UNIVERSITÀ DI PISA

Scuola di Ingegneria

Corso di Laurea Magistrale in

INGEGNERIA CHIMICA

Dipartimento di Ingegneria Chimica e Industriale (DICI)

Tesi di Laurea Magistrale

"Modelling the behaviour of pressurized vessels exposed to fire with defective thermal protection systems"

Relatore

Dott. Ing. Gabriele Landucci

Candidato

Federica Ovidi

Controrelatore

Prof. Leonardo Bertini

Anno accademico 2014/2015

UNIVERSITÀ DI PISA

Scuola di Ingegneria

Corso di Laurea Magistrale in

INGEGNERIA CHIMICA

Dipartimento di Ingegneria Chimica e Industriale (DICI)

Tesi di Laurea Magistrale

"Modelling the behaviour of pressurized vessels exposed to fire with defective thermal protection systems"

Autore:

Federica Ovidi *Firma:* _____

Relatore:

Dott. Ing. Gabriele Landucci *Firma:* _____

Controrelatore:

Prof. Leonardo Bertini *Firma:* _____

Anno accademico 2014/2015

To my Mum and Dad,

and Chicco

Abstract

Industrialized society is linked to the transport of hazardous materials by road and rail, among other. During transportation, accidents may occur and propagate among the tankers leading to severe fires, explosion or toxic dispersions. This may increase the level of individual and social risk associated to those activities, since the transport network often crosses densely populated area. The escalation of a primary event, in this case the fire, is typically denoted as domino effect, and the triggered secondary events typically are amplified.

In the framework of liquefied petroleum gas (LPG) transportation, severe fire and explosion hazards are associated to the possible catastrophic rupture of tankers, which may be induced by domino effect of accidental fires. Heat resistant coatings may protected tankers against the fire, reducing the heat load that reaches the tank shell wall and the lading. Indeed, the rupture is the result of the double effect of thermal weakening of the tank material and the increasing pressure due to LPG evaporation. However, this protection systems are not ideal and undergo defects due to both material degradation and accidental damage. Therefore, protection may be ineffective. The present work is aimed at characterizing the performance of defective coatings.

The first part of the work is devoted to the characterization of past accidents occurred in the framework of road and rail transportation of hazardous materials. The *ARIA* and *MHIDAS* databases are adopted as data sources, identifying 245 road and 220 rail accidents involving hazardous materials. The analysis highlighted the importance of protecting tank from heat load to avoid the rupture and related severe scenario. For these reasons, in North America the installation of a heat resistant coating is used to protect dangerous good tankers from accidental fire exposure. In Europe, *ADR* and *RID* regulations govern transnational transport of hazardous materials by road and by rail, respectively, and still not include any section about thermal protection systems of tankers.

Possible concerns related to the installation of these systems is due presence of defects that may be formed accidentally in the fireproofing layer. It is therefore important to establish what level of defect is acceptable in order to avoid the failure of tankers, in the prospective of a wider implementation of tankers fire protections in the European framework. Since large scale bonfire tests are expensive and difficult to be carried out in order to verify the thermal protections adopted, modelling the behaviour of pressurized insulated tankers when exposed to the fire is a possible solution to test the adequateness of defective protections.

In order to describe the thermal behaviour of real scale LPG tanks exposed to fire, a lumped model (namely, ‘RADMOD’) and a Finite Elements Model (FEM) are developed. The models are validated against available experimental data and allow predicting the thermal behaviour of tankers with defective coating when exposed to fire, with the aim to assess the thermal protection performance. The phenomena taking place through the vessel in presence of defects are investigated and characterized, in order to reproduce the experimental data on thermal behaviour of defective thermal protection systems exposed to fire.

The FEM model allows to determine the wall temperature profile and the stress distribution over the vessel, determining, in the end, a critical defect size that lead to the tank failure, with respect different fire conditions. A sensitivity analysis is performed on the FEM model in order to identify the parameters that mostly affect the heat

exchanges of the system. This analysis highlights the main relevance of the flame temperature against other parameters, such as convective heat transfer coefficients and emissivity of flame and steel.

The complex analysis performed by FEM model, requires high computational times, which may be prohibitive when a wide number of runs is required. The RADMOD code is a simplified lumped model, which allows to assess the behaviour, among other, of the pressure and the fluid temperature with lower, and thus acceptable, computational time. Another plus of the RADMOD model is that it can be run for a wide range of materials, substances, geometries and fire scenario, estimating a conservative but credible time to failure of the tank. The novel mathematical code for defective thermal protection system is added to the previous version of the RADMOD model, which was implemented for unprotected or completely coated tanks, thus all the phenomena related to the defect enclosure are characterised. In addition, other phenomena, already present in the RADMOD model, are revised to enhance the potentiality of the code. The comparison of results with available experimental data on small-scale shows that the model proposed in this thesis work can reasonably predict the thermal response. The application of the modelling tool to different geometries is performed considering real-scale defects. Thus, several case-studies were defined in order to reproduce medium- and large-scale tanks varying a few parameters, such as defect size and liquid filling level, for testing the reproducibility of the new model. The results from the case studies highlight the potentiality and the flexibility of the RADMOD code in modelling the thermal response.

The ultimate goal would be to apply the data collected from RADMOD code about temperature and pressure of lading, as boundary condition in the FEM model for an improved modelling of thermal behaviour of real-scale LPG tanks in fire scenarios even if there is a defective thermal protection system.

Sommario

La società industrializzata è inevitabilmente legata al trasporto di sostanze pericolose che, tra le altre modalità, viaggiano giornalmente su strada e su rotaia. Durante questi trasporti, esiste la possibilità che si verifichino incedenti con sviluppo d'incendio, in questi casi le fiamme possono estendersi alle cisterne e provocare altri incendi, severe esplosioni o dispersioni tossiche. L'esistenza di queste casualità nel trasporto di materiali pericolosi porta ad un aumento del livello di rischio associato a tali attività, sul piano del rischio individuale e sociale, visto che la rete dei trasporti attraversa spesso aree densamente popolate. L'escalation di un evento primario, in questo caso l'incendio, è generalmente indicata come effetto domino, e gli eventi secondari che vengono innescati sono tipicamente amplificati.

Nell'ambito del trasporto di gas di petrolio liquefatti (GPL), gravi incendi e severe esplosioni possono verificarsi a seguito della rottura catastrofica della cisterna, causata, ad esempio, dall'effetto domino di incendi accidentali. Un modo per proteggere la cisterna da tali eventualità potrebbe essere installare un rivestimento termico sul serbatoio. Questo ridurrebbe il calore ricevuto sia dalle pareti della cisterna che dal fluido al suo interno, ottenendo un duplice effetto protettivo. Infatti, le cause che portano alla rottura della cisterna sono due: l'alta temperatura raggiunta delle pareti, che indebolisce termicamente i materiali di costruzione, e l'aumento della pressione interna dovuto all'evaporazione del GPL. Tuttavia, questi sistemi di protezione termica non sono ideali e sono soggetti alla formazione di difetti, che possono essere dovuti sia alla degradazione del materiale stesso che a danneggiamenti accidentali del coibente. Pertanto, l'azione di protezione può risultare inefficace. Lo scopo del presente lavoro è quello di caratterizzare le prestazioni dei rivestimenti termici affetti dalla presenza di questi difetti.

La prima parte del lavoro è dedicata allo studio di incidenti avvenuti in passato nell'ambito del trasporto stradale e ferroviario di sostanze pericolose. I dati sono raccolti da due diversi database: ARIA e MHIDAS; identificando 245 incidenti stradali e 220 incidenti ferroviari in cui sono stati coinvolti materiali pericolosi. L'analisi evidenzia l'incidentalità delle rotture dovute ad incendi esterni e la gravità degli scenari associati alla rottura dei serbatoi pressurizzati. Per queste ragioni, in Nord America le cisterne adibite al trasporto di sostanze pericolose vengono equipaggiate con rivestimenti termici in grado di proteggerle dall'esposizione al fuoco. Al contrario, le regolamentazioni europee sul trasporto stradale e ferroviario, rispettivamente gli accordi ADR e RID, non prevedono ancora nessuna sezione sui sistemi di protezione termica delle cisterne.

Una problematica relativa all'installazione di tali sistemi è legata proprio alla possibile formazione di difetti nello strato termico protettivo. Quindi, stabilire quale livello di difetto può considerarsi accettabile per evitare la rottura del serbatoio, risulta importante sia dal punto di vista della sicurezza ed anche nella prospettiva di una più ampia implementazione di questi sistemi nel panorama europeo. Per testare l'adeguatezza delle protezioni termiche in presenza di difetti si può ricorrere ad esperimenti su grande-scala di serbatoi incendiati. Poiché tali esperimenti sono molto costosi e difficili da realizzare, una delle possibili alternative è modellarne il comportamento tramite software specifici.

In questo studio sono implementati due diversi modelli, al fine di descrivere la risposta termica dei serbatoi GPL incendiati su grande-scala: un modello a parametri concentrati (chiamato 'RADMOD') ed un modello ad elementi finiti (FEM). Entrambi sono validati a fronte di dati sperimentali e consentono di predire il comportamento delle cisterne coibentate esposte al fuoco, con l'obbiettivo di valutare la prestazione della protezione termica difettata. Per permettere la modellazione di tale problema tutti i fenomeni ad esso legati sono prima analizzati e caratterizzati.

Il modello FEM esegue un'analisi avanzata tramite la quale è possibile calcolare, in funzione di diverse condizioni di incendio, i profili termici delle pareti e la distribuzione delle tensioni sul serbatoio, determinando, infine, una dimensione critica del difetto capace di portare alla rottura della cisterna. In questo studio il modello FEM viene utilizzato al fine di identificare i parametri che maggiormente influiscono sugli scambi di calore del sistema, tramite l'esecuzione di un'analisi di sensitività. I risultati dell'analisi evidenziano la rilevanza della temperatura di fiamma come parametro nella risposta termica, a fronte di altre variabili come i coefficienti di scambio convettivo o l'emissività della fiamma e dell'acciaio.

Le simulazioni eseguite con il modello FEM sono complesse e richiedono tempi di calcolo elevati che possono risultare proibitivi, ad esempio quando sono richieste simulazioni multiple. Per questo motivo viene implementato un secondo modello: il modello RADMOD. RADMOD, infatti, è un modello semplificato che permette di determinare l'andamento della temperatura del fluido e della pressione nel serbatoio, con tempi di calcolo minori e, quindi, accettabili. Un altro vantaggio di RADMOD è quello di riuscire a simulare diversi tipi di materiali, sostanze, geometrie e scenari d'incendio, stimando un tempo di cedimento della cisterna conservativo ma comunque credibile. In questo studio, il codice per la simulazione di sistemi coibenti difettati viene implementato ed aggiunto alla precedente versione del modello RADMOD, sviluppata solo per la simulazione di serbatoi non protetti o completamente coibentati. Quindi, tutti i fenomeni legati alla presenza del difetto vengono prima caratterizzati e poi modellati all'interno del codice; ed alcuni fenomeni già presenti nel modello vengono rivisitati per aumentarne le potenzialità. Il confronto dei risultati ottenuti dal codice con i dati sperimentali su piccola-scala, evidenzia la potenzialità del modello RADMOD nel prevedere la risposta termica di tali sistemi. Successivamente il codice è applicato a diversi difetti, considerando geometrie reali. Vengono, quindi, definiti diversi casi-studio relativi a serbatoi di media e grande scala variando alcuni parametri, come la dimensione dei difetti ed il livello di riempimento del serbatoio, per testare la riproducibilità del nuovo modello. I risultati dei casi-studio evidenziano la potenzialità e la flessibilità del modello RADMOD.

L'obiettivo finale dell'implementazione dei due modelli è quello di ottenere i dati su temperatura del fluido e pressione nel serbatoio tramite il modello RADMOD, ed usarli come condizioni a contorno nel modello FEM, per migliorare la modellazione della risposta termica di cisterne GPL coibentate in scenari d'incendio, anche in presenza di difetti nel sistema di protezione.

Summary

List of Figures

List of Tables

1 Introduction

All over the world, and particularly in industrialized countries, the transport of hazardous materials has till years continuously increasing trend. [Paltrinieri et al. 2009] The transportation of chemicals is necessary for the manufacturing and distribution of products within and across regional and international borders. Although, transportation of hazardous materials is affected by severe accidents. Public concern is focused mainly on road and rail transport, since the road and rail networks used in transportation of hazardous materials necessarily come closer, and sometimes also cross, densely populated areas. Transport of dangerous goods need to be regulated in order to prevent, as far as possible, accidents to persons or property and damage to the environment, the means of transport employed or to other goods. [UNECE, Model Regulations Volume I , 2013]

In Europe, the legislation for hazardous materials transportation is designed and managed by ONU through the UNECE. The legislation is divided into several documents tailored to the specific needs of the various means of transport, covering transport of dangerous goods by road, rail and inland waterways. In particular, the road and rail transportation are regulate, respectively, by the ADR and RID agreement. The ADR agreement, for instance, concerns determination and classification of dangerous substances, characteristics of packaging and containers, construction, equipment and operation of the vehicle carrying the goods in question. [ADR, 2015]

Focusing attention on the transportation of liquefied flammable products (such as liquefied petroleum gas – LPG, propylene, butadiene, etc.) an accidental spill may lead to severe fire and explosion scenarios having the potential to cause injuries and fatalities also among the off-road population. Among them, one of the more severe is the BLEVE, which consists in the explosive release of expanding vapour and boiling liquid when a container holding a pressure-liquefied gas fails catastrophically. [Birk & Cunningham, 1994] The pressurized liquefied gas vaporizes instantly and expands, originating a blast that is often followed by a fireball due to the ignition of the flammable substance. [Reid, 1979]

The BLEVE may be caused by an external fire that impinges the tank. The fire exposure causes a temperature increase of the tank wall and, thus, of the fluid inside the tank. The mechanical resistance of the shell material is compromised by high wall temperature and by pressure-induce stress, due to the evaporation of the liquid. Even with a properly working and sized pressure relieving device, able to keep the internal pressure within the vessel design limits, the tank can rupture due to wall material degradation at high temperature. Thus, the combination of both these factors may lead to the catastrophic rupture of the tank, and consequent BLEVE and fireball. Hence, the chance of BLEVE can be reduced by the installation of systems able to prevent or, at least, to delay for a time lapse sufficient for emergency response, the thermal collapse of the tank.

In North America, specific transport regulations have been adopted, requiring road and rail tankers carrying flammable liquefied gases to be equipped with pressure relief valves and, mainly, rail tank-cars have to be thermally insulated. For instance in Canada the thermal protection system is designed so that the tank-car will not rupture for 100 minutes in an engulfing pool fire or 30 minutes in a torching fire [CFR Code of Federal Regulation, 2015; CGSB, 2002] However, such protective measures are not compulsory in Europe. In fact ADR and RID regulations do not require any passive fire protection

on LPG tankers. Possible concerns related to the implementation of protections on tankers is related to the possible formation of defects, that may deplete the thermal protection performance.

There are intrinsic defects related to the installation of a coating, i.e. in correspondence of joints or external hooks the coating can not cover the entire surface of the tank. Moreover, as thermal protection system on tank undergoes wear or insufficient maintenance, it is possible that the insulation degrades. Vibrations and shocks may cause the slippage or the crushing of insulation blanket, reducing the thermal protection to the tank.

It is therefore crucial to assess whether or not a given degree of defect is acceptable. Addressing this issue requires a deep understanding of the phenomena which take place when a tank-car covered by defective thermal protection is exposed to fire. For instance, the slippage of the blanket results in the formation of an air gap between the external steel jacket, that covers the coating, and the tank-car shell. In case of exposure to fire, complex mechanisms occur for heat transfer from the flame through the several layer of the tank, i.e. steel jacket, undamaged coating or air gap, shell wall and, finally, to the lading which is in vapour or liquid phase. [Scarponi et al. 2016]

The thermal response of such system needs to be investigated deeper. The best way to achieve this aim would be reproducing real-scale bonfire tests concerning pressurized insulated tankers and testing the behaviour of several insulation deficiencies. Trials of this kind are not nimbly feasible, since they are almost prohibitive under the economical point of view and also for safety and environmental concerns. The implementation of simulation tools overcomes the impossibility of testing the effect of defects on real-tanks, the closer the model reproduces the reality, the lower the need to perform bonfire tests. Modelling the thermal behaviour through a computer model also allows the simulation of a wide range of geometries, materials, fire conditions and other parameters.

In the present work, two different models are presented in order to determine the thermal behaviour of real-scale LPG tanks with defective insulation system, involved in accidental fire impingement: a FEM model and a lumped parameters model.

The FEM method divides the vessel in elements and nodes and allows to obtain the approximated value of exact solution of temperature and equivalent stress, in each nodes. The model is based on two distinct simulations, thermal and mechanical, which are concatenate in order to obtain accurate modelling of pressurized vessels exposed to fire. In detail, the model determines the wall temperature profile by a thermal analysis, the results of which are extracted and used in a mechanical analysis, determining the stress distribution over the vessels. The results obtained in each nodes allows the use of correct failure criteria to evaluate the time to failure of the tank. The computational time of this analysis is very high and being not acceptable in case multiple runs are required. A sensitivity analysis is performed on a thermal FEM model reproducing the experiments carried out by Birk and VanderSteen [VanderSteen & Birk, 2003] on a portion of tanker shell, with several insulation deficiencies. The sensitivity analysis aims to identify the most critical parameters affecting the heat exchange in tankers exposed to fires, therefore varying a few of several parameters, as the flame temperature and the steel emissivity, the temperature behaviour of the defect is analysed.

In order to reducing the computational time of the FEM model, a lumped parameters model (namely ‘RADMOD’) is developed. The lumped parameters analysis

substantially reduces computational costs dividing the system in different zones (macro-nodes), depending on the fire conditions, in which are defined and obtained by the model, averaged value of parameters.

The RADMOD model is developed, based on a previous model developed by [Landucci et al. 2013]. With respect to the previous version of the model, the novel developed tool defective insulation systems. The model was further enhanced for different types of heat exposure conditions, the heat and material balances were revised for fully engulfing fire and for half engulfing fire. Complex phenomena are also enhanced, as the liquid thermal stratification. The novel sub-model is developed for small-scale tanks, in order to validate it against experimental test data on a 1.9 m^3 tanks conducted by Birk et al. in 2006. [Birk et al. 2006]

The model was then extended to medium- and large-scale vessels in order to run different real-scale geometries of defects. The latter were identified by Birk and Cunningham through a thermographic method for the inspection of tank-car thermal insulation in 1994. [Birk & Cunningham, 1994] Several case studies were defined and analysed varying some parameters, as the liquid filling level and the vessel geometry, in order to test the potentialities of the present approach.

2 Safety issues in the transportation of hazardous materials

2.1 Transportation of hazardous materials in European framework

In everyday language the term hazardous materials also referred to as dangerous/hazardous substances or goods solids, liquids, or gases that can harm people, other living organisms, property, or the environment. They not only include materials that are toxic, radioactive, flammable, explosive, corrosive, oxidizers, asphyxiates, biohazards, pathogen or allergen substances and organisms, but also materials with physical conditions or other characteristics that render them hazardous in specific circumstances, such as compressed gases and liquids, or hot/cold materials. [TSO, 2012]

2.1.1 Transport volume of hazardous materials

All over the world, and particularly in industrialized countries, the transport of hazardous materials (hazmat) rise continuously in years. [Directive 94/55/CE] Every day large amounts of these materials are involved in road, rail and inland waterway transport. It was estimated that more than 4 billion of hazmat tons were transported annually at worldwide level in the first half of the past decade [Zografos & Androutsopoulos, 2004]: in USA, there are at least 300 million hazmat shipments each year, and totally approximately 3.2 billion tons. In Germany, each year around 300 million tons of dangerous goods are conveyed, around 140 million tons of which by road. In Italy, 74 millions of hazmat tons were transported on trucks in 2001, [BAM, 2012] while table 2.1 contains data on the rail transport of dangerous goods on national territory in 2011-2012, [MIT, 2012/2013] according to the RID classification, which is discussed in the following paragraph.

Table 2.1 – Rail transport of dangerous goods in Italy during 2011-2012 [MIT, 2012/2013]

RID class	**Dangerous Good**	**2011**		**2012**	
		Tonn-km x 1000	Averaged travel (km)	Tonn-km x 1000	Averaged travel (km)
1.1	Explosive	1.407	286	661	237
2.1	Gases (compressed, liquefied or dissolved under pressure)	385.978	399	350.359	384
3	Flammable liquid	388.331	269	384.845	268
4.1	Flammable solid	6.850	163	3.122	155
4.2	Spontaneously combustible substance	1.229	190	1.990	530
4.3	Substance which in contact with water emits flammable gas	7.419	255	2.904	291
5.1	Oxidising substance	10.291	302	7.886	204
5.2	Organic peroxide	1.849	601	2.385	590
6.1	Toxic substance	84.110	284	73.746	259
6.2	Infectious substance	-	-	-	-
7	Radioactive material	72	166	41	167
8	Corrosive substance	144.567	304	125.224	329
9	Miscellaneous dangerous goods	169.862	283	198.584	250
Total		**1.201.965**	**308**	**1.151.745**	**296**

2.1.2 The ADR / RID agreements

Since hazmat daily cross international borders an harmonized regulation system was needed. The different regulations from country to country make international trade in chemicals and dangerous products seriously impeded, if not impossible and unsafe. [UNECE, 2016] In the European Community, the hazmat transportation is regulated by ONU through the United Nations Economic Commission for Europe (UNECE). The agreement is divided into several documents tailored to the specific needs of the various means of transport, starting from a common basis:

- RID *(Règlement concernant le trasport International ferroviaire des merchandises Dangereuses)*, for the railway sector
- ADR (*Accord Européen Relatif au Transport International des Marchandises Dangereuses par Route*), for the road sector
- IMDG (*International Maritime Dangerous Goods)*, for shipbuilding, maritime sector
- ADN (*Accord Européen Relatif au Transport International des Marchandises Dangereuses par Voies de Navigation Intérieures)*, for inland waterways

The ADR agreement was signed in Geneva on September 1957 and entered into force in January 1968. [ADR, 2015] In 1962 Italy adhered to the ADR agreement [L. 1839/1962] and it was originally applied to international transport only. Than the ADR, RID and ADN agreements were extended to internal transport under the intention of European Union to harmonize across the Community the conditions under which dangerous goods are transported [Directive 94/55/CE] and Italy transposes that directive in January 1996 [D.M. 4 settembre 1996] The agreement itself is brief and simple, most of the provisions are indicated in the annexes: A - *General provisions and provisions concerning dangerous articles and substances*, and annexes B - *Provisions concerning transport equipment and transport operations*. [ADR, 2015]

The ADR agreement regulates:

- the classification of dangerous substances in regard to the road sector
- standards and tests that determine the classification of individual substances as dangerous
- the conditions of packaging of goods, characteristics of packaging and containers
- construction methods for vehicles and tanks
- the requirements for the means of transport, including travel documents

Moreover, the agreement refers to employees who are involved in hazmat transport at various levels: from the drivers of vehicles to people loading and unloading to operations managers. Persons of those categories must have been trained and often have achieved patent permits. [ADR, 2015] The prevision laid down the ADR do not apply to the transport of dangerous goods by private vehicles or under the responsibility of the armed force. [D.M. 4 settembre 1996]

2.1.3 Classification of dangerous goods

The ADR agreement classifies the substances in nine hazard classes that define the type of risk that hazardous material may pose. Some substances have main risks and secondary risks, and thus meet the definition of more than one hazard class. To further group substances with similar risks, some hazard classes contain divisions. [ADR, 2015] The ADR classification is reported in table 2.2.

Table 2.2 – ADR classification of dangerous good [ADR, 2015]

Class	Dangerous Goods
1	Explosive substances and articles
2	Gases
2	Flammable liquids
4.1	Flammable solids, self-reactive substances and solid desensitized explosives
4.2	Substances liable to spontaneous combustion
4.3	Substances which, in contact with water, emit flammable gases
5.1	Oxidising substances
5.2	Organic peroxides
6.1	Toxic substance
6.2	Infectious substances
7	Radioactive material
8	Corrosive substances
9	Miscellaneous dangerous substances and articles

ADR also defines three packing groups, which indicate the degree of risk a hazardous material may pose in transport in relation to other materials. Packing group is not applicable to all hazard classes divisions, it refers to classes 1, 2, 5.2, 6.2, 7 and to self-reactive substances of class 4.1. This classes are assigned to packing groups in accordance with the degree of danger they present [ADR, 2015] as follow:

- Packing group I – Substances presenting high danger
- Packing group II – Substances presenting medium danger
- Packing group III – Substances presenting low danger

Then, once the dangerous goods class has been defined, the European legislation give some provisions of how to avoid or reduce the accident of the tanks subjected to an external heat load, such as an accidental fire. For flammable substances the most hazardous condition of transportation is the state of pressurized liquefied gas, in case of sub cooled liquids or high pressure gases the consequences are not as much severe [Landucci et al. 2013]. Therefore in the former scenario (and also for toxic gases) the European Agreements RID and ADR, commit all filling and discharge openings of tanks be equipped with an internal instant closing stop-valve which closes automatically in the event of unintended movement of the vessel or in the event of fire (for tank-containers, this requirements only applies if they have a capacity of more than 1 m^3) for risk reduction. In addition it also contains requirements for pressure relief devices to ensure the integrity of the tank even if the tank is fully engulfed in fire. For example, for tanks of non-refrigerated liquefied gases, the internal pressure does not exceed 20% of the working pressure. [ADR, 2015]

The present work focuses on liquefied petroleum gas (LPG) which transportation is extremely frequent in Europe. LPG is a mixture of saturated hydrocarbons, primarily propane and butane, in their liquid state, that is, under pressure at ambient temperature. It is a useful fuel for mobile and remote applications, because it requires only moderate pressure (< 2 MPa) to remain liquid form at ambient temperature and it readily vaporized when the pressure is released. This is the main advantage of LPG as fuel, because it is liquid for transportation and storage, but gaseous for use. The composition of LPG consequently depends on the season and the location where it is marketed. In fact, propane evaporates at -42 °C, at atmospheric pressure, instead at 0.6 °C, which is

the boiling point of butane at the same pressure condition. Thus, different grades of LPG can be produced. In regions where the winter temperatures drop below 0°C, the main constituent of LPG is propane, because butanes are liquids at such conditions. In hot climates, LPG can be a butane-propane mixture. [Maitlis & De Klerk, 2013]

In the ADR classification LPG belongs to class 2, division 2.1. As mentioned before, the hazard related to LPG is also due to its liquefied gas condition. A flammable gas liquefied through pressurization is a gas that has internal energy sufficient to suddenly evaporates and turns out in a flammable mixture with air.

2.2 Past accidents data analysis

In order to identify the major safety issues associated to the transportation of hazardous materials, past accidents data analysis was carried out. In fact, this type of analysis grants valuable information on causes, dynamics and consequences, which can provide the necessary experience to be used for safety improvement and to the characterization of accidental scenarios.

2.2.1 Past accident report – Viareggio 2009

One of the most severe accident connected with the rail transportation of hazmat occurred in Viareggio (Italy) in 2009. On Monday June 29th 2009, a freight train was composed of 14 tank wagons, each having a nominal capacity of about 46.7 t (100,000 L) was passing through Viareggio. At 23:45 the first tank wagon derailed and overturned after passing through Viareggio railway station at a speed of 90 km/h, below the imposed limit of 100km/h. The following 4 tank cars also derailed and overturned. The train engine did not derail and stopped few meters ahead of the first car. After derailment, an intense loss of containment took place from the first tank wagon. The entire inventory of a commercial LPG mixture was released from the breach. No loss of containment occurred from the other 13 tank vessels. Firemen emptied all the derailed cars on July 2nd. According to the report of the engine drivers, no immediate ignition followed the release. Before the ignition of the gas cloud, the drivers had time to shut-down the engine, to remove the documents from the engine and to run about 200m away from the railway. Several witnesses remember a cloud of cold and white mist propagating around the area where the derailment took place. The cloud ignited few minutes after the start of the release. It is still uncertain which was the ignition point. A flash fire resulting in severe damage took place. Several houses were involved in the fire and 31 fatalities were caused by intense heat radiation exposure or collapse of building. [Landucci et al. 2011]

2.2.2 Methodology and selection criteria

The data were collected from two different databases, the ARIA (Analysis, Research and Information on Accidents) database and the MHIDAS (Major Hazard Incident Data Service) database; the first one was used as primary source while the second one was used as supplement since it is no longer updated. The MHIDAS database was hosted by United Kingdom Health and Safety Executive. The ARIA database operated by the French Ministry of Ecology, Sustainable Development and Energy lists the accidental events, which have, or could have damaged health or public safety, agriculture, nature or the environment. [ARIA, 2016] It collects events that are mainly caused by hazardous industrial or agricultural facilities and also by transportation of hazardous materials.

The research was carried out on all countries but France, this is due to the 40000 accidents collected in France against the 6000 collected in other countries, but France. The French data also concern small accidents which are not important for this research

that aiming at the classification of substances and primary causes involved in hazmat transportation. The selection of contextual accidents would be laborious and it would not have lead to significant changes in the final results, assuming that there is no reason why France should be out of European average accidents in hazmat transportation. For this reason it was assessed the exclusion of the France from the location of accidents.

The following scenarios were considered during the research:

- Accidents occurred during transport of dangerous goods by road, inside a company or on the road
- Accidents occurred during transport of dangerous goods by rail, in or outside of an classified installation

This analysis has taken into account all accidents of this type occurred from 1980 to September 2015.

Three categories of substances were individuated and classified by the physical state in which they were transported, through the following methodology:

- Liquid
- Liquefied gas
- Other

The flammable and toxic substances transported in liquid phase, at ambient temperature, are classified as liquid if their boiling point is under 30°C, otherwise they are classified as liquefied gas, if their boiling point is over 30°C. Solid, gaseous and cryogenic substances, both flammable and toxic, are classified as other. In addition to the above classification, substances were divided by hazardous properties (flammable or toxic) specifying what type of substance were involved in the accident (ammonia, LPG, etc.).

Primary causes are the events that turn out in the involvement of hazmat transportation tank in the road or rail accident, which is followed by the failure of the tanker an subsequent leakage of substance. The analysis of primary cause was conducted by classifying them in the following categories:

- Human error
- Failure of truck/locomotive
- Failure of tanker
- Failure of rail/rail control system, for rail transportation
- External event

Human error includes all the events which were not intended by the actor, which are a deviation from intention, expectation or desirability. Collision, truck overturns, lost of control of the vehicle, derailment, failure to close the valves, unsafe welding, failure of operating hook, etc. are some example of what the human error category contains.

The failure of truck or locomotive includes the failure of every elements belonging to the truck or convoy except the tankers; such as the breakdown of a wheel, lost of the tanker, fire on truck not related to an external event, failure of the axle, etc.

The failure of the tanker could occur in several modes including the failure of a valve or pressure relief valve, the premature opening of rupture disk, the crash of a part of the tanker which was deformed. The leakage from the tank was also included in this category, as well as the fire on the tanker, which was considered as the consequence of a leakage.

In the rail transportation it was necessary to add another category: the failure of the rail or of the rail control system, which includes the causes related to the rail damage, such as fracture, corrosion, defective rail, misalignment; and to the failure of "rail" control system, such as the failure of automatic stop device, of a switch and, more generally, of traffic control system.

The external event is the last category, it includes: external impact, sabotage, earthquakes, hurricane and external fire. The latter is the cause on which this work will focus. The external fire could occur, amongst other events, from another tank or from another unit, by the ignition of a flammable substance leakage during the tank loading/unloading operations or from a short circuit of electrical cable. All the unknown causes were included in the external event category.

Focusing on the LPG transportation, the primary causes were investigated as the causes that led to the tank failure; if a human error caused the accident it may lead to a cold BLEVE (Boiling Liquid Expanding Vapour Explosion), with the instantaneous loss of containment, or it may generate a fire which engulfs the tank and may turns out in the failure of the tank. In the first scenario the primary cause was considered as the human error, while the external fire was considered as the cause of the second scenario. The same classification of primary causes of accidents reported above were used for LPG tanks causes of failure.

Also the consequences were collected for the LPG accidents and they were classified as follows:

- Release → only leakage without ignition
- Instantaneous release → cold BLEVE
- Release, ignition and fire → no BLEVE occurred
- Release, ignition and fire → with consequent fired BLEVE

2.2.3 Results of the historical analysis

As mentioned before, the data were collected principally from ARIA database, which lists 339 occurrences referred to road transportation and 320 occurrences referred to rail transportation, in relation to the selection criteria aforesaid between 1980 and 2015. After selection of contextual accidents and implementation with MHIDAS database, 245 occurrences referred to road transportation and 220 occurrences referred to rail transportation have been examined. The results of the analysis is reported and than discussed in this section.

Road transportation results

Figure 2.1 reports the category of substances involved in severe accidents in road transportation while Figure 2.2 shows the primary causes of accidents occurred in hazmat road transportation. Figure 2.3 and 2.4 respectively reports the primary causes of accidents in road transportation which involve LPG and the consequences of these category of accidents.

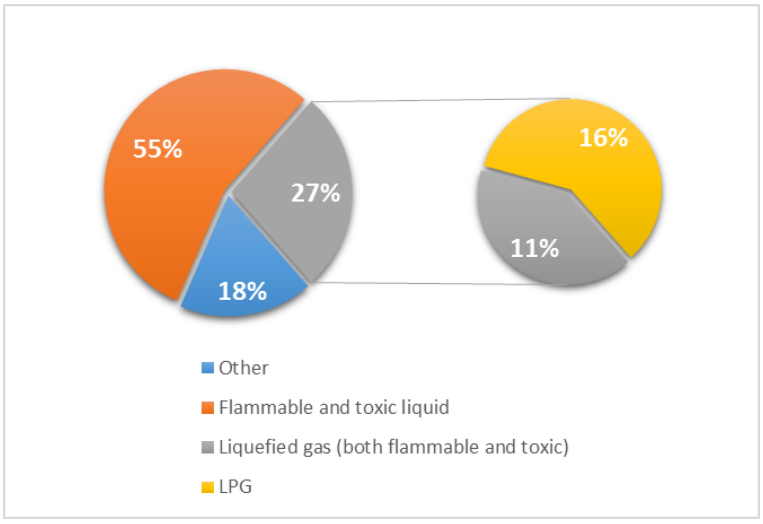

Figure 2.1: Classes of substances involved in hazmat road transportation accidents

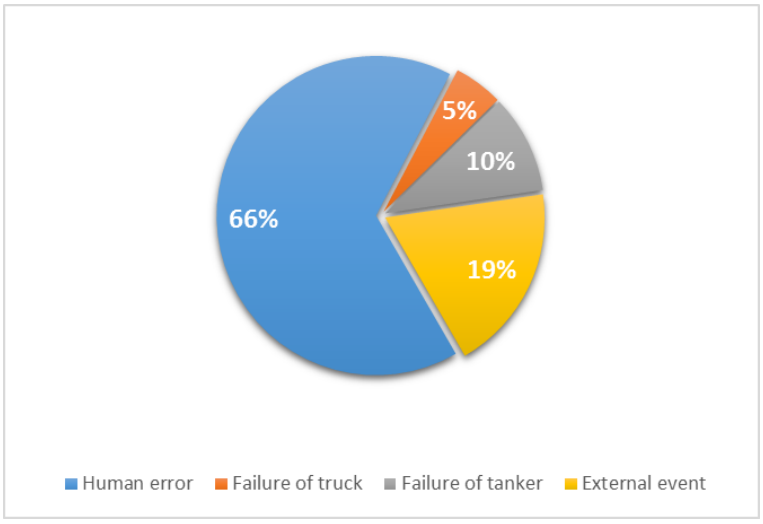

Figure 2.2: Primary causes of accidents occurred in hazmat road transportation

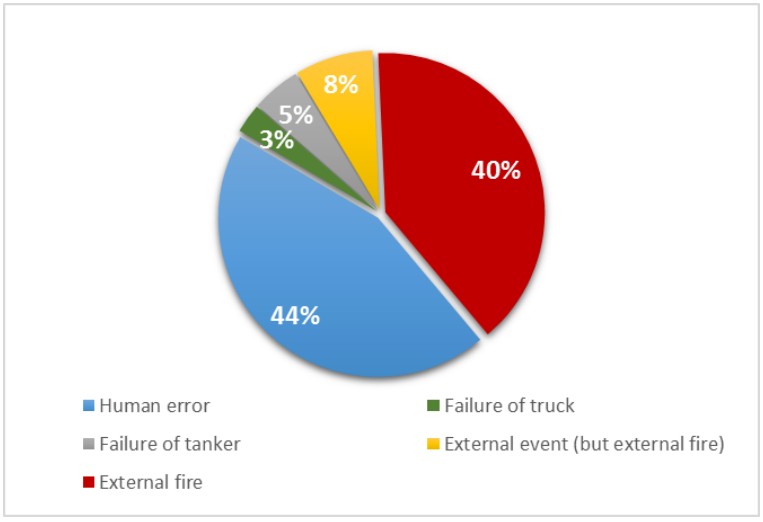

Figure 2.3: Primary causes of accidents occurred in LPG road transportation

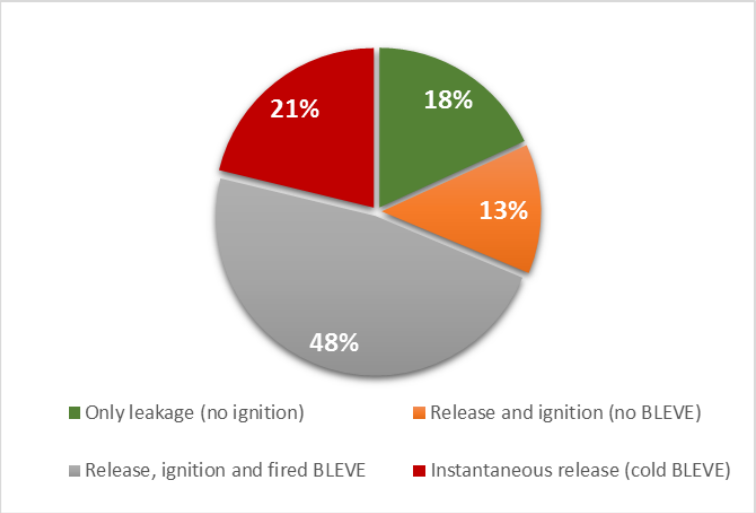

Figure 2.4: Consequences of accidents occurred in LPG road transportation

Rail transportation results

Figure 2.5 reports the category of substances involved in severe accidents in rail transportation, while Figure 2.6 shows the primary causes of accidents occurred in hazmat rail transportation. Figure 2.7 and 2.8 respectively reports the primary causes of accidents in rail transportation which involve the LPG and the consequences of these category of accidents.

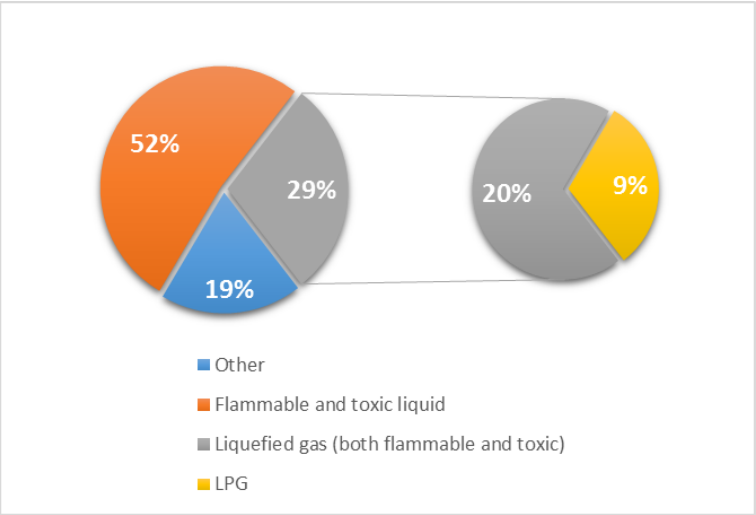

Figure 2.5: Classes of substances involved in hazmat rail transportation accidents

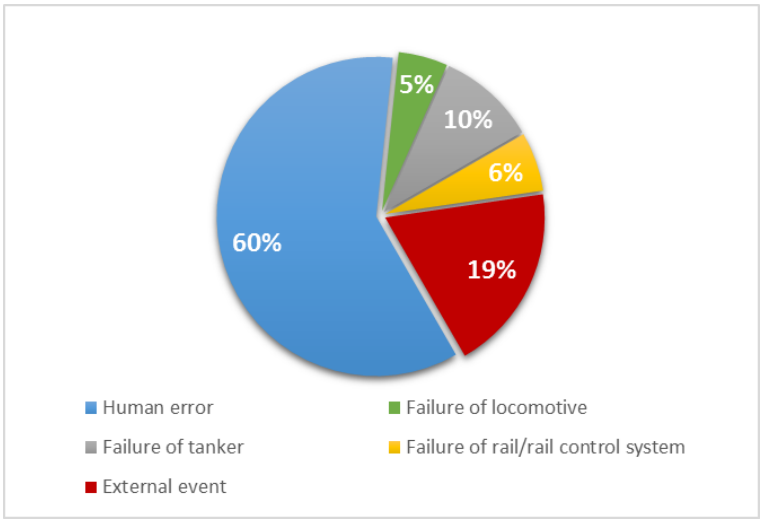

Figure 2.6: Primary causes of accidents occurred in hazmat rail transportation

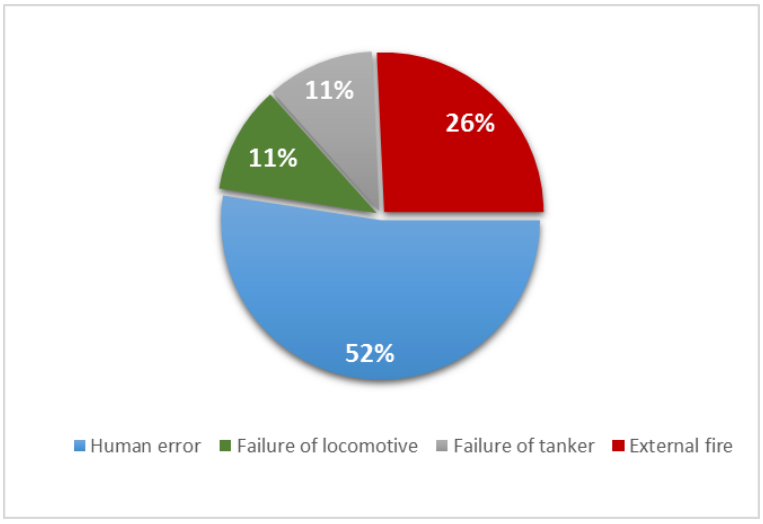

Figure 2.7: Primary causes of accidents occurred in LPG rail transportation

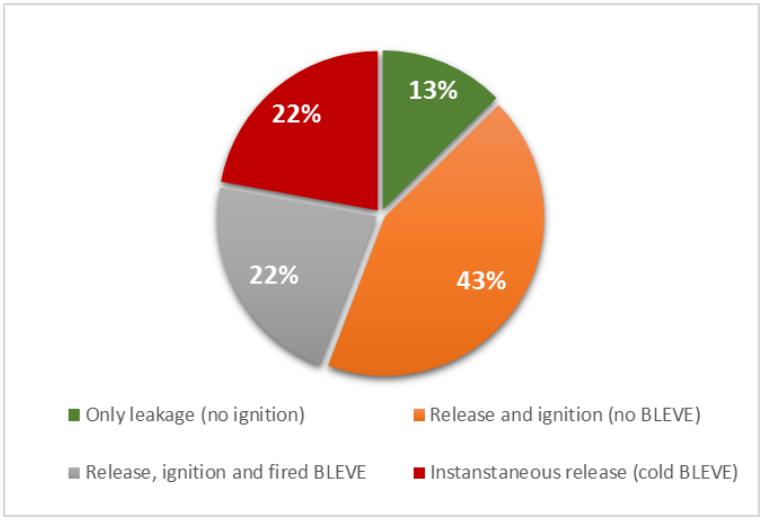

Figure 2.8: Consequences of accidents occurred in LPG rail transportation

2.3 Safety issues related to the transportation of pressurized flammable gases

Past accidents data analysis identified the relevant accidents occurred in years during the road and rail transportation of dangerous goods, around the world. The classes of substances involved and the main causes of accidents are classified, with particular focus on accidents occurred during LPG transportation, the consequences of which are also identified and classified. It is timely, therefore, to detailed analyse the safety issues related to LPG transport. They are discussed in this section to complete the picture and come to some conclusions.

Dangerous goods are carried through a transportation network, which civilians daily use and which crosses vulnerable and densely populated areas. During the transportation of LPG or, generally, pressurized flammable gas, if an accidental leak occurs it may lead to catastrophic event which can harm people and neighbouring buildings, as occurred in the Viareggio accidents. (see paragraph 2.2.1)

2.3.1 BLEVE definition

As evidenced by past accident data analysis, one of the most critical scenarios that may follow an accidental leakage of LPG is the boiling liquid expanding vapour explosion (BLEVE). This event typically follows the catastrophic rupture of a tank containing the pressurized liquefied gas, which instantly vaporizes and expands. The liberated energy in such cases is very high, causing high blast pressures and generation of fragments with high initial velocities, and resulting in propulsion of fragments over long distances. [TNO Yellow Book, 2005] The blast is often followed by a fireball due to LPG ignition. [Reid, 1979] In the end of the 1970s, the BLEVE was a mysterious phenomenon, several theories have been put forward to explain this very energetic event but none have been proved. [Birk & Cunningham, 1994] Among the large number of definitions that can be found in literature, [Hemmatian et al. 2015] Walls defined BLEVEs for first time in 1957 [Walls, 1979] as a failure of a major container into two or more pieces occurring at a moment when the container liquid is at a temperature above its boiling point at normal atmospheric pressure. Then Reid in 1976 [Reid, 1979], defined BLEVEs as the sudden loss of containment of a liquid that is at a superheated temperature for atmospheric conditions. More recently, on the basis of some observations which highlight that there is no practical reason why fragments or superheat limits need to be mentioned in the definition, some authors proposed less restrictive definitions. In particular, Birk and Cunningham in 1994 have defined BLEVEs as the explosive release of expanding vapour and boiling liquid when a container, holding a pressure-liquefied gas, fails catastrophically. Catastrophic failure was defined as the sudden opening of a tank/container to release its contents nearly instantaneously. [Birk & Cunningham, 1994; Eckhoff, 2014]

In the present work the latter definition of BLEVEs will be used. The TNO definition is also reported: BLEVE is an explosion resulting from the sudden failure of a vessel containing a liquid at a temperature significantly above its boiling point at normal atmospheric pressure, e.g. pressure liquefied gases. The fluid in the vessel is usually a combination of liquid and vapour. Before rupture, the liquid contained is more or less in equilibrium with the saturated vapour. If the vessel ruptures, vapour is vented and the pressure in the liquid drops sharply. Upon loss of equilibrium, liquid flashes at the liquid-vapour interface, the liquid-container-wall interface, and, depending on temperature, throughout the liquid. [TNO Yellow Book, 2010]

Usually two types of BLEVE are defined: “fired” BLEVE and “unfired” or “cold” BLEVE. [Paltrinieri et al. 2009] The first one is thermally induced by an external fire, thus it usually follows the tank collapse due to fire engulfment. If the ignition of the vapour is immediate, and very often it is because the external fire, a fireball occurs. The “cold” BLEVE is not thermally induced, it may be caused by a violent impact on the tank during a traffic accident or by the tank sudden failure due to material defect or to overfilling. [Prugh, 1991] In a cold BLEVE there is no certain ignition so the fireball may not be present, surely it is easy that in a road/rail environment there is enough energy and sources to ignite the flammable cloud. If the ignition is delayed the cloud will cause a flash fire rather than a fireball. [TNO Yellow Book, 2005]

The primary causes of a “cold” BLEVE are wholly incidental, as this type of BLEVE, of course happens only if the severity of the accident is enough for the tank strength, but it cannot be delayed or avoided at the time of accident. The focus in this work is on “fired” BLEVE, which can be avoided, or at least delayed, through the installation of an adequate fireproofing system in combination with appropriate designed pressure relief valves (see the detailed analysis in Section 2.3). Moreover in a statistic on several transport accidents reported by Paltrinieri et al. more than 85% of BLEVEs recorded are thermally induced. [Paltrinieri et al. 2009]

2.3.2 Fireball definitions

As seen above, when a BLEVE occurs a given amount of flammable vapour is suddenly released into the atmosphere. A fraction of liquid droplets can deposit on the ground (rain-out fraction) and form a flammable pool, while another part is entrained by the vapour causing an aerosol cloud. If the cloud is immediately ignited it turns out in a phenomenon called fireball. A fireball is defined as a fire, burning sufficiently rapidly for the burning mass to rise into the air as a cloud or ball. [TNO Yellow Book, 2005] The ignition must be immediate for the fireball to occur, if the mass of flammable vapour mixes sufficiently with air, the delayed ignition will give rise to a flash fire rather than a fireball. Since the mixing with air is limited, the flame is only on the external surface of the volume of the released gas, thus it can be considered a diffusion flame.

While the external surface burns, the internal fuel droplets act as fuel reservoir. In fact they progressively vaporize, mix with air and burn. The resulting fireball is a transient phenomenon the duration of which lasts up to a minute. The fireball passes through three phases [Lees, 1996] :

- growth → growth to half diameter upon final diameter
- steady burning → roughly spherical
- burnout → size held steady

The growth phase may be divide into two intervals, each lasting about 1 second. In the first interval the flame is bright and the flame temperature is about 1300°C, the smaller droplets of fuel vaporize and the fireball grows to about half its final diameter. In the second interval of the growth phase, the fireball grows to its final volume, the surface starts to be dark and sooty and the flame temperature decreases by approximately 200°C. In the second phase, which lasts some 10 seconds, the fireball, which is now roughly spherical, is no longer growing. At the start of this phase, it begins to lift off. It rises and changes to the familiar mushroom shape. The estimated effective flame temperature is 1100-1200°C as in the second interval of the growth phase. In the third phase, which lasts some 5 seconds, the fireball remains of the same size, but the flame becomes less sooty and more translucent. [TNO Yellow Book, 2005] Once there is no more fuel the fire extinguish itself. The radius of the fireball can be calculated from the

quantity of combusting material. It was found that peak emissions came from areas at the top of the expanding fireball whereas the emission was lower from lower portions of the fireball because of increased soot shielding and poorer mixing with ambient air. [TNO Yellow Book, 2005]

2.3.3 Analysis of cascading scenarios in the transportation of LPG

As mentioned before, the most dangerous scenario that may follows an accidental leakage of LPG is the BLEVE with consequent fireball.

The typical mechanism which leads to the fired BLEVE can be considered as a domino effect or "cascading event" [TNO Yellow Book, 2005], consisting in the following steps:

- occurrence of primary event → a road or rail accident occurs with development of fire
- propagation of the event → the fire extends to LPG tankers
- starting of BLEVE mechanism → temperature of the tank walls increases, thus pressure increases by LPG evaporation
- tank catastrophic rupture due to increased pressure and thermal weakening of materials → BLEVE with blast wave and possible debris thrown away
- rapid ignition of flammable aerosol → fireball with high radiation heat flux

When a road or rail accident happens, it is likely that a fire develops from the ignition of the fuel that leaks from the vehicle. The ignition sources in these situations can be many, e.g. the metal sheets of the vehicle involved in the crush easily generate sparks. Moreover there are several flammable materials in vehicles that may go to feed the flames. If one or more, as is easily in rail transportation, LPG tanks are involved in the accident, directly or indirectly, the flames may extend up to them.

From this moment on, the situation becomes much more critical. The heat is transferred from the fire to the tank outer surface by convection and thermal radiation. If the fire is large or if the tank is sufficiently distant from the flame radiation will dominate, otherwise also convection must be taken into account. [Landucci et al. 2013] The heat is transferred by conduction through all layers of tank: through external jacket and insulation blanket (if present) and through the tank shell.

The heat is now received by the internal load by convection and radiation. The liquid-side tank wall usually has high heat transfer coefficients, particularly if the liquid is boiling, resulting in a cooling effect. On the contrary, the vapour-side tank wall has a less efficient heat exchange due to low heat transfer coefficients, with consequent wall temperature increase. The latter weakens the tank materials which are, moreover, subjected to the differential dilation in correspondence of liquid-vapour interface. At this stage, LPG starts boiling and inner pressure of tank increases; one must recall that the LPG is a liquefied pressure gas, thus in saturated condition in vapour-liquid equilibrium. Although the tank is constructed to withstand the internal pressure that is generated, the combination with the weakening of materials can lead to the catastrophic failure with instantaneous release of the contents. The time between the start of the fire and the tank rupture is defined as time to failure (ttf). [Landucci, 2008] The energy released in the physical explosion following the rupture of the vessel, is the work of expansion of the LPG from the burst pressure to atmospheric. The burst pressure depend from the situation in which the tank fails, in case of external fire the pressure at failure is estimated as the 21% more of the opening pressure of safety valves. [TNO Yellow Book, 2005] Part of the released energy is spent for the projection of fragments and the rest for the formation of pressure wave. Primary fragments have high kinetic energy and

are projected at distance, they impact what is surrounding causing damages and secondary fragment. The explosion overpressure affects buildings, vehicles and humans nearby. The damage to humans are due to the action of shock wave on the sensitive organs, i.e. lungs and tympanic membrane, and to the impact of debris fragments and collapsed buildings. The ignition of the cloud generates a heat flux, which affects a large area around the accident. For instance, an LPG fireball generated from 10 tonn of substance, after 5 second from the ignition has a radiative heat flux with a lethality zone of about 80 meters diameter and it causes irreversible injuries up to 100 meters, at ground level. [TNO Yellow Book, 2005]

It is clear that if a road or rail accident may be confined in its close proximity, an accident that involves one or more LPG tanks may afflict people and buildings relatively distant. Taking into account the mechanism described above, it is evident that the catastrophic rupture of the tank can be avoided by controlling the load temperature, thus the wall temperature. When it is possible and only after the safety enhancement for workers, the temperature increase is controlled by fire fighters spaying water on the wall of the tank until the external fire is extinguished.

2.4 Safety devices adopted for the protection of the tank

BLEVEs caused by fire can be avoided or at least delayed providing tank with adequate thermal protections. [Paltrinieri et al., 2009] Thermal protections consist of an insulating coating layer and a pressure relief valve (PRV). The insulating coating is aimed at reduce the heat flux reaches by tank shell walls, so as avoid the thermal weakening of material. PRVs are aimed at preventing the pressure build up during fire exposure by venting the overpressure. The benefits of safety device coupled with thermal insulation on LPG tank will be developed in this section.

2.4.1 Passive fire protection systems

A generic passive protection is defined by CCPS as a barrier which does not require any external activation to perform the safety function. [CCPS, 2010]

Passive fire protection (PFP) systems consist in coating, cladding or free-standing system which, in the event of fire, will provide thermal protection to restrict the rate at which heat is transmitted to the object or area being protected. [EN ISO 13702, 1999]

Firewall are thermal shields placed between the targets and the potential fire sources, which are able to absorb the thermal radiation ensuring the survivability of the target. Clearly enough they are only applied in fixed installations. [Landucci, 2008]

PFP through PFP coatings can be suitable for transport vessels, since they are directly applied on the tank shell.

The PFP systems are differentiated according to the materials they are made of, whether organic or inorganic. Inorganic-based materials are typically vermiculite sprays or cement boards that are inert to flame impingement and keep the initial structure with good thermal resistance. They are not able to adapt their configuration to the fire aggression so they may become brittle after fire exposure. Due to high thickness applied and consequent weight, they are mostly only suitable for fixed installations. [Landucci et al. 2009] The cementitious products protect the tank by evaporation of the moisture trapped within the material, keeping the underlying steel temperature around 100°C. [Zuccaro, 2012] The heat input is also reduce by the concrete high mass and low thermal conductivity. The weight of concrete can be lightened by aggregation with lightweight

products, as vermiculite. In this case due to the lower mass and in order to obtain the appropriate water content, structural steel shell are typically covered with a very thick coating layer. [Landucci et al. 2009] Another type of inorganic materials used as fireproofing are the thermal insulation systems, such as mineral wool and cellular glass. Both are lightweight, dimensionally stable, essentially impermeable to moisture, and they are non-combustible. [Zuccaro, 2012] The density of these materials is one order of magnitude lower than other products and these property makes it a convenient solution even if it needs higher thickness to perform adequate protection. Thus, different layers of material are applied on equipment to protect and than stainless steel jacketing is employed to obtain fire resistance. [Landucci et al. 2009] The latter type of fireproofing materials are particularly suitable for the application on tanks for the transport of hazardous goods.

Organic-based materials present better mechanical properties and they may be more adequate to obtain light structures, like portable tanks of dangerous goods. [Landucci et al. 2009] Intumescent coatings are the organic-based material normally used in hydrocarbon-processing complexes, generally they are epoxy based, spray or hand applied. When exposed to sufficient heat, intumescent coating expands to form a thick, insulating carbonaceous char. The reduction of the heat load to the steel substrate relies on the thermal insulating capability of the char and the ability of the char to remain adherent and physically intact. [Zuccaro, 2012] The application of several layers of material is necessary to assure a sufficient duration of the fire protection, since the material tends to be slowly burned by the flames. [Landucci et al. 2009] One main problem with intumescent coatings is related to corrosion of steel substrate that has been sometimes reported beneath apparently intact coating. Moreover, intumescent products and in general organic-based materials may degrade with prolonged outdoor weathering and exposure to slightly elevated temperatures. [Zuccaro, 2012] This does not render organic-based materials optimal for protection of tanks for the transport of goods.

2.4.2 Pressure relief valves

As mentioned before, pressure relief valves are also common tool in the passive fire protection, they don't reduce the heat flux entering the system, but reduce the pressure ejecting mass from the process. [Crowl & Tipler, 2013] The pressure relieving devices are designed to open during emergency or abnormal conditions to prevent rise of internal fluid pressure in excess of a specified design value. [CCPS, 1998]

A pressure relief valve has the task to vent off excess pressure enough quickly and re-close for preventing the further flow of fluid after normal conditions have been restored. The required relieving area of the safety valve depends on scenario and this aspect is the basis for the selection of the type and size of device. The standard regulations API 520 [API 520, 2014] is a design manual widely used for sizing of relief valves on both liquid and gas filled vessels and the standard API 527 [API 527, 2014] gives permissible leakage rate of valves and testing procedure.

During the relief the fluid may be in liquid, liquid-vapour mixture, gas or supercritical phase. Thus, the safety system must be able to handle various process condition.

Pressure relief valves have spring-loaded disks that close a main orifice against a pressure source. As pressure rises, the disk begins to rise off the orifice and a small amount of fluid passes through the valve. Continued rise in pressure above the opening pressure causes the disk to open the orifice in a proportional fashion. The safety valve

is similar to the relief valve except it is designed to open fully, or pop, with only a small amount of pressure over the rated limit. Conventional safety valves are sensitive to downstream pressure and may have unsatisfactory operating characteristics in variable back pressure applications. The balanced safety relief valve is available and minimizes the effect of downstream pressure on performance. [ASM, 2015]

2.4.3 Safety requirements for the effective fire protection of LPG tankers

Focusing on LPG transportation, if a severe accident occurs the emergency teams should have the time for the intervention, since, in the fired-domino described in previously section, the tank failure due to the propagation of fire is delayed respect to primary event, i.e. the external fire. The problem is the tank resistance, which in the case of absent protection may withstand fire conditions for a limited period (5-30 minutes). This lapse of time is usually not sufficient to avoid the safe suppression of the fire due to fire brigade intervention. A realistic evaluation of the time required for effective mitigation by the fire brigades, based on actual data available from past accidents in the Netherlands, evidenced that a time lapse of 75 minutes is required to allow an effective protection or prevention of BLEVE by active measures upon the arrival of the fire brigades. [Molag & Kruithof, 2005] Therefore the comparison between the ttf of tank and the time for arrival of rescuers shows that the intervention time is not sufficient for avoid the rupture unless the tank resistance has been enhanced. Thermal insulation around the tank can reduce the excessive heating of the steel wall and PRV can reduce the internal pressure. These coupled actions extend the time to BLEVE and can avoid the failure of the tank. [Landucci et al, 2009]

In North America specific transport regulation [CFR, 2015; CGSB, 1997] have been adopted, requiring road and rail tankers carrying flammable liquefied gases to be equipped with pressure relief valves. In addition, rail tankers have to be also thermally insulated. The Canadian General Standards Board requires that the thermal insulation system must be able to avoid the rupture of the tank for 100 minutes in an engulfing pool fire, or 30 minutes in an engulfing torching fire. One common system includes a 13 mm blanket of high-temperature ceramic fibre thermal insulation covered with 3 mm steel jacket. [Birk & Cunningham, 1994] This insulation system is the one used in the model development later in this work.

Even if the double action of thermal insulation and PRV seems to be the answer of safety issues related to transportation of LPG, it may be insufficient to avoid the vessel catastrophic rupture. Indeed, the fireproofing system is not ideal and it may degrade during its lifetime. The PFP effectiveness can be influenced by damages or defects which lead to a double negative effects: the thermal weakening of the constriction material, due to the temperature increase, and strong local thermal dilatation. In fact, the shell wall in contact with the liquid undergoes a cooler effect while the shell wall in contact with vapour does not. If a defect in the thermal insulation system is present, the difference of the vapour and liquid temperatures is very strong, the vapour-side wall thermal dilation will be much higher than the liquid-side wall one, these phenomenon at the interface leads to the increase of the mechanical stress distribution in the defective part.

Characterization of thermal insulation defects is the central purpose of this work and it will be deeply analysed in Section 3.

2.5 Discussion and conclusions

In the present Chapter Past accident data analysis, which results are reported in Section 2.2.3, showed that the percentage of classes of substances involved in severe accidents are in line with the percentage of hazardous materials transported by road and rail. It was estimated that over 50% of hazardous materials transported (both by rail and road) are liquids, while gases (compressed, liquefied) occupy around 10%. [Paltrinieri et al., 2009] In fact, flammable and toxic liquid is the class of substances more involved in severe accidents both in road and rail transportation. This is due to the global quantities of hazardous materials transported, as said, but also due to the lower thickness of the shell of the tank used for transportation at ambient pressure, as in the case of liquids, than the tanks used for liquefied gases, which have to resist a higher pressure. If an accident occurs, the tank with the thicker shell is more likely to resists.

The results of accidents involving LPG highlight that the problem related to the transportation of such hazardous substance is relevant to public safety. The external fire is the cause of the 40% for road and 26% for rail transportation accidents, approximately half party of which led to fired BLEVE in the road transportation, while in the rail transportation BLEVE occurs in 22% of accidents. The percentage of accidents in which LPG does not ignite after leakage is 18% in road transportation and 13% in rail transportation, this means that in the remaining 82% and 87%, respectively road and rail, of accidents there is development of a fire. These results highlight that the safety issues related to the hazmat transportation is relevant for public safety in order to avoid severe consequences from transportation accidents and prevent Viareggio-like accidents. In the Viareggio accident only a series of random events avoid the BLEVE occurrence and the propagation of fire to other LPG tankers. The LPG leak found many obstacles through the expansion area, such as wall of the station, car and tree. This type of confinement could have caused an overpressure in case of ignition. When such overpressure occurs, the event is a vapour cloud explosion (VCE) rather than a flash fire. [TNO Yellow Book, 2005]

Finally, even if other worst-case scenarios have been avoided, the flash fire resulted in 31 fatalities and in extended damages to residential buildings around the railway line. The need of specific regulations which concern the possible implementation of safety devices is now evident. As mentioned before, the European framework, the installation of thermal insulation system on transportation tankers is still not approved because of defects and degradation in which these systems undergo. Since the coating systems are not ideal, they have to be well characterised in terms of protection performance, in particular if defects are present. Assessing the acceptability levels for the coating defects, in order to avoid vessels failure when exposed to fire, is of utmost importance for the wider implementation of coatings as relevant safety measure.

3 Characterisation of defective coatings for fire protection

As mentioned in the previously section, a coating defect is not always able to cause the fired tank failure. Both size and features of the defect can influence the heat conduction into the steel-wall and limit the temperature growth. [Landucci et al. 2011b] Therefore, it is crucial to understand what kind of defect can be considered dangerous and determine a critical defect size that leads to the tank failure. The characterization of defects is of underlying importance to achieve this aim and to assess the thermal response of defective coatings.

The first step for characterisation is to analyse the nature of this defects. It was assess that defects in coating system can be accidental or intrinsic. [Birk & A.M. Birk Engineering, 1999] The accidental defects may be caused by material matters, such as erosion and degradation, or by external event such as human damages, creeping on the terrain, the incidental crash with other tank-car or hurdles. [Landucci et al. 2011b] On the other hand, intrinsic defects are related to the discontinuities that exist in a normal tank-car, such as the manway nozzle, jacket spacers and body boisters. [Birk & A.M. Birk Engineering, 1999]

3.1 Insulation discontinuities

Discontinuities are direct metal conduction paths that are present due to tank design features. The effect of heat flow through discontinuities might lead to local "hot spots" at these locations particularly if the discontinuity were in the vapour space region of the tank, and could be of concern with commodities where a chemical reaction may be initiated if they are raised to a certain temperature. [Birk & A.M. Birk Engineering, 1999] Discontinuities and associated heat transfer coefficient (U coefficient) values were suggested by Johnson. [Johnson, 1998] Those data are shown in table 3.1. Birk suggested to consider these U values based only on thermal conductivities of the tank wall materials. [Birk & A.M. Birk Engineering, 1999]

Table 3.1 - Summary of Insulation Discontinuity U values, from [Johnson, 1995]

Location	**U (W/k)**
manway nozzle and cover	2.4
siphon and air vent nozzle	1.0
safety relief valve nozzle	0.52
jacket spacers	2.5
bottom outlet saddle	2.1
draft sills	11.9
body bolsters	10.6
brake cylinder support	0.75
brake lever support	0.52
Total U for discontinuities (sum of individual U's)	**32.3**
Total U for thermally insulated tank (assuming conductance of 0.426 W/m2 K)	**74.3**
Total U for thermally protected tank (assuming conductance of 22.7 W/m2 K)	**3960**

The table shows that the discontinuities are not very significant for a thermally protected tank with a 13 mm insulation. Indeed, the insulation discontinuities increase overall U by 1%. [Birk & A.M. Birk Engineering, 1999] For these reason, the discontinuities of insulation system will be ignored during this thesis work.

However discontinuities are significant for thermally protected tank, i.e. a tank car with just the steel jacket and no thermal insulation in the gap. The tank may be protected by the steel jacket which behaves like thermal radiation shield and this reduce the heat flow by about half. [Birk, 1983] The overall U coefficient, in this case, is increased by 43% by the insulation discontinuities. This result is somewhat misleading because the 43% increase represents a small overall increase in heat transfer when compared to what a large insulation defect would produce. For instance 1 m^2 of defect can be more important than all the discontinuities. [Birk & A.M. Birk Engineering, 1999]

3.2 Insulation defects

As mentioned before, the defects in thermal insulation system are due material degradation or due accidental damages. In case of silica blankets, the insulating layers can also slip out by the position resulting in a long flatted defect. [VanderSteen & Birk, 2003] This insulation defects usually leave a large percentage of the tank surface uncovered [Birk & Cunningham, 2000] and thus, in case of exposure to fire, a large percentage of heat can reach the internal shell wall and the lading, may leading to the tank failure. The available data on the characterization of defective coatings are reported in this section.

As argued in the previously sections, the implementation of computer models is of underlying importance to test the thermal response of a wide range of conditions, such as testing different vessel materials, fire exposures, geometries of defect and so on. To show the reliability of this models, comparison with experimental data is required. Nevertheless, real-scale experiments on filled tank-car expose to fire are lacking for coated (undamaged or defective) tanks, as well as for unprotected tanks. The only available trial of this kind dates back to 1974, it was carried out on two rail-tanks, each with a total capacity of 128000 litres and filled with 96% of propane. One of the rail-tanks was coated. [Anderson & Townsend, 1974] From there onwards only smaller scale experiments were carried out on filled tanks. On the other hand, it is worth to mention that reproducing a real-scale experiment, is almost prohibitive under the economical point of view as well as for safety and environmental concerns.

For what concerns experiments on tanks with defective insulation system, only two bonfire trials were performed. One of which was carried out on a filled tank [Birk et al. 2006], while the other tested the defects on a portion of tank shell [VanderSteen & Birk, 2003]. The tests carried out in this trials are reported in this section, as the only available experimental data for the validation of models presented in this thesis work. More experiments would be needed in this experimentation area, in order to better understand the thermal response of different defect geometries and thus, for the development of enhanced computer models.

3.2.1 Real-scale defects geometries identified by thermographic inspection of tank-car

An inspection technique was developed by Birk and Cunningham in 1999 [Birk & Cunningham, 2000] to find thermal insulation deficiencies on rail tank-cars. This method uses a thermal imager to find insulation gaps under the tank steel jacket. The method relies on a small temperature difference existing between the tank lading and the surroundings. Solar heating can also assist in generating thermal gradients that the thermal imager can identify. The effectiveness of using a thermal imager for detecting insulation deficiencies was validated against simulated tank-car tests carried out in the laboratory. After validation, field tests were conducted on real rail tanks with the aims to identify which have insulation deficiencies. The field study consisted of several field trips to industries and railway yards to image uninsulated and insulated tank-car and stationary tank. [Birk & Cunningham, 2000] The results of the field test shown that the thermography is an effective technique for inspecting insulated tank cars and that several tank-cars have deficiencies on their thermal insulation system, as shows in figure 3.1.

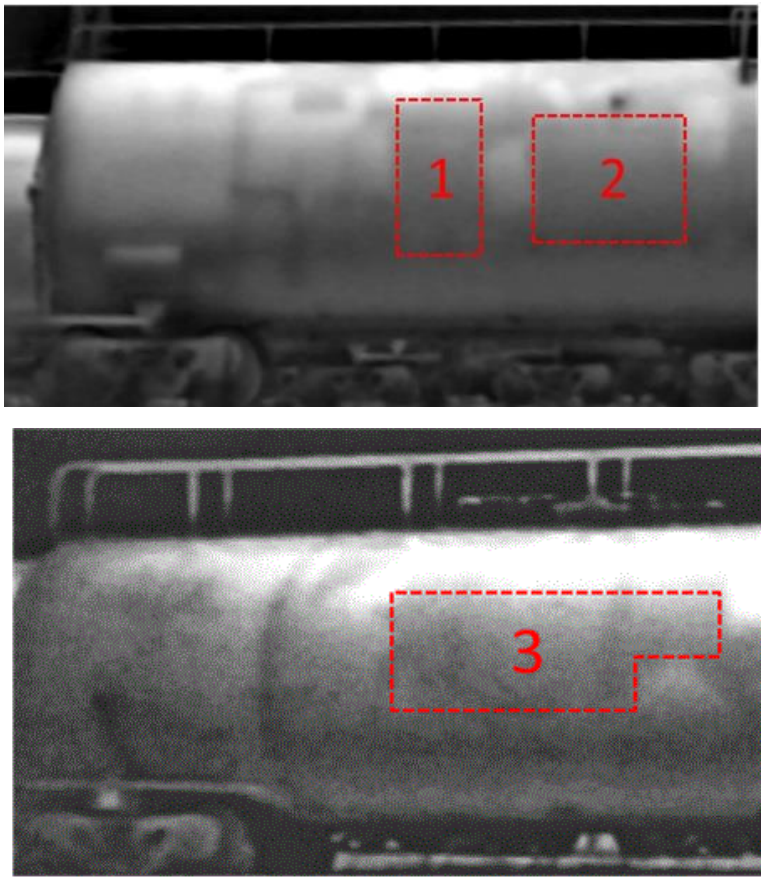

Figure 3.1 – Two different tank-cars, each with underlined insulation deficiencies [Birk & Cunningham, 2000]

The parts of the tank that the thermographic images identified as lighter are those in which the insulating material is intact, while in the darker parts the insulation is defective. This shows that the coating defects on rail-tank currently in use are not rare and are not negligible.

Three different geometries can be identified on the two different rail-tanks. Defect 1 and 2 have a rectangular geometry with a different value of aspect ratio. This is defined as the ratio between the longest edge and the shortest one and represents how much the defect geometry is close to a square, whose aspect ratio is 1. Defect 3 is L-shaped due to the formation of two rectangular defects, which are adjacent forming a single defect. [Scarponi et al. 2016] Aspect ratio and areas of the defects are reported in table 3.2.

Table 3.2 - Geometries of real-defects individuated by Birk and Cunningham in 1999 [Scarponi et al. 2016]

	Aspect ratio	**Area (m2)**
Defect 1	0.45	1.68
Defect 2	0.93	2.51
Defect 3	-	3.86

The geometries of defect 1 and 2 are investigated in the case studies implemented with the RADMOD code. They are analysed and their influence on the thermal response is discussed in Section 7.

3.3 Thermal protection deficiency fire tests on a quarter section tank-car – FEM validation data

Fire test data is provided that will be useful in developing a guideline to assess different thermal protection deficiencies. Thus, a total of 12 thermal protection deficiency fire tests were conducted in 2003 by Department of Mechanical Engineering of Queen's University, Canada. [VanderSteen & Birk, 2003] Identical fire conditions were used and only the thermal protection defect was changed.

Five different-sized square thermal protection defects were studied. These data are used in the present work for the finite volume model validation.

3.3.1 Tests conditions

Apparatus

The apparatus consisted of a 2.1 m long quarter section of a tank-car. The primary wall is tank-car steel and has a thickness of 16 mm and a radius of curvature of approximately 1.5 m. The outer steel jacket is plain carbon steel and has a thickness of 3 mm. Both the shell and the jacket were painted flat black in order to ensure high emissivity. This was measured to be around 0.9 - 0.95. Therefore, this value was also considered in the FEM model validation in this thesis work. Holes were drilled through the tank wall to allow either the addition of 13 mm spaces or for clamping the steel jacket against the tank wall. Most tests required the 13 mm spaces to keep the jacket from crushing the 13 mm thick insulation. If the test required crusher insulation, however, the spaces were removed and the jacket was bolted to the tank wall.

According to the standard, the pool-fire environment must have a fire temperature of 871 $\pm$ 56 °C [CGSB, 2002]. To achieve this aim, and other conditions to represent a credible pool fire, an array of nine propane utility burners was used to uniformly heat the tank wall. These burners are nominally rated at 586 kW when the propane is supplied at 240 kPa, but the propane pressure was regulated down to approximately 10 kPa, for the reasons above.

An imagine of the apparatus can be seen in figure 3.2.

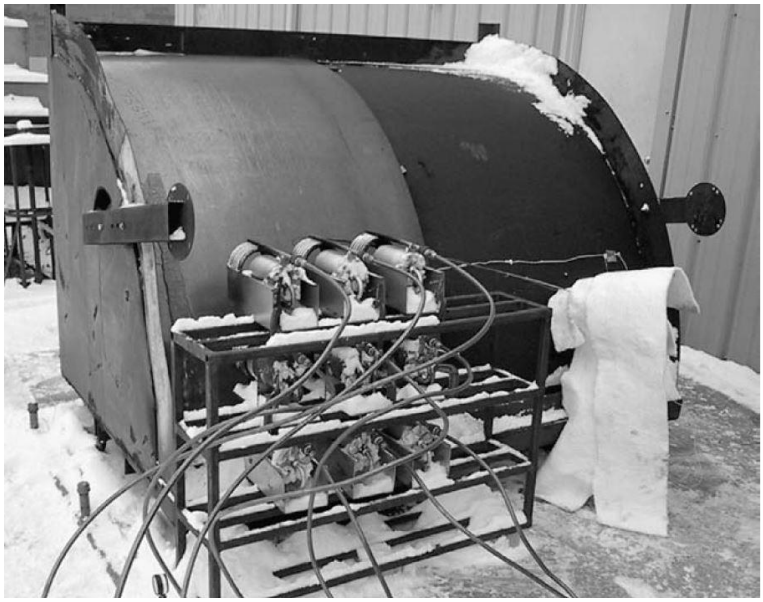

Figure 3.2 – Front view of test apparatus, showing the outer steel jacket (no insulation) [VanderSteen & Birk, 2003]

Insulation system

The type and thickness of the thermal insulation used in this testing was the same as that found on actual tank-car. The thermally protected configuration consisted of 13 mm of ceramic insulation placed on top of the tank wall and covered with a 3 mm out steel shell. As mentioned before, the spacing was maintained using spacers bolted to the tank wall. Specifications of the insulation are given in the table 3.3.

Table 3.3 – Properties of insulation used in the trial [VanderSteen & Birk, 2003]

Specification	**Property**	
Material	Ceramic fibre blanket	
Vendors	Fiberfrax - Unifrax	
Thickness (mm)	13	
Density at new condition (kg/m^3)	72	
Thermal conductivity, *k* at new condition	Temperature (°C)	*k* (W/m K)
	200	0.06
	400	0.11
	600	0.18
	800	0.28

Instrumentation

The test instrumentation consisted of a a wall thermocouple, an infrared (IR) thermal imager, an infrared thermometer gun and two fire thermocouples. Still photography were also used to collect data from the testing. A digital camera was used in each fire test to record the shape of the flame from several different locations.

The wall thermocouple and the IR thermal imager were used for the measurement of the inner wall temperature. Whereas the flame temperature and the black body temperature of the fire were measured through the IR thermometer gun and the fire

thermocouples. The black body temperature determines the thermal radiation emitted by the fire. The wall thermocouple was mounted on the black unheated surface of the tank wall in the centre of the region where the defects were positioned.

3.3.2 Tests results

In tests with square defects cut out of the insulation, the thermal image data was very useful in study the temperature rise with time, and also the temperature gradients across the defect. [VanderSteen & Birk, 2003]

The imagines of the fire engulfment can be seen in figure 3.3.

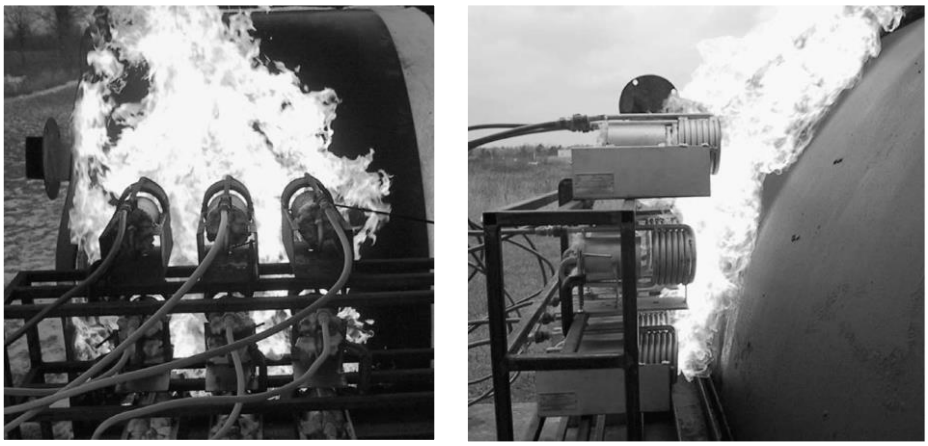

Figure 3.3 – Front (sx) and side (dx) views of fire engulfment [VanderSteen & Birk, 2003]

Table 3.4 summarizes the validation data used for the validation of the FEM model, the cells marked represent an available data set. Further details on the experimental results obtained are reported elsewhere. [VanderSteen & Birk, 2003] The FEM validation will be discussed in the Section 8.1.

Table 3.4 - Summary of the validation data adopted for the FEM validation presented in this thesis work. The cell marked with an "X" represent an available data set [Scarponi et al. 2016]

Type of configuration	**Defect size (cm)**	**Ambient temperature (°C) as initial condition**	**Transient temperature in the defect**	**Temperature profile in the defect at different time**			
				5 min	**10 min**	**15 min**	**20 min**
Fully protected	0 [a]	-9	X				
Steel jacket only	- [b]	-13	X				
Squared defect	15.2	-10	X	X	X	X	X
Squared defect	24.4	0	X	X	X	X	X
Squared defect	40.6	0	X	X	X	X	X
Squared defect	61.0	0	X	X	X	X	X

[a] The insulation is undamaged

[b] The insulation was removed from the space between vessel wall and steel jacket

An example of the thermal imager data obtained in the fire tests are reported in figure 3.4. The figure shows the temperature distribution on the inner wall of the tank. In particular, the temperature profile along a horizontal line passing through the center of the defect are show for different defect sizes. The distance from the center of the defect is normalized on the semi-length of the defect edge (d/2). These data were measured after 20 minutes from the beginning of the test. It is important to note that for the larger defects, the temperatures at the center of the defect are almost the same, regardless the defect size.

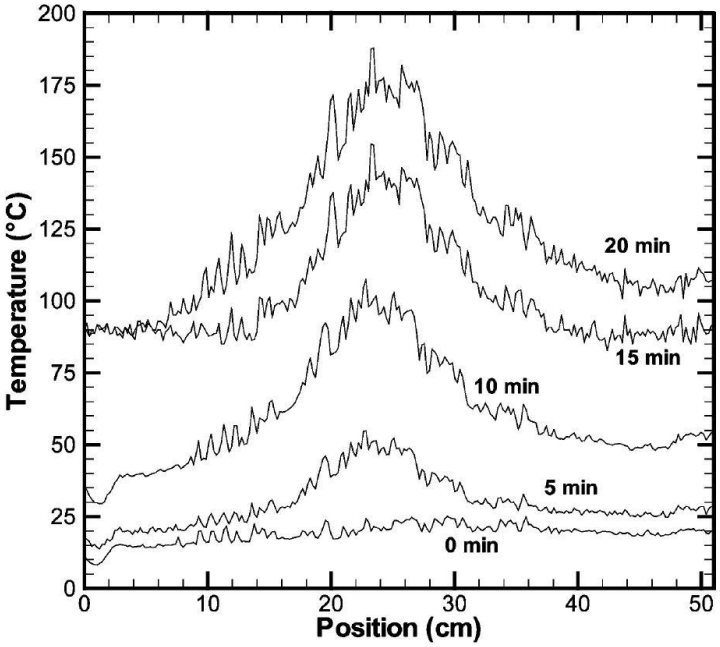

Figure 3.4 – Temperature profile across defect at various times during one of the tests (test 4) [VanderSteen & Birk, 2003]

3.4 Fired tests on propane pressure vessels with defective coating – RADMOD validation data

In order to generate fire test data on a propane-filled pressure vessel with defect in its thermal protection system, six instrumented small-scale tanks (1.9 m^3) were exposed to controlled fire in 2004. [Birk et al. 2006]

Two of the tanks were unprotected and they were used for comparison with the full-scale unprotected test of the propane-filled rail tank-car, named RAX 201, conducted in 1974 by Townsend et al. [Anderson & Towsennsend, 1974] The remaining four tests considered defects covering 8% and 15% of the tank surface area. One of those were aborted due to burner system problem, the other three are used for the validation of lumped sub-model for defective thermal protection system presented in this work.

3.4.1 Tests conditions

Apparatus

In the tests series, the tanks were ASME code 1890 litres, which were used as approximate 1/3rd scale models, based on diameter, for 125 m3 112J type rail-tank-cars, RAX 201. The tanks were horizontal steel cylinders, their design gauge pressure at 46°C was 1.72 MPa. The white tanks were painted black in the region of the defect to ensure a high emissivity.

The tanks specifications are given in the table 3.5.

Table 3.5 – Tank properties and geometry used in the trial [Birk et al. 2006]

Specification	Property
Capacity (l)	1890
Length (m)	3.07 end to end
Diameter (m)	0.953
Minimum wall thickness – shell (mm)	7.4
Minimum wall thickness – head (mm)	5.3
Material – shell	SA-455 ASME Steel
Material – head	SA-414 gr.C ASME Steel
Design pressure at 46°C (MPa)	1.72
Calculated burst pressure at 46°C (MPa)	7.1

To ensure proper scaling against RAX 201, and controllable test condition the mechanical PRV was replaced with computer controlled valve and its set pressure was increased, moreover the engulfing fire was replaced with 25% partially engulfing generated through an array of liquid propane burners. The 25% fire engulfment gives vapour space peak wall temperatures similar to 100% engulfment. However the tank will pressurized and empty through PRV about four times slower. It has been estimated that the 25% engulfed tanks should fail a little later, order of 1 minute later, than if were 100%. [Birk et al. 2006]

The fire was designed to represent a full-scale pool fire with an effective blackbody temperature in the range of 815-927°C. This temperature is specified for fire testing of tank-car protection systems in North America. [CGSB, 2002] To respect this and other conditions, in order to represent a credible pool fire, a 5 x 5 array of liquid propane torches and a liquid propane evaporator, were designed and used in the trial. The propane was supplied to the evaporator at approximately 205 kPa.

A sketch of the burners position with respect to the tank is shows in figure 3.5.

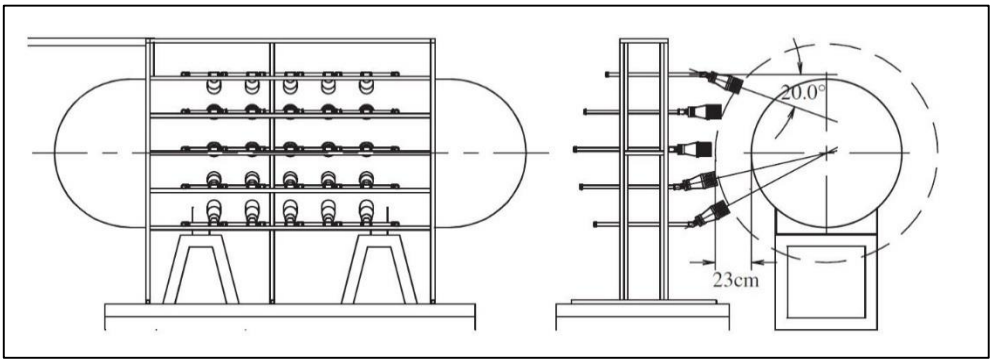

Figure 3.5 – Burner array configuration over the tank [Birk et al. 2006]

Insulation system

In the insulated tests, the tanks were covered with ceramic blanket insulation. This insulation was covered with 3 mm carbon-steel jacket in the flame impingement zone. Specifications of the insulation are given in the table 3.6.

Table 3.6 – Properties of insulation used in the trial [Birk et al. 2006]

Specification	**Property**	
Material	Ceramic fibre blanket	
Vendors	Unifrax	
Width (m)	1.2	
Thickness (mm)	13	
Density at new condition (kg/m^3)	72	
Thermal conductivity, *k* at new condition	Temperature (°C)	*k* (W/m K)
	-20	0.03
	100	0.05
	300	0.09
	500	0.15
	650	0.20
	800	0.30

The thermal conductivity is a function of temperature and the different values of the conductivity will be use in the RADMOD code depending on the temperature of the wall which is in contact with the insulation. More specifically the liquid wetted wall temperature is expected to be within the first couple range, the protected vapour space wall temperature in the second range (300-500°C) and the jacket temperature in engulfing fire is expected to be in the last couple of values (650-800°C).

Figure 3.6 shows the location and size of of both large and small insulation defects, 15% and 8% respectively, and the protective steel jacket used.

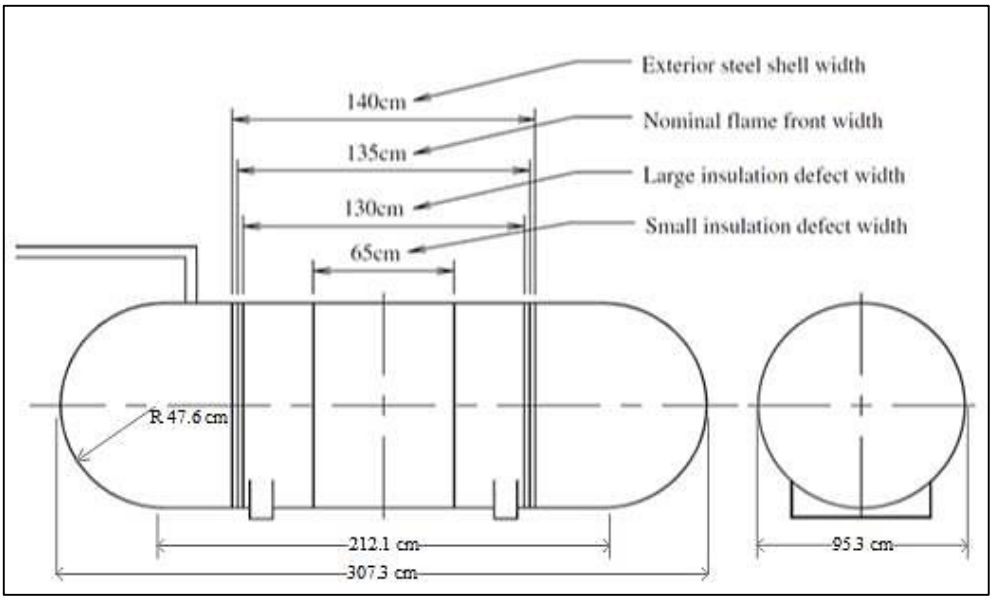

Figure 3.6 – Standard ASME 18901 test tank and nominal flame width and location relative to tank insulation defects and steel jacket [Birk et al. 2006]

Instrumentation

Each test tank was instrumented with 48 sheathed lading thermocouples, one static pressure transducer, and from 11 to 17 wall thermocouples. The lading thermocouples were contained in five vertical bundles with each bundle containing a full range of thermocouple lengths, each of which represents a specific fill level, figure 3.7 shows the lading thermocouples location. The wall thermocouples were welded directly to the wall and they were typically located as show in figure 3.8.

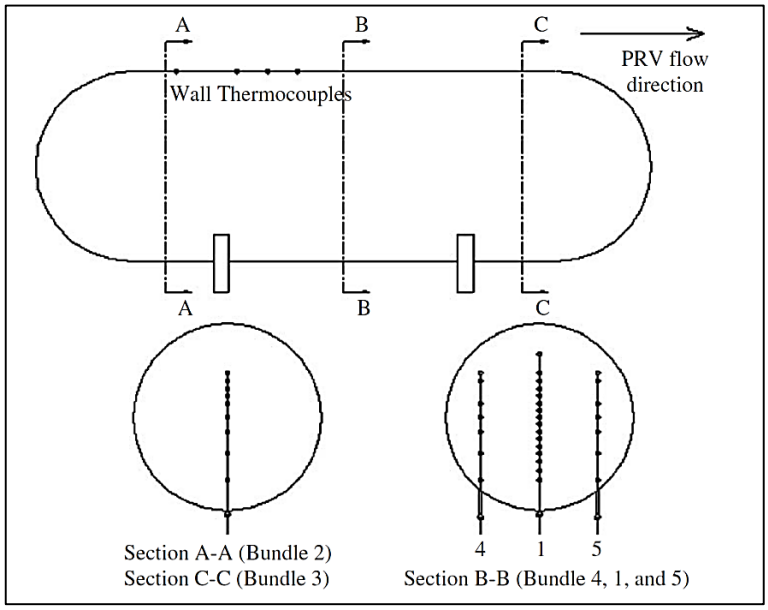

Figure 3.7 – Lading thermocouple location [Birk et al. 2006]

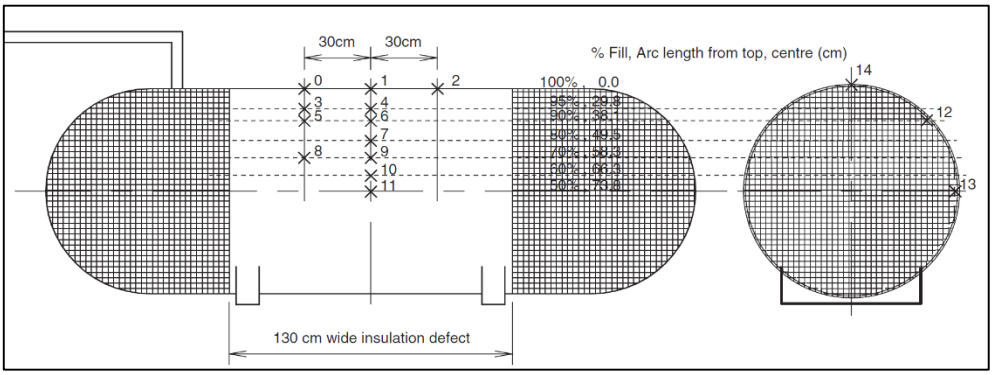

Figure 3.8 – Wall thermocouple layout for one of the tests (test 04-03) [Birk et al. 2006]

3.4.2 Tests results

An imagine of the fire engulfment can be seen in figure 3.9.

Figure 3.9 – Burner array and evaporator set-up [Birk et al. 2006]

Large thermal defect, test 04-03

The tank for 04-03 had 15% insulation area defect, it was filled and purged with 1300 l of propane, about 71% fill by volume. The PRV was set to pop at 2.63 MPa and close at 2.39 MPa. The simulated PRV had a 15 mm orifice. The fire exposure generally was good. The fire had an effective black body temperature in the range 860-940°C. The tank failed at 1420 seconds (24 minutes). The tank pressure was about 2.55 MPa and the PRV never opened. It was expected that the PRV would have happened at about 25 minutes. Just before failure, the peak wall temperature increased rapidly to about 780°C; it is likely that the tank had bulged to make direct contact with the hotter jacket.

Figure 3.10 – Test 04-03 tank after rupture. The steel jacket split open at the top tack weld. [Birk et al. 2006]

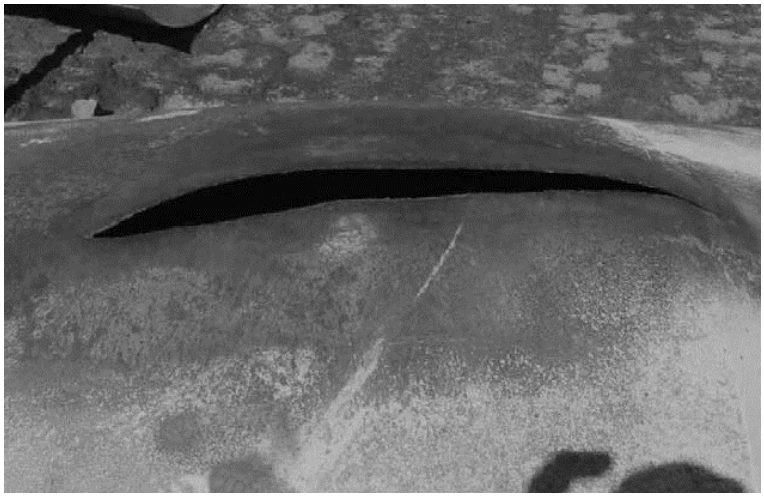

Figure 3.11– Tank failure, test 04-03 [Birk et al. 2006]

Large thermal defect, low hoop stress, test 04-04

The tank for 04-04 was a repeat of test 04-03 with two modification: the PRV was set to pop at 2.12 MPa and close at 1.93 MPa, in order to give about a 20% reduction of hoop stress, and the fill was increased to 78%. The wind caused fluctuations in the fire. The tank failed at 54 minutes, if the time span when the fire was poor were removed, the adjusted failure time would be about 35 minutes.

Figure 3.12 – Tank rupture test 04-04 [Birk et al. 2006]

Small thermal defect, test 04-04

This test involved a tank with 8% insulation defect area. The defect spanning almost the entire tank circumference except for the bottom 20-30°. As in the test 04-03 the tank was filled and purged with 1300 l of propane, about 71% fill by volume. The PRV was set to pop at 2.63 MPa and close at 2.39 MPa. The simulated PRV had a 15 mm orifice. The test started off well so it has been up to 2000 seconds (33 minutes) when the wind increased for about 1200 seconds dropping the wall and jacket temperatures substantially. The wind speed then dropped and the test continued with rising wall

temperature. The PRV initially opened at 2130 seconds (35.5 minutes) and cycled 16 times before the tank failed at about 3550 seconds (59 minutes). The adjusted failure time would be 2400 seconds (40 minutes).

Summary

The summary of the tests used in this work for the validation is reported in table 3.7, further details on the experimental results obtained in tests are reported elsewhere. [Birk et al. 2006] Whereas, RADMOD validation will be discussed in the Section 8.3.

Table 3.7 – Summary of data adopted for the RADMOD validation presented in this thesis work.

	Test 04-03 15% area defect	**Test 04-04** 15% area defect	**Test 04-05** 8% area defect
PRV settings (MPa)	2.63	2.12	2.63
	9% blowdown	9% blowdown	9% blowdown
Nozzle (mm)	15	15	15
Initial fill	71	78	71
Approximate volume (l)	1300	1430	1300
Initial lading temperature (°C)	11	21	13
Time to failure (s)	1425	3360	3545
Adjusted time to failure (min)	20	24-36	29-46
PRV pops (# time)	0	79	16
Time to first PRV pop (s)	NA	1063	2133
Fill at failure	71%	64%	65%
Liquid temp at failure (°C)	37	60	50

4 Methodological approach

In this chapter the aims of the work are briefly described and the core methodological steps are reported in flow chart form, in Figure 4.1.

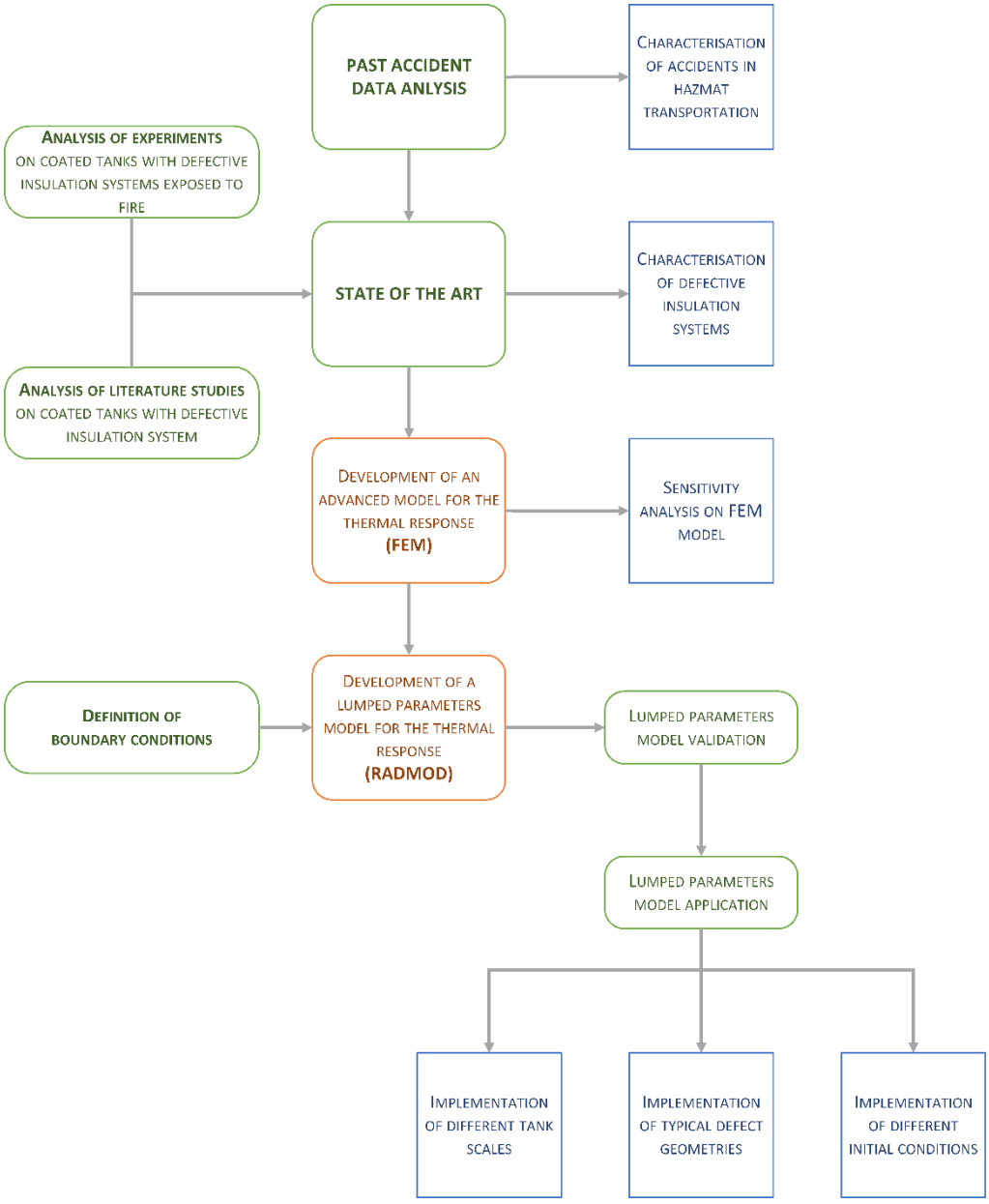

Figure 4.1 – Flow chart describing the methodology used in the present work

The analysis of past accidents data allowed for the characterisation of the main causes and main consequences related to the transportation of hazardous materials, focusing on the scenarios involving LPG. This analysis aimed to assess the need of a passive fire protection system for LPG tanks, in order to avoid their catastrophic failure due to external heat load. The presence of deficiencies in such insulation system was characterised first through the analysis of bonfire experiments [VanderSteen & Birk, 2003; Birk et al. 2006] and then, through the analysis of literature studies [Scarponi et al. 2016], both, experiments and literature, focused on coated tanks exposed to fire with defective insulation systems.

This basis permits to characterise the problem and achieve the two aims of this thesis work:

1. The development of an advanced finete elementes method (FEM) model able to predict the thermal response of insulated tanks exposed to fire in presence of defects in their insulation systems. The FEM model is validated [Scarponi et al. 2016] against available experimental data [VanderSteen & Birk, 2003] and then a sensitivity analysis is performed. This part of the work is aimed at evaluating the dependence of the temperature reached by the wall of the tank in correspondence of defect on main parameters, such as temperature and emissivity of the flame, steel emissivity and convective heat coefficients.

2. The more innovative progress of this thesis work is the development of a lumped parameters model for evaluation of thermal behaviour of tanks exposed to fire with defective coating system. The goal is to implement a simplified model with low time of simulation and adaptable to different materials, tank and defect geometries, and configurations, which allows to obtain informations on the fluid lading behaviour, among other parameters, during the fire exposure. The model is validated against available experimental data [Birk et al., 2006] showing also a conservative but credible prediction of the time to failure of the tank. The model is then applied to different reale-scale tanks and reale-scale defect geoetries, varying some of the several parameters, such as the initial filling, in order to assess the thermal response of the system. This model requires less dettailed informations to run and obtains less dettailed results giving in any case a credible response of the performance of defective insulation systems installed on tanks in case of flame impingement.

5 Analysis of the behaviour of pressurized vessels exposed to fire: theoretical considerations

In case fire scenario affects one or more transport tankers, thermal radiation and convection associated to the flame may trigger a domino-effect chain with associated escalation of events, as it was shown in paragraph 2.3.3. In the framework of the LPG transport, accidental fire may develop and affects the pressurized vessel, the heat from the flame is transferred to the tank by radiation and convection. This causes the tank shell to heat up, conduction takes place through the tank walls up to the lading which reaches the heat by means of convection mainly, and radiation. [Moodie, 1988] Where the tank inner surface is in contact with the lading in vapour phase, the heat exchange coefficients are relatively low and the wall temperature in these regions increases rapidly. [Birk, 1988] The increase of the wall temperature causes a degradation of the shell material properties and thus a decrease in the material strength. Otherwise, the heat transfer coefficients in the regions where the wall is wetted by the liquid are relatively high and the wall is cooled by the liquid as a result. The liquid phase is not usually homogeneous and while heated, the near-wall liquid becomes hotter and less dense so it rises reaching the interface with the vapour. This leads to a stratification phenomenon [Aydemir et al. 1988] which determines the increasing liquid temperature and thus the internal pressure to rise until it reaches a level where the pressure relief valve will open venting mass and resulting in the mixing of lading. The thermal rupture of the tank depends on the tank internal pressure, the tank wall temperature distribution, and the tank material strength at the elevated temperature which exist during the fire. [Birk, 1988] In this chapter all the phenomena and the related issues tanking place in such scenario are discussed.

5.1 Material balances

The material balances are strictly dependent by the presence of the PRV. The flux through the valve depend on the discharge pressure for which two fluxes can be registered:

- Sonic flux
- Supersonic flux

The discharge pressure determines the critical conditions for which the supersonic flux occurs. This critical conditions are due to the compressibility of the vapour, in fact the flow through the PRV nozzle will increase to a maximum value as the downstream pressure is reduced, and any further decrease in the downstream pressure will not affect the flow. [Perry & Green, 2007] The determination of the appropriate methodology for the evaluation of mass flow through the PRV depends on the approximation considered for the situation:

- Ideal gas → [API 520, 2014]
- Non-ideal gas → [Leung & Epstein, 1988] or [CCPS, 1998]
- Two-phase relief → [Leung & Nazario, 1992] or [Leung & Epstein, 1990]

The methods reported above are some of the guidelines available for determine the mass vented by the PRV ($\dot{\Phi}$). From this evaluation is possible to define the mass balances that relates the mass liquid variation to the vapour mass variation (eq. 5.1):

$$\frac{dm_v}{dt} = \frac{dm_l}{dt} - \dot{\Phi} \quad (5.1)$$

Where m_v and m_l are respectively the vapour and the liquid mass. The rate of liquid evaporated is related to the liquid conditions (T_l and P), if the temperature of the liquid is lower that the boiling temperature of the liquid at the pressure inside the vessel then the heat absorbed by the liquid causes an increase in the liquid temperate (eq. 5.2), on the contrary the heat absorbed by the liquid causes an evaporation of the liquid itself, if the temperature of the liquid is higher than the boiling temperature (eq. 5.3).

Not boiling liquid: $\frac{dm_l}{dt} = 0$ (5.2)

Boiling liquid: $-\Delta H_{vap} \frac{dm_l}{dt} = \dot{q}_l^{in}$ (5.3)

Where ΔH_{vap} is the latent heat of vaporisation of the liquid and $\dot{q}_l^{in}$ is the heat load to the liquid and it will be discussed in the Paragraph 5.2.3.

5.2 Heat transfer mechanisms and balances

5.2.1 Fire

Fire heat transfer to a tank is very case-specific. The fire heat input will depend on many variables, such as the fuel type, the wind conditions, the size of the fire, etc. It is only possible to discuss trends and likely case situations. [Birk, 1995] The fire that a general equipment can be subjected to is generally categorized as either a pool fire or a jet fire. A jet fire is a pressurized release of flammable gas and/or liquid with a high momentum, forming a cone shaped flame envelope in the direction of the release. Jet fires radiate high heat fluxes of about 230 kW/m2 when JP-type fuels are involved, and the momentum can push firewall protection away and burn through steel like a blow torch. Heat fluxes of hydrocarbon pool fires are significantly lower than for jet fire, due to the limited convective term associated to the flame velocity. May be expected to reach effective flame temperature of between 700-800 °C [Keltner et al. 1990] which gives a heat fluxes in the range of 70-100 kW/m2. [Birk, 1995] In this thesis work the focus is on LPG transportation issues, thus the fire impingement considered here is the pool fire. The flammable pool may develop from leakage of the fuel of vehicles involved in an accident or from the leakage of flammable liquid content, if hazmat tankers are involved in the accident.

The thermal load from the flame to the tank is a combination of convection from the hot combustion products passing over the tank surface and radiation emitted by the flame to the tank surface. This event is complex and depends on several issues. [Landucci et al. 2009] In fact, the relative proportions of radiative and convective load from a flame varies depending on the fuel type and location of the tank within the flame, while the total heat loads depends on the fuel type, the size and shape and the location of the tank within the fire. Moreover the heat loads are not constant over the surface of the tank surface. [Roberts et al., 2004] In most cases, it can be assumed that the flame and the tank wall are diffuse grey bodies and that the ambient temperature of the surroundings

is low compared to the flame temperature. With this assumptions the heat flux absorbed by the tank wall can be expressed as:

$$\dot{q}_{flame \rightarrow wall} = \dot{q}_{rad}\left(\sigma \varepsilon_s\left(\varepsilon_f T_f^4 - T_w^4\right)\right) + \dot{q}_{conv}\left(h\left(T_f - T_w\right)\right) \qquad (5.4)$$

Where ε_s and ε_f are the flame and the steel surface emissivity, respectively, σ is the Stefan-Boltzmann constant, T_f and T_w are the flame and the wall temperature respectively, and h is the convective heat transfer coefficient of the flame. The worse case if the fire is sooty, in this case the vessel will become a black body ($\varepsilon_s = 1$) receiving all the heat radiation. [Birk, 1995]

5.2.2 Tank insulation and shell

The heat transfers through the tank wall and associated coverings is determined by the temperature gradient in the radial direction. [Aydemir et al. 1988] The heat load is transported by mean conduction through the tank layers. In case of protected tank, the wall have an outer passive fire protection coating and the surrounding steel jacket. The conduction through a solid material, written in cartesian coordinate system, is:

$$\dot{q}_{in} - \dot{q}_{out} = \frac{\delta}{\delta x}\left(k_x \frac{\delta T}{\delta x}\right) + \frac{\delta}{\delta y}\left(k_y \frac{\delta T}{\delta y}\right) + \frac{\delta}{\delta z}\left(k_z \frac{\delta T}{\delta z}\right) \qquad (5.5)$$

Where *T* is the temperature, *t* the time, *c* the heat capacity, *ρ* the density and *k* the thermal conductivity.

The terms of heat entering and leaving the wall depend on the layer considered. The insulating material reaches the heat from the fire and transfer through conduction to the vessel inner walls. The latter then exchanges with the lading through both convection and radiation. The wall in contact with the vapour phase has low convective heat exchange coefficient and thus the heat is not easily dispersed to the vapour and the temperature increases. As the wall reaches higher temperature, thermal radiation from the tank to the lading becomes increasingly important. A small part of radiation is absorbed by the vapour, because of the transparent nature of vapour, and the major proportion of radiative heat transfer is to the liquid surface facing to vapour-space wall. [Moodie, 1988]

5.2.3 Liquid phase

In the liquid zone the temperature is lower one, since the heat transfer coefficients are higher and the heat is dispersed from the wall to the liquid. The heat transfer mechanism at the initial phase is pure natural convection. In fact the liquid is heated from the bottom and by side, temperature difference between the liquid in contact with the walls and the liquid bulk, generate density gradients that drive the natural flow and it can give stratification, leaving a cold bulk in the middle and a hot layer around and at the top. [Birk, 1995] The effects of this phenomenon are discussed in section 5.3. If the heat flux is high enough the wall temperatures rises up and saturated or sub cooled nucleate boiling will start. Bubbles of gas start to form in contact with the wall and grow up, until they become big enough to go up to the liquid surface. If the heat flux is even bigger, there is a point where a film of gas is created by the wall and the heat transfer coefficient drops down intensely, and that is the critical flux. The qualitative behaviour of the liquid heat transfer coefficient, as called h, is illustrated in figure 5.1. The last transition indicates in the graph is from nucleate boiling and film boiling, this occurs when the temperature gradient increases and radiation takes place in the gaseous film on the wall.

As shown in section 5.2.1, a jet fire and a pool fire, are not credible that can provide a heat flux higher than critical heat flux: consequently, the transition from nucleate boiling and film boiling does not occur in the scenario considered here.

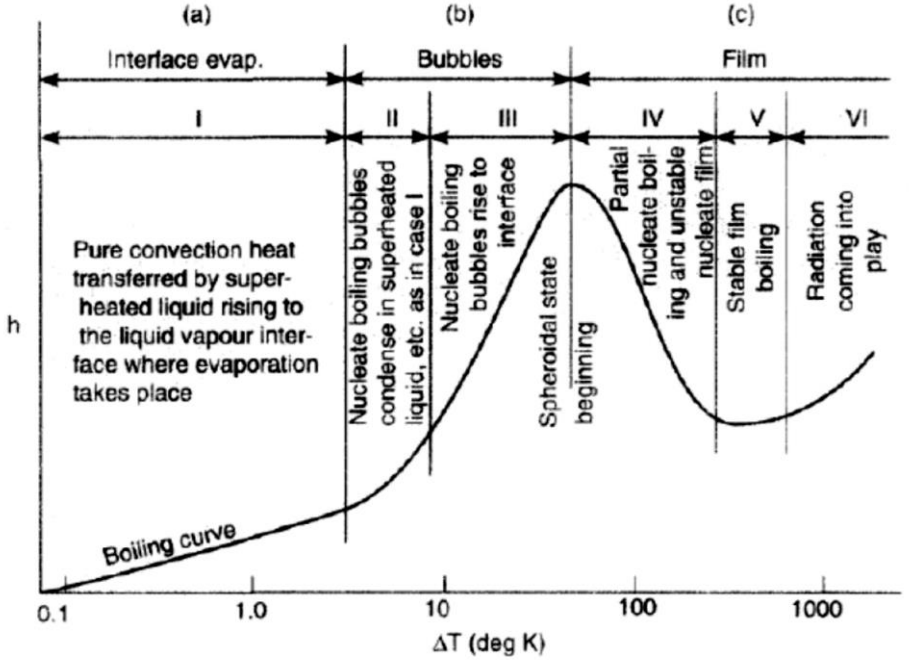

Figure 5.1 - Behaviour of the liquid heat transfer coefficient with the driving force, the difference of temperature between the wall and the saturation temperature of the liquid at a given pressure [Kern, 1965]

When the PRV opens up there is a quick drop in pressure, all the mass of liquid becomes superheated and it begins to boil. So, when the PRV opens, there is a good mixing effect in the liquid and the stratification disappear. Two different situations must be considered to write appropriate heat balance in the liquid phase:

- Not boiling → temperature of liquid lower than boiling temperature of liquid at the internal pressure of vessel (eq. 5.6)
- Boiling → Temperature of liquid higher than boiling temperature of liquid at the internal pressure of vessel (eq. 5.7)

In the not boiling case the heat absorbed by the liquid causes an increase in the liquid temperature (eq. 5.6) while in the boiling case the heat absorbed by the liquid causes an evaporation of the liquid itself and thus the temperature of the liquid remain approximately constant (eq. 5.7) assuming that all the heat received is used for the evaporation, the balances follow:

$$m_l c_{v,l} \frac{dT_l}{dt} = \dot{q}_l + \dot{q}_{lv} \quad (5.6)$$

$$m_l c_{v,l} \frac{dT_l}{dt} \cong 0 \quad (5.7)$$

Where m_l and $c_{v,l}$ are respectively the mass and the specific heat of the liquid, and T_l is the liquid temperature. The terms $\dot{q}_l$ and $\dot{q}_{lv}$ are the heat loads to the liquid, $\dot{q}_l$ is the heat received from convection with the liquid-space tank wall and the radiation from the vapour-space tank wall, $\dot{q}_{lv}$ is the heat exchange between the liquid and the vapour.

The latter is due the temperature difference between the two phases which determines a heat transfer process in the phase interface. The two equations are approximate, in fact another transfer mechanism is present in the liquid phase when stratification occurs, that is the transferring of heat to the sub-cooled bulk fluid (see section 5.3). [Aydemir et al. 1988]

5.2.4 Vapour phase

The convective heat transfer coefficient for the vapour space is low and the wall temperature increases as the vapour temperature. The gas in the vapour space is superheated and severely stratified. [Aydemir et al. 1988] The entering heat load is by convection from the vapour-space tank wall and a small account of radiation, considering the vapour not transparent, in addition there is the heat provided from the liquid mass evaporated. The situations in which the heat balances change are in function of:

- PRV opening (eq. 5.8)
- PRV stay closed (eq. 5.9)

if the PRV is open, a term is added to the stay closed balance (eq. 5.8) this term is related to the PRV which vents out mass dissipating heat from the vapour, as shown in eq. 5.9.

$$m_v c_{v,v} \frac{dT_v}{dt} = \dot{q}_v + \dot{q}_{lv} + \frac{dm_l}{dt} H_l \qquad (5.8)$$

$$m_v c_{v,v} \frac{dT_v}{dt} = \dot{q}_v + \dot{q}_{lv} + \frac{dm_l}{dt} H_l - \dot{\Phi} H_\Phi \qquad (5.9)$$

Where m_v and $c_{v,v}$ are respectively the mass and the specific heat of the vapour and T_v is the vapour temperature. $\dot{q}_v$ is the heat received by convection and radiation from the tank wall and $\dot{q}_{lv}$ represent sthe heat exchange with the liquid phase. H_l and H_Φ are the entalpies associated respectively to the mass of liquid evaporated $\left(\frac{dm_l}{dt}\right)$ and to the mass vented by the PRV ($\dot{\Phi}$) (see Section 5.1).

5.3 Stratification phenomenon

When a tank is heated from a fire the liquid is not usually heated uniformly, from experimental evidence the liquid at the bottom of the tank is cooler than the liquid on the top. [Birk, Cunningham, 1996] Thermal stratification occurs frequently in vessels of liquefied gases, such as LPG, due to external heating. This stratification effect has a relevant effect on safety aspect like BLEVE prediction and energy. [Birk & Cunningham, 1996]

As said in paragraph 5.2.3, due to the heating of inner tank walls in the liquid-space, the fluid particles near the wall are heat and thus became less dense. They begin rising along the walls of the vessel. Upon reaching the liquid surface, these particles spread towards the centre and fall back into the cooler regions of the fluid, they then re-enter the boundary layer to repeat the above process. This recirculating natural convective flow establishes a vertical temperature gradient inside the tank, and thus the liquid became thermally stratified. [Aydemir et al., 1988] Due to this phenomenon, the liquid on the free surface has a higher temperature than the bulk liquid: the pressure in the vessel is controlled by this warmest liquid layer. It is possible to divide the lading liquid domain in three different zones [Aydemir et al. 1988] :

- a bulk liquid → in which the subcooled liquid is present;
- a stratified liquid layer → zone from bulk to liquid–vapour interface
- a boundary liquid layer → zone near to the hot walls, in which the liquid rises up to reach the interface due to the natural convection

Figure 5.2 shows a schematisation of the several formed in the liquid-phase containing in the vessel exposed to fire. [D'Aluisa et al. 2014]

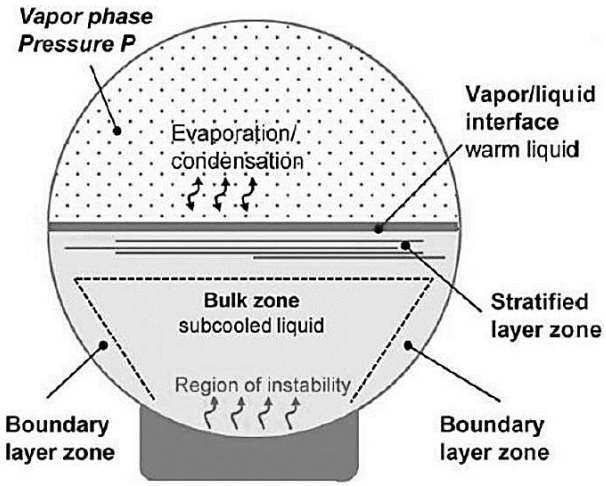

Figure 5.2 – Schematisation of the thermohydraulic behaviour of liquid-phase lading in the vessel exposed to fire [D'Aluisa et al. 2014]

The magnitude of the temperature gradient is a function of several parameters but for a given fluid and heat flux, experience indicates that the depth of lading is of primary importance; the lower the filling level, the less severe the stratification. Another observation from the laboratory vessel is the existence of vertically-upwards fluid motion near the bottom of the cylinder. In this region, fluid particles rise directly upwards and mix with the bulk of the fluid instead of attaching to the wall to form a boundary layer. This mechanism is important since it provides direct heating to the central core regions and also retards the initiation of boundary layer. [Aydemir et al. 1988]

The stratified temperature distribution is present until other processes dissipate the temperature gradient. The liquid stratification is affected by thermal and transport properties of the fluid, by the liquid vertical dimension and geometry, by distribution and rate of the heat source, by the PRV operation. Immediately after the start of fire exposure, stratification phenomena begin till the eventual opening of PRV. Then, the resulting boiling causes mixing effects reducing massively the stratification. If the PRV closes it is then observed that the stratification starts again. [Birk & Cunningham, 1996] So the de-stratification phenomena mainly depends on the behaviour and sizing of the PRV and on the heat power heating the tank. [Birk & Cunningham, 1996]

The temperature-stratification effect is seen at all scales and it plays an important role in the outcome of an accident situation. Temperature stratification determines the time to first opening of the PRV and it also affects the severity of the outcome since it affects the liquid energy at the time of failure. [Birk, 1995] The role of thermal stratification on BLEVE is important; for a given tank pressure, the average temperature of the liquid decreases as the liquid become more stratified. That is because the tank pressure is given by the top warm layer. So for a given release valve opening pressure there is less energy

in the liquid the more it is stratified. The response upon sudden depressurization does not only depend on the average liquid temperature. If the liquid is stratified, then the hot layers will be more super-heated than the cool layers, so the pressure recovery given by the boiling of the liquid will start earlier from the warm layer. Eventually, this can suppress the boiling from the cold layers, since also the hydrostatic pressure is contributing to this. If the temperature of the liquid is uniform the pressure recovery after the opening of the PRV is going to be stronger and therefore more likely to fail the tank. [Birk & Cunningham, 1996]

On the other hand, the more the liquid is stratified the faster the pressure rises, so the time to PRV opening will be shorter if the liquid is stratified respect to a situation in which the liquid is homogenous. [Birk & Cunningham, 1996] The effect of the PRV opening are discussed in the following section 5.5.

5.5 PRV opening effects

When the PRV opens and vents vapour, the depressurization leads a boiling process, that consumes energy in the warmest liquid layers and the resulting bubble rise causes mixing in the warmest layer, so the combination of these effect reduces the stratification. So, as time progresses, continuous mixing of the fluid results in more uniform temperatures throughout the liquid. [Aydemir et al. 1988]

The time to destratify depends on the tank scale and the PRV action which itself is controlled by the degree of fire exposure. If a tank is engulfed in fire the resulting large PRV flow will tend to destratify the liquid quickly, whereas if the tank is exposed to a small fire the liquid may not destratify at all. [Birk & Cunningham, 1996] While destratification takes place, little mass is being lost from the tank through the PRV, since most of the heat input is going into the bulk of the liquid (sub-cooled boiling where vapour-bubbles collapse into cooler core liquid) and not into vapour generation for venting. when the liquid temperature becomes uniform, the mass flow through the PRV increases because all of the fire heat is now going into vapour production at the PRV set pressure. This is when the liquid level starts to drop more rapidly. [Birk, 1995] While the liquid level decreases the tank surface area in contact with the vapour phase increases, and thus reducing the area with the liquid cooler effect.

5.4 Vessel failure mechanisms

A tank may suffer a failure during a fire for a number of reasons, for the horizontal cylindrical vessel these include:

- uncontrolled pressure built-up due to heating or reaction
- wall-thinning due to hoop stress and high-temperature material degradation
- severe bending stressess due to thermal stresses induced by differential temperature on tank top and bottom
- mechanical damage due to impacts, corrosion or poor manufacture

Of the above types of failure, mechanical damage is difficult if not impossible to identify in an accident situation, as the severe bending stresses. The latter may not alone be capable of causing a failure but may cause premature failure when coupled to mechanical damage of some kind. Uncontrolled pressure build-up is strictly related to

the design and sizing of pressure relief system. While, wall thinning due to hoop stress and high-temperature material degradation is a likely scenario in the event that a tank in good condition is exposed to severe fire impingement. [Birk, 1995] In this scenario, with continuing fire attack the vapour metal walls weaken and commence plastic deformation at the hottest locations eventually leading to the formation of a creep. If the PRV opens the liquid level decreases and the tank surface in which the creep may form increases. Over some period of time, the creep results in the formation of a fissure or hole in the tank wall. This fissure may grow leading to the catastrophic failure or it may stop leading to a depressurisation due to the content discharge. This two scenarios depend on the condition of the wall and the thermodynamic condition of the tank contents. [Venart, 2000]

6 Modelling the thermal response of insulated vessels exposed to fire in presence of defective coatings: FEM simulations

6.1 Theoretical background on defective coating assessment

Scant data are available for the characterisation and the modelling of defective coating used for the thermal insulation of vessels. The possible presence of defects in the thermal coating and the critical size of a defect in compromising the performance of the thermal protection system were never systematically explored before the past decade. [Scarponi et al. 2016] In fact, as discussed in paragraph 3.2.1, the first step through the characterisation of defective coatings has been through the thermographic inspection method proposed by Birk and Cunningham in 2000. [Birk & Cunningham, 2000] Subsequently, two bonfire trials were performed aimed at the definition of criteria to tests the performance of defective insulation system, one of which aimed to test the effect on a portion of tank shell of different coating deficiencies [VanderSteen & Birk, 2003] and the other one tests the effect of small and large insulation defects on LPG filled tanks. [Birk et al. 2006]

Nevertheless, there weren't any studies on insulated tank exposed to fire with defective coating, the thermal behaviour of such system was investigated only in the past year by G. Emrys Scarponi et al. [Scarponi et al. 2016] which developed a thermal model supported by finite elements analysis and perform a study on the heat transfer mechanism inside the enclosure, which is discussed below. The finite elements method, discussed in this section, is aimed to reproduce the thermal response of defective coatings in order to define a specific set of key performance indicators (KPIs) aimed at provide a tool to facilitate the task of assessing the acceptability of a given degree of defectiveness.

6.1.1 Heat transfer mechanism inside the defect enclosure

Coating defect forms an enclosure between steel jacket and tank shell-wall, within there is a layer of air which can transfer the heat through convection, conduction and radiation. The hypothesis is that radiation is the dominant heat transfer mechanism. In fact, the radiative heat flux is proportional to the temperature raised to the fourth power and in the enclosure there is a high temperature gradient between the steel jacket temperature, which rises quickly up near to flame temperature, and the shell-wall temperature, which remains much lower especially if in contact with liquid-phase. [Landucci et al. 2011] On the other hand, the conductive and convective transports are expected to be low.

The three mechanisms were modelled and tested in order to assess which of those is dominant and which is negligible. The tests were conducted through a mono-dimensional finite volume model developed by Scarponi et al. [Scarponi et al. 2016] Therefore, three models were applied: the first model considers only the radiation mechanism, in the second also convection was considered and the third model considers a static layer of air in which the heat is transferred by conduction, in addition to the radiation between the two walls. In the computation of the radiation flux, it is assumed that each point forming the enclosure radiates and receives radiation towards and from all other points according to a view factor, which depends on the reciprocal position of the points. In the case of convection model, a convective heat transfer coefficient in the enclosure and the heat flows entering and leaving the latter, all solved in function of a

bulk temperature of the air in the gap. The heat transferred by conduction is written as the transient heat conduction equation for the air in the enclosure as a static layer, considering an air thermal conductivity. The three models were tested both for the case in which the inner wall is wetted by the liquid and for that in which the vessel content is in the vapour phase.

The results confirm the hypothesis that the radiation is the dominant heat transfer mechanism and that the contribution of conduction and convection can be neglected, since the temperature profile in the air gap obtained from the second and third models have not appreciable deviation from the profile obtained with the first model. [Scarponi et al. 2016]

6.2 Modelling approach and energy balace

As mentioned before, the model supported by finite element analysis was developed by G. Emrys Scarponi et al. [Scarponi et al. 2016] and it is reported in this section.

The Finite Element Method (FEM) is a numerical analysis technique with which is possible to obtain approximated solutions of exact solutions of interest. [Gubinelli, 2003] The mathematical approach consist in the definition of a domain and the identification of a model describing the relations between the variables, coupled with proper boundary conditions. The FEM analysis discretizes the domain through a "mesh" of finite elements and calculates the solution of the problem in particular points, called "nodes".

In the model presented in this work, the domain of interest is an insulated vessels with deficiencies in its coatings. The model describing the problem consists in a transient heat balance and it is coupled with differential equations, as boundary conditions, which depend on the different zones identified in the domain. In an insulated vessels exposed to fire in presence of defective coatings, four different zones can be identified and thus four different boundary conditions are defined. Figure 6.1 shows the geometry of the problem with the different zones.

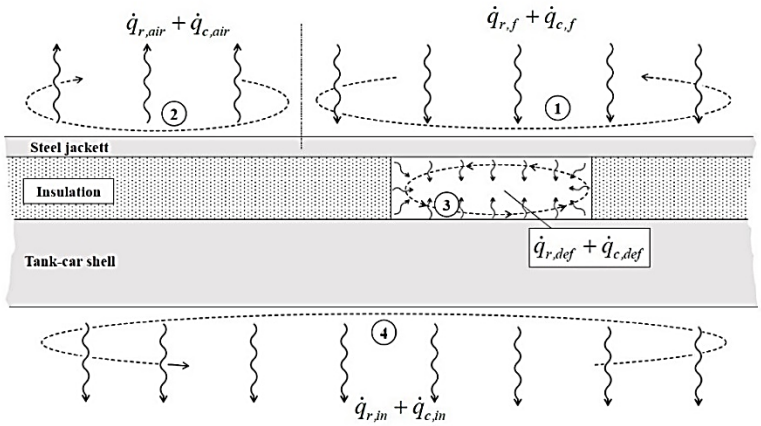

Figure 6.1 – Sketch of the zones identified for the domain in the FEM model and assignment of boundary condition [Scarponi et al. 2016]

Zone 1 and 2 are the external surfaces of the steel jacket. The first zone is impinged by the flames, while zone 2 considers the case of partially engulfing fire and represents the

not impinged area. In zone 1 the flame exchanges with the steel jacket through both radiative and convective mechanism, expressed respectively by eq. 6.2 and 6.3. The sum of these boundary conditions represents the total heat power entering the system. The mechanisms governing the first region are the same for zone 2 but the heat leaves the system. So, for zone 2 the radiative and convective flows are from the steel jacket to the ambient air, with the corresponding temperatures and properties, as shown in eq. 6.4.

Zone 3 is the defect enclosure, the insulation is missing forming an air gap. The heat transport mechanisms in this region is discussed in paragraph 3.2.2, where is stated that radiation is the main heat transport mechanism inside this enclosure. Therefore, the boundary condition zone 3 is a radiative flux in which each point radiates and receives radiations towards and from all the other points forming the enclosure according to a view factor, which depends on the reciprocal position of the points. A deeper discussion of radiative heat exchange in enclosures can be find elsewhere [Modest, 2003].

The last zone, zone 4, is the internal surface of the tank shell, where heat reaches the lading, both in vapour or in liquid phase, depending on the liquid level. In this thesis work, the model is used in its validation form. Thus, the entire internal surface was supposed to be in contact with air according to the experimental setup [VanderSteen & Birk, 2003] reported in section 3.3. So, the convective flux leaving the system written for zone 2 is used also here, as eq. 6.5 shows, but changing the correlation for the convective heat exchange coefficient.

The governing equation, i.e. the transient heat balance, for a solid material can be written as:

$$\rho c \frac{\delta T}{\delta t} = \frac{\delta}{\delta x}\left(k_x \frac{\delta T}{\delta x}\right) + \frac{\delta}{\delta y}\left(k_y \frac{\delta T}{\delta y}\right) + \frac{\delta}{\delta z}\left(k_z \frac{\delta T}{\delta z}\right) \quad (6.1)$$

Where T is the temperature, t the time, c the heat capacity, ρ the density and k the thermal conductivity.

While the boundary conditions coupled with eq. 6.1 are:

Zone 1 – radiative and convective flows entering the system:

$$\dot{q}_{r,f} = \sigma \varepsilon_s (T_{BB}^4 - T_w^4) \quad (6.2)$$

$$\dot{q}_{c,f} = h_f (T_f - T_w) \quad (6.3)$$

Zone 2 – radiative and convective flows leaving the system:

$$\dot{q}_{r+c,out} = \sigma \varepsilon_s \left(T_w^4 - T_{air}^4\right) + h_{air}(T_w - T_{air}) \quad (6.4)$$

Zone 4 – validation model, convective heat flux leaving the internal wall:

$$\dot{q}_{r+c,valid\_air} = \sigma \varepsilon_s \left(T_w^4 - T_{air}^4\right) + h_{valid\_air}(T_w - T_L) \quad (6.5)$$

Where σ is the Stefan-Boltzmann constant, T_w and ε_s are the temperature and the emissivity of the steel wall respectively, T_{BB} is the black body temperature of the fire, T_f is the flame temperature, T_{air} is the ambient temperature. The black body temperature depends on the flame temperature and the emissivity assigned to the flame.

ε_s is the emissivity of the steel wall, it depends from the temperature reached by the wall. Both the steel jacket and the tank wall are made of carbon steel, thus the average

value of the emissivity is set to 0.7 according with the temperature range of interest (0 – 700 °C) [Eurocode 1, 2005].

The convective heat exchange coefficients h_f and h_{air} are, respectively, between the flame and the tank wall (zone 1) and between the tank wall and the ambient air (zone 3). While h_{valid_air} is between the internal tank wall and the air (zone 4). For each convective coefficient is needed a correlation for evaluate its value.

The convective coefficient h_f is a function of the fluid dynamic regime of the flame impinging the tank wall, which depends in turn on the burning rate of the fire. For low momentum flames, as in the case of the simulated pool fire in the experiments, the coefficient can be estimated as follows [Knudsen et al. 1999]:

$$Nu = \frac{h_f L}{k_f} = 0.26\, Re^{0.6}\, Pr^{0.3} \qquad (6.6)$$

Where Nu, Re and Pr are the Nusselt, Reynolds and Prandtl numbers respectively, L is the characteristic dimension of the system and k_f is the thermal conductivity of the flame. Reynolds number introduces the regimes of flow, laminar or turbulent, with respect flame velocity, while Prandtl merges the fluid properties, function of temperature. [Mauri, 2012]

For the determination of the natural convective heat transfer coefficient h_{air} for cylindrical geometry, several correlation can be found in literature [Boetcher, 2014]. Most of them require the preliminary calculation of the Nusselt number (Nu) by empirical correlations:

$$Nu = \frac{h_{air} L}{k_{air}} = \alpha\, Ra^{\beta} \qquad (6.7)$$

Where k_{air} is the thermal conductivity of the air, L is the characteristic dimension of the system and Ra is the Rayleigh number. Ra number is associated to the natural convection and, in the conditions considered here, its expected value varies between 10^{10} and 10^{11} . [Scarponi et al. 2016] According to King [King, 1932] for the expected Ra value range, the coefficients α and β are assumed equal to 0.13 and 0.33 respectively.

The convective heat exchange coefficient h_{valid_air} was calculated using eq. 6.8, valid in case of natural convection under an inclined plate [Churchill & Chu, 1975].

$$Nu = \left(0.825 + \frac{0.387\, Ra^{1/6}}{\left(1+\left(\frac{0.492}{Pr}\right)^{9/16}\right)^{8/27}} \right)^2 \qquad (6.8)$$

In addition to the assignment of the boundary conditions, material properties have to be defined for the steel and the insulation. Both the tank shell and the jacket are made of carbon steel, for which detailed thermal properties can be easily find in literature [Eurocode 1, 2005]. The thermal protection used in the test and its properties are reported in paragraph 3.3.1.

6.3 Numerical implementation on a distribuited parameters code

The model was implemented on the ANSYS® software, using the ANSYS® Mechanical APDL Release 14.5 module [ANSYS inc, 2013], based on finite elements approach. The problem geometry was defined in order to reproduce the experimental apparatus describes in paragraph 3.3.1. The time step adopted in each implementation is set to 5 seconds.

6.3.1 Types of models

Three different models are implemented through a distributed parameters code:

- Fully protected
- Sealed
- Defect 15.2

A schematisation of the models is shown in figure 6.2, while table 6.1 reports a summary of the geometries and their properties.

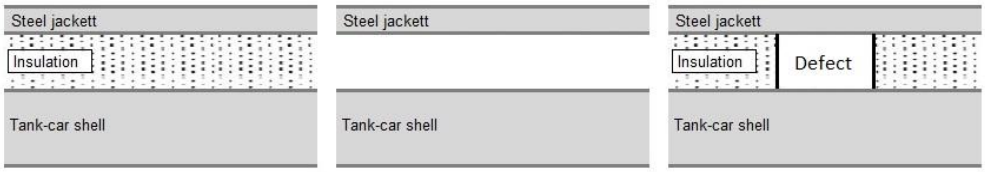

(a) (b) (c)

Figure 6.2 – sketch of geometries (a) fully protected (b) sealed (c) defect 15.2

The fully protected model has an insulation layer between the steel jacket and the tank wall. In the sealed geometry the coating is removed and air fills the empty space. The last model is a defective coating with a square air gap of 15.2 x 15.2 cm, which correspond to one of the defect geometries tested by Birk and VanderSteen. [VanderSteen & Birk, 2003]

Table 6.1 – Summary of the models implemented with the FEM model

	Fully protected	**Sealed**	**Defect 15.2**
Steel jacket	yes	yes	yes
thickness	3 mm	3 mm	3 mm
material	carbon steel	carbon steel	carbon steel
Tank shell			
thickness	16 mm	16 mm	16 mm
material	carbon steel	carbon steel	carbon steel
Insulation	yes	no	yes
thickness	13 mm	-	13 mm
material	ceramic	-	ceramic
Defect	no	-	yes
area	-	-	231 cm^2

6.3.2 Mesh

The volumes are meshed with the element SOLID90, indicated in the ANSYS [ANSYS inc, 2013] as suitable for transient thermal analysis. SOLID90 has 20 nodes and 6 faces.

Considering the cylindrical geometry, the axial and annular length of the elements are set at 50 mm whereas the radial dimension is 3 mm for the steel jacket, 3.25 mm for the insulation blanket and 3.2 mm for the tank shell.

The mesh obtained using such geometric parameters is shown in figure 6.3.

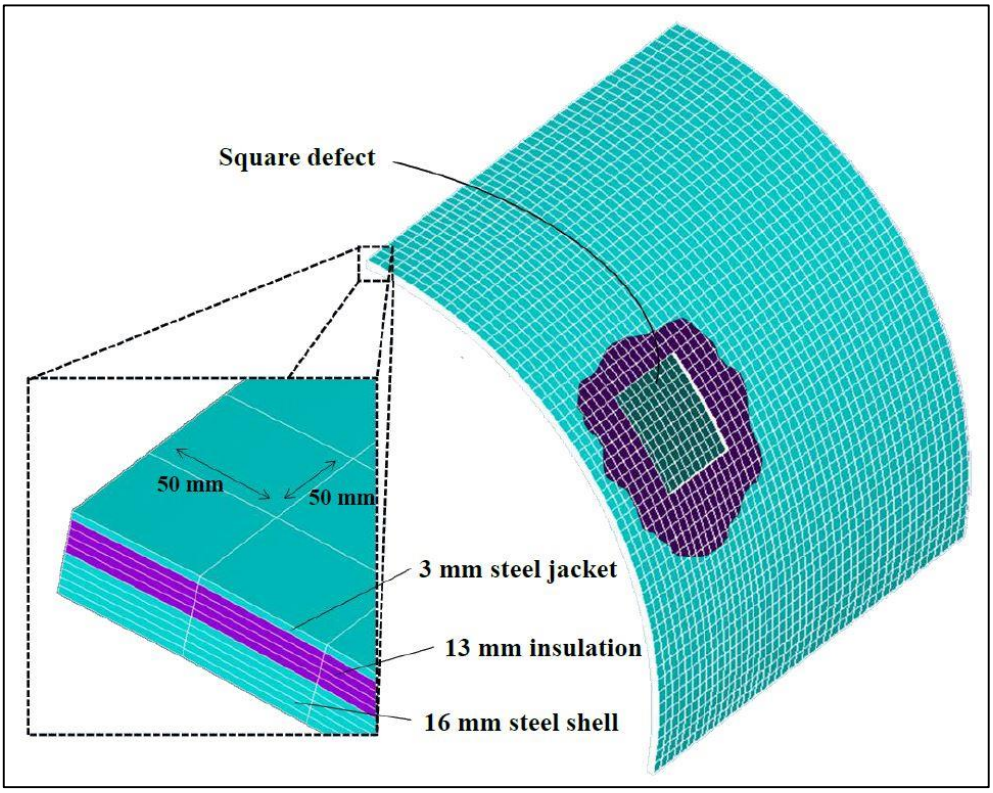

Figure 6.3 – Mesh implemented in the FEM model [Scarponi et al. 2016]

6.3.3 Mesh independence

Four simulations are set in order to run an independence analysis, the aim is to prove that the solution obtained with the previous setting is independent both from mesh and time step. Thus, a finer mesh is also implemented and the time step is reduced by half, the setting of the independence analysis is shown in table 5.1. The analysis is conducted on the geometry with square defect 15.2.

In the fine mesh the axial and annular lengths of the elements are reduced from 50 mm to 30 mm, the radial dimensions of the insulation blanket and of the tank shell are reduced by half, 1.63 mm and 1.6 mm respectively, while the steel jacket radial dimension is kept unaltered (3 mm). Not all lengths are reduced by 50% because halving the dimensions generates an aspect ratio forbidden by the SOLID90 element. Nevertheless, the number of element created in the fine mesh is more that seventeen times the number of element of the coarse mesh, as shown in table 6.2.

Table 6.2 – Summary of independence tests conducted on the FEM model mesh

Test ID	Mesh	Number of elements	Time step (s)
Baseline	Coarse	1440	5
01	Coarse	1440	2.5
02	Fine	24624	5
03	Fine	24624	2.5

The results of the analysis are shown in figure 6.4, where the percentage difference of temperatures (see eq. 6.9) is reported in function of time. The temperatures refer to the centre of the defect and their are obtained with the baseline (coarse mesh, wider time step) and with the finer mesh.

$$\Delta T\% = \frac{T_{test} - T_{baseline}}{T_{baseline}} * 100 \qquad (6.9)$$

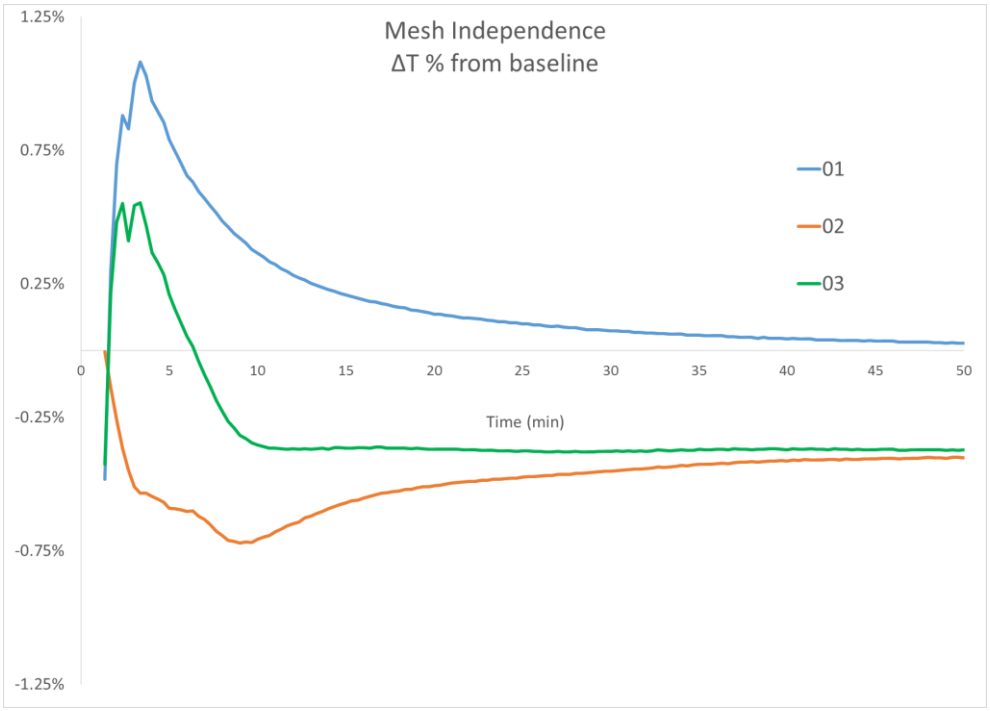

Figure 6.4 – Mesh independence results

In the first minute the results of tests with halving time step (01 and 03) diverge from the baseline of about 12% and thus, for graphic reasons, the first minutes is not reported in figure. Up to minute 2 the differences from the baseline is about 1% , from this point onward the percentage is less than unit. The results show that the solution of the coarse mesh is invariant with both the finer mesh and the shorter time step. This allow to use the coarse mesh and the wider time step for the simulations, saving computational time without compromising the results.

7 Evaluation of pressure build-up in tankers exposed to fire through lumped codes

7.1 Overview of the lumped modelling approaches

The modelling of the the pressure build-up of an equipment exposed to fire is a very complex problem. Different and particular problems must be solved, more specifically, the radiant flux over the target and the wall temperature behaviour must be modelled, then the possible failure conditions have to be analysed in order to assess the proper failure criteria to be adopted in the evaluation of the time to failure. The use of a distributed parameter approach (see chapter 6) would require many hours for preparation and for run time, which may be unacceptable even in the case of the analysis of a single scenario, limiting the analysis to a reduce number of accidents. Moreover, the uncertainty that affects the definition of the primary accidental scenarios will in any case affect the precision of the modelling results. [Landucci et al. 2009] Thus a lumped model approach was developed to evaluate the performance of tankers exposed to fire. This method requires less detailed information and it also obtains less accurate results which provides anyway a conservative but credible behaviour of the system. [Landucci et al. 2009] The easiness of use and the time-saving, few minutes for running, are key advantages of the lumped approach.

The lumped model is based on the division of the domain in different zone, called "nodes". In each node conditions and properties of the material can be considered uniform, averaged over the node, and the variable of interest (pressure, temperature, ..) are function of time alone. Then is set the heat balance in each node, with attention at the boundary conditions between different region, and the global conservation laws, concerning both mass and heat, obtaining a set of equations time-dependent able to assess the thermal behaviour of the different nodes as the pressure behaviour of the system. [Landucci et al. 2009; Landucci et al. 2013]

Several lumped models were developed from 1970 to nowadays for assessment of the thermal response of the vessels and its contents in case of fire exposure. These models generally concern horizontal cylindrical LPG vessels to engulfing fire and they allow the analysis of phenomena as the fire protection system influence or the PRV. [Landucci et al. 2009] The models and their developed setting are shown in tables 7.1.

Table 7.1 – Available lumped parameter models, for the predicting the consequences of fire attack [Landucci et al. 2016]
(FE = fully engulfed; PE = partially engulfed; JF = jet fire engulfment)

Reference	date	Model Name	Fire exposure	Thermal insulation
[Graves, 28]	1973		FE	Yes
[Johnson, 25 26]	1980-1998		FE	Yes
[Aydemir et al. 1988]	1987	PLGS-I	FE	No
[Beynon et al. 1988]	1987	HEAT-UP	FE	Yes
[Ramskill, 1988]	1984-1987	ENGULF I & II	FE, PE	No
[Forrest, 1985]	1986	SAFIRE	FE	No
[Birk, 1988]33	1988-2006	TANKCAR	FE, PE	No
[Shebeko et al. 2000]	2000		FE	Yes
[Salzano et al. 2003]	2003		FE, JF	No
[Gong et al. 2004]	2004		FE	No

[Lautkaski, 40]	2009	ENGULF II	FE, PE	No
[Landucci et al. 2009] 23	2009	RADMOD	FE, PE, JF	Yes
[Heymes et al., 42]	2013		DS	No
[Birk et al. 24]	2013		FE, PE	No

Between the models reported above, before 2006 only few models manage different vessel geometries and different vessel categories (e.g. ENGULF and SAFIRE) and only few models are able to predict correctly the influence of the PRV action (e.g. HEAT-UP and Salzano et al. codes). Hence the need to develop a lumped model able to predict the time to failure of insulated and unprotected vessels of any type, atmospheric and pressurized, undergoing different modes of fire exposure, taking into account the influence of the PRV action. [Landucci et al. 2009] This model, namely RADMOD, and its enhancement for defective coatings, are the main items of this work. In the next section the novel RADMOD model implementations are described, section 7.2 focusing on the enhancements of the previously code and the novel implementation for defective coating is discussed in section 7.3.

7.2 RADMOD code

The RADMOD code was developed first by the PhD project of Gubinelli and then by [Landucci et al. 2013]. The novel versions of the RADMOD model for horizontal cylinders was developed by Bazzocchi [Bazzocchi, 2014] and subsequently enhanced by Nigro [Nigro, 2015] who also extended the model for vertical configurations.

The last version of RADMOD model [Nigro, 2015] for horizontal cylinders is the basis of the code novel implementation for defective coatings presented in this thesis work. The updating are discussed in this section (7.2.2) and the fundamental equations implemented in the model are reported in appendix A. For what concerns the failure criteria adopted in the code, they are reported in Section 7.2.4.

Moreover, three sub-models are available for the evaluation of thermal stratification phenomena, two of which are implemented in the novel RADMOD model and discussed in paragraph 7.2.5. Whereas, the more improvement of the RADMOD code for defective coatings is discussed in section 7.3.

For further details on the RADMOD model and sub-models implementation refer to [Nigro, 2015] and previously works [Bazzocchi, 2014; Landucci et al. 2013].

7.2.1 Model set-up

The thermal model was setup in MatLab, with a link to the Excel to allow the insertion of initial condition and have a simplified view of the results of the simulation which are collected in another Excel spreadsheet. In order to solve a system of First-Order differential equations an explicit solution procedure was chosen, i.e. Matlab ODE45 solver. Explicit procedure in time is more simple to program, but requires small enough time steps to prevent numerical instability. So its simplicity and a medium order of accuracy has led us to choose this calculation procedure. [Nigro, 2015]

Another assumption made is that the fluid inside the tank is a pure substance (propane). If a mixture (propane-butane for LPG case) is considered the simulation will be more complex because the different concentrations in vapour and liquid have be calculated.

[Landucci et al. 2009] So the mixing rules should be used to obtain an accurate thermal analysis.

7.2.2 RADMOD nodes

The first version of the code was developed for coated or unprotected equipment, vertical and horizontal pressurized vessels and for vertical or spherical atmospheric vessels. All mathematical equations consider a simplified framework of the equipment, without further details about nozzles, instrumentation or piping system. Moreover for both horizontal and vertical cylinders also the two semi-elliptical heads are neglected. The focus in this thesis is on the pressurized vessels, the nodes individuated for such problem by the fist version of RADMOD are schematic described in Figure 7.1.

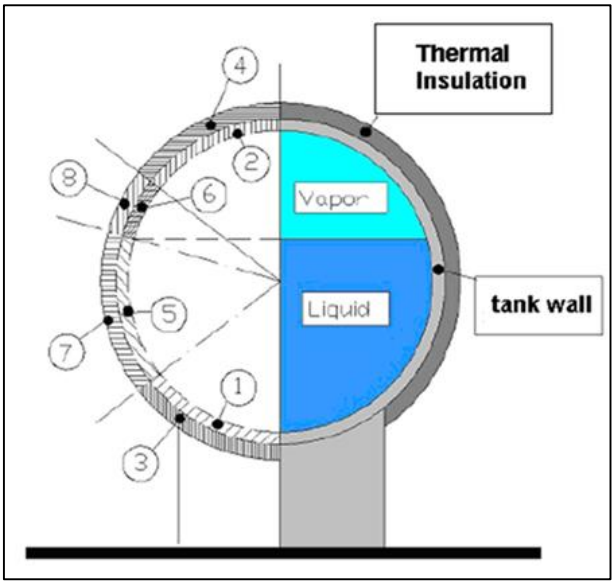

Figure 7.1 – Sketch of horizontal cylindrical tank of the RADMOD code [Landucci et al. 2013]

The nodes are numbered from 1 to 8 and each of them indicates a specific zone of the tank wall or the thermal coating:

- Node 1 → Inner shell wall in contact with the liquid (not with the flame)
- Node 2 → Inner shell wall in contact with the vapour (not with the flame)
- Node 3 → Coating of the liquid side (not in contact with the flame)
- Node 4 → Coating of the vapour side (not in contact with the flame)
- Node 5 → Shell wall in contact with the liquid and not with the flame
- Node 6 → Shell wall in contact with the vapour and not with the flame
- Node 7 → Coating of the liquid side in contact with the flame
- Node 8 → Coating of the vapour side in contact with the flame

This plan of the nodes is valid for the partial fire engulfment. In the novel version of the RADMOD code, the nodes not directly in contact with the flame (nodes 1,2,3,4) are not contemplated in the novel version. It is assessed to denominate the nodes keeping the pair of numbers and add two extra nodes in order to perform a better study of the behaviour of the protection layer and shell , as suggest by [Butler et al. 2001]. So six nodes for shell and coating are available:

- Node 1-5 → Inner shell wall in contact with the liquid
- Node 2-6 → Inner shell wall in contact with vapour

- Node 3-7 → Coating of the liquid side
- Node 4-8 → Coating of the vapour side
- Node iV → intermediate node between shell and coating of the vapour side
- Node iL → intermediate node between shell and coating of the liquid side

After these modification the final sketch for the RADMOD model for horizontal vessels is shown in Figure 7.2.

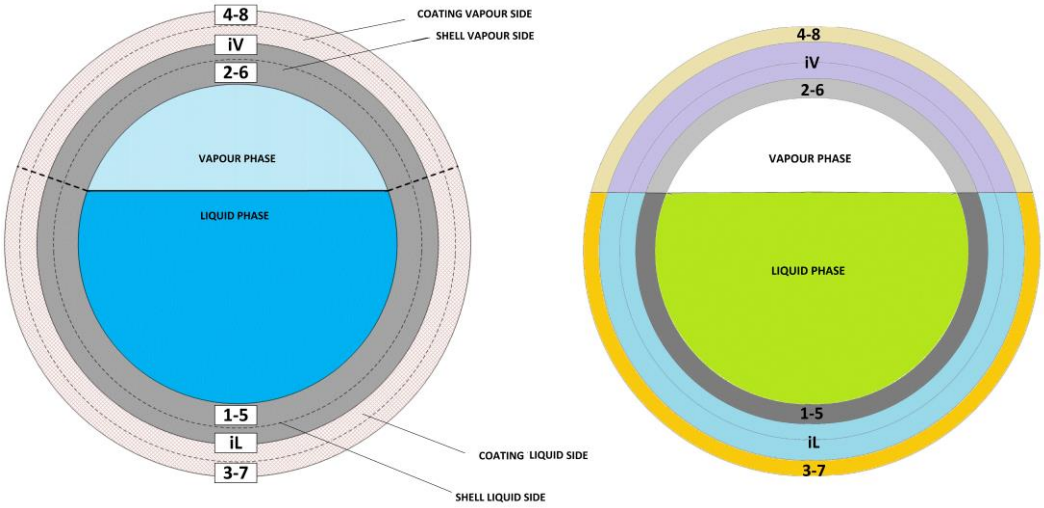

Figure 7.2 Nodes illustration of horizontal cylindrical tank of the RADMOD code

The mathematical formulation of the model is different in the cases with or without coating, depending on the shape. When an unprotected vessel is analysed, nodes 3-7 and 4-8 are not present, so the two associated equations are not solved. However, in both cases the equations describing the behaviour of the liquid and vapour are the same.

7.2.3 RADMOD variables and equations

In the complete version of RADMOD Baseline applied to a coated horizontal tank there are 12 unknown variables so 12 equations are needed. The unknown variables are:

- Liquid temperature T_L
- Vapour temperature T_V
- Internal pressure P
- Level inside the tank L
- Liquid mass m_L
- Vapour mass m_V
- Temperature of shell in contact with the liquid T_{15}
- Temperature of shell in contact with the vapour T_{26}
- Temperature of shell in contact with the flame on liquid side T_{iL}
- Temperature of shell in contact with the flame on vapour side T_{iV}
- Temperature of coating in contact with the flame on liquid side T_{37}
- Temperature of coating in contact with the flame on vapour side T_{48}

The thermodynamic implies to split the problem in two parts depending on the liquid saturation (see chapter 5), the system of equations is different if the liquid is sub-cooled or super-heated. So at every iteration through the check of pressure against the saturation pressure (P_{sat}) at the liquid temperature (T_L) is needed in order to have the right system of equations. If the pressure of the system is higher than saturation pressure the liquid

is sub-cooled otherwise it is superheated. The saturation pressure is evaluated through Antoine equation. The only energy balances to split in this two cases are the ones written for the lading (liquid and vapour phase) since the heat transfers through the tank layer (shell, coating and jacket) are not related to the liquid saturation.

The improvements of the heat balances are reported below, whereas the failure criteria adopted in the code are reported in paragraph 7.2.4.

Vapour transparency

The first improvement of the RADMOD code regards the radiation received by the vapour phase. The vapour is not considered transparent to the radiation from the vapour-space wall, thus the radiation received by the liquid is reduced by a quantity which is added to heat loads to the vapour, with respect to heat transfer coefficients between the vapour and the wall. Thus, the liquid and the vapour temperature balances are modified as shown in equation (7.1) and (7.2) for the liquid node and (7.6) and (7.7) for the vapour node.

Liquid temperature (T_L) → Not boiling liquid:

$$m_L cv_L \frac{dT_L}{dt} = q_{L,boil} + q_{L,rad} + q_{LV} \quad (7.1)$$

Liquid temperature (T_L) → Boiling liquid:

$$\frac{dT_L}{dt} = 0 \quad (7.2)$$

Where m_L is the liquid mass, cv_L is the heat capacity of liquid at constant volume. Since the liquid can be assumed uncompressible, the specific heat at constant volume is considered equal to the specific heat at constant pressure (cp_L). q_{LV} is the convective and radiative heat power between the vapour-phase and the liquid-phase. The terms $q_{L,boil}$ and $q_{L,rad}$ are the convective and radiative heat powers received by the liquid from the walls, the convection is from the liquid-space walls and the radiation from the vapour-space ones. The radiative contribution is define as:

$$q_{L,rad} = A_{26int}\sigma\varepsilon F_{v,L}(T_{26}^4 - T_L^4) - q_{V,rad} \quad (7.3)$$

Where ε is the steel emissivity, σ is the Stefan-Boltzmann constant (5.6703×10^{-8}) , $F_{v,L}$ is the view factor between the tank wall and the liquid surface, A_{26int} and T_{26} are the internal surface of node$_{26}$, facing on the lading and its temperature. $q_{V,rad}$ is the radiation received by the vapour, thus, the novel term, defined as:

$$q_{V,rad} = A_{26int} h_{V,r}(T_{26} - T_V) \quad (7.4)$$

Where the radiative heat-transfer coefficient from the wall to the vapour-phase ($h_{V,r}$) is calculate by the empirical correlation [Perry & Green, 1997]:

$$h_{V,r} = 5.6783 \frac{\left[\left(\frac{T_{26}}{100}\right)^4 - \left(\frac{T_V}{100}\right)^4\right] 0.173}{(T_{26} - T_V)} \quad (7.5)$$

The term of absorbed radiation by the vapour-phase in then added to the vapour node energy balance, as follows:

Vapour temperature (T_V) → Not boiling liquid:

$$m_V cv_V \frac{dT_V}{dt} = q_V + q_{V,rad} - q_{LV} - zz\phi \frac{RT_V}{MW} \quad (7.6)$$

Vapour temperature (T_V) → Boiling liquid:

$$m_V cv_V \frac{dT_V}{dt} = q_V + q_{V,rad} - q_{LV} - zz\phi \frac{RT_V}{MW} + \frac{dm_L}{dt}\left(cv_V(T_V - T_L) - zz\frac{RT_L}{MW}\right) \qquad (7.7)$$

Where m_V is the vapour mass, cv_V is the heat capacity of vapour at constant volume, zz is the compressibility factor, Φ is the mass flux discharged from PRV, R is the ideal gas constant and MW is the molecular weight. If the pressure relief valve is not installed or it is closed Φ is equal to zero simplifying the equation. The heat power q_V is the convective contribution pf the vapour-space walls.

Heat load from the flame

The heat flux from the flame to the shell was set as a constant input data in the previously version of the RADMOD code, in the novel implementation the input data are different and require to set the flame temperature and the flame emissivity, allowing the evaluation of a dynamic heat flux with respect to the wall effective temperature. The total flux from the flame to the external nodes can be expressed as the sum of a convective and a radiative contribution ($I_{ext} = I_{conv} + I_{rad}$). The radiative term is written in function of the generic temperature of the wall, in order to adapt the equation by replacing the generic wall temperature with the specific temperature, as shown below:

$$I_{ext} = \left(\sigma\varepsilon_s\left(\varepsilon_f T_f^4 + \left(1-\varepsilon_f\right)T_{amb}^4\right) - \left(\sigma\varepsilon_s T_w^4\right)\right)F_{v,a} + \left(1 - F_{v,a}\right)\sigma\varepsilon_s T_{amb}^4 \qquad (7.8)$$

Where T_w is the generic wall temperature, T_f is the flame temperature, ε_f and ε_s are the emissivity of the flame and of the steel wall, respectively, σ is the Stefan-Boltzmann constant (5.6703×10^{-8}). $F_{v,a}$ is a shape factor, it takes into account the case of distant source, in which the near-flame shell exchanges both with the ambient air and with the distant flame. Equation (7.8) is suggested by Heymes et al. through the study of an LPG tank exposed to fire. [Heymes et al. 2013] In the novel version of RADMOD $F_{v,a}$ is implemented to allow further development, thus its value is currently set equal to the unit.

Partial engulfment

In case the flame impingement affects only a portion of tank, the equations set remains unchanged as well as the nodes division, the only difference concerns the exchange areas between the flame and the external nodes. Thus, the temperatures obtained by the code are average over the nodes. The idea comes from the first RADMOD version [Landucci et al. 2013] where, in case of distant source, the nodes kept their configuration and only the external areas of exchange were modified. This improvement affects the balances of external nodes, $node_{37}$ and $node_{48}$ in case of coated tank or $node_{iL}$ and $node_{iV}$ if the vessel is unprotected, since the other two external nodes are not present, see Figure 7.2.

Unprotected tank → external $node_{iL}$ and $node_{iV}$ (T_{iV} and T_{iL})

$$d_s cp_{sL} \frac{s_s}{2}\overline{A_{iL}}\frac{dT_{iL}}{dt} = A_{iL,F}I_{ext,L} - A_{iL,A}I_{amb,L} - A_{iLint}\frac{k_{sL}}{s_s}(T_{iL} - T_{15}) \qquad (7.9)$$

$$d_s cp_{sV} \frac{s_s}{2}\overline{A_{iV}}\frac{dT_{iV}}{dt} = A_{iV,F}I_{ext,V} - A_{iV,A}I_{amb,V} - A_{iVint}\frac{k_{sV}}{s_s}(T_{iV} - T_{26}) \qquad (7.10)$$

Coated tank → external $node_{37}$ and $node_{48}$ (T_{37} and T_{48})

$$d_i cp_i \frac{s_i}{2} \overline{A_{37}} \frac{dT_{37}}{dt} = A_{37,F} I_{ext,L} - A_{37,A} I_{amb,L} - A_{37int} \frac{k_{iL}}{s_i} (T_{37} - T_{iL}) \quad (7.11)$$

$$d_i cp_i \frac{s_i}{2} \overline{A_{48}} \frac{dT_{48}}{dt} = A_{48,F} I_{ext,V} - A_{48,A} I_{amb,V} - A_{48int} \frac{k_{iV}}{s_i} (T_{48} - T_{iV}) \quad (7.12)$$

Where *d*, *cp*, *k* and *s* are respectively the density, the heat capacity, the thermal conductivity and the thickness of the steel, with subscript, or relative to the insulation, depending by the subscript *s* or *i*.

The areas ($\overline{A_{node}}$) represent the average nodal areas, the heat leaving the systems to the inner nodes is expressed in each equation as: $A_{node,int} \frac{k}{s} (T_{node} - T_{internal\ node})$, and represents the power heat transferred by conduction from the node of interest to the internal layer of the tank with which the node is in contact.

In case of partial engulfment $I_{extL/V}$ and $I_{ambL/V}$ are respectively, the heat flux that the shell receives from the flames and the heat flux transferred by the shell wall to the ambient air, on the liquid or vapour shell space depending by the subscript L or V.

The areas with the subscript *F* or *A* represent the surfaces engulfed by the flame (*F*) and the not engulfed surfaces in contact with ambient air (*A*). They are defined in equations set (7.13) and (7.14) respectively.

Fully engulfed tank

$$A_{ext\_node,F} = A_{ext\_node} \quad (7.13a)$$

$$A_{ext\_node,A} = 0 \quad (7.13b)$$

Half engulfed tank

$$A_{ext\_node,F} = \frac{A_{ext\_node}}{2} \quad (7.14a)$$

$$A_{ext\_node,A} = \frac{A_{ext\_node}}{2} \quad (7.14b)$$

The total external area of the node is A_{ext_node}, and it is calculated only on geometrical considerations on the tank geometry and on the liquid level. Whereas, the other terms depend on the engulfment degree, when the tank is partially engulfed the external surface of the nodes are halved and each half is redefined as the subscripted areas (*F*) and (*A*), respectively (eq. set 7.14). If the tank is fully engulfed in the flame, the areas which exchange with ambient (*A*) are set to zero, whereas the areas which exchange with the flame (*F*) are set equal to the totality of the external nodal surface (eq. set 7.13). So, in this case, the outgoing terms from the walls to the air being zero.

Thermal conductivity of insulation

The last novel implementation regards the input data required for the coating layer. This include the setting of the thermal conductivity, which could be insert as a constant or, if more information are available, as temperature dependent values. The second case is the new implementation, there are three values to insert depending on the temperature range and defining three thermal conductivities: k_{iL}, k_{iV} and k_{iJ}. The subscripts refer to different zone with which the insulation is in contact: the liquid wetted wall (*L*), the vapour space wall covered by the coating (*V*) and the external steel jacket (*J*). Each thermal conductivity differs from the others by the temperature range which is expected

to be reached in the zone in contact with the insulation. Thus, for coated tank, k_{iJ} is associated to the external nodes ($node_{37}$ and $node_{48}$), k_{iL} and k_{iV} are indeed associated to the intermediate nodes ($node_{iL}$ and $node_{iV}$) respectively.

7.2.4 Failure criteria

Two different failure criteria are used in the RADMOD code for the evaluation of the time to failure (ttf) of the tank. Both predict a conservative ttf, the first is the more simplified and conservative using the Von Mises criterion for the evaluation of ttf, whereas the second criterion is based on the standard BS7910:2013 "Guide to methods for assessing the acceptability of flaws in metallic structures". [BS7910, 2013]

Von Mises criterion

The axial (σ_{ax}), the circumferential (σ_{circ}) and the equivalent (σ_{eq}) stresses, according to Von Mises, are calculated as follows:

$$\sigma_{ax} = \frac{PR_e}{2s_s} \tag{7.15a}$$

$$\sigma_{ax} = \frac{PR_e}{s_s} \tag{7.15b}$$

$$\sigma_{eq} = \sqrt{\sigma_{ax}^2 + \sigma_{circ}^2 - \sigma_{ax}\sigma_{circ}} \tag{7.16}$$

The equivalent stress is compared with the admissible stress of the material (σ_{adm}) that is a function of temperature. For the evaluation of the admissible stress, the yield strength of the material (σ_Y) is divided for a safety factor (*S.F.*), considered equal to 1.1 in this work, which considers all the welds and the other unknown details that makes the vessel weaker:

$$\sigma_{adm} = \frac{\sigma_Y(T_{shell})}{S.F.} \tag{7.17}$$

The temperature at which is evaluated the yield strength is the maximum temperature among those of the shell nodes. This approach is the most easy and conservative for the evaluation of the ttf because the yield strength is calculated at the 0.2% of deformation, so it considers only the elastic field. The time to failure of the vessel is predicted through equation (7.18) as the first time when the following inequality is no more verified:

$$\sigma_{eq} > \sigma_{adm} \tag{7.18}$$

As already said, the results obtained from this criterion are very conservative, anyway in an actual accident there can be unpredictable severe damage on the shell itself and this results gives an idea of the worst real-case.

Standard BS7910:2013

The criterion used in the code is the basic application, low level called option 1, of the standard "Guide to methods for assessing the acceptability of flaws in metallic structures". [BS7910, 2013] It evaluates the ductile rupture considers the flaws in the material, in particular the weld as the critical zones. The crack propagation mode considered in this work is Mode I where the crack is opened by a tensile stress normal to the plane of the crack. Knowing detailed information on metallic surface much more detailed results could be obtained compared with the simplified approach explained above.

This criterion can be seen graphically in Figure 7.3, the assessment line is obtained by two dimensionless parameters: the load ratio (L_r) and the fracture ratio (K_r), defined in eqations (7.80 and 7.82) respectively. Inside the curves the stress is acceptable and the crack won't propagate, outside the curve the stress is too high so the tank is expected to fail:

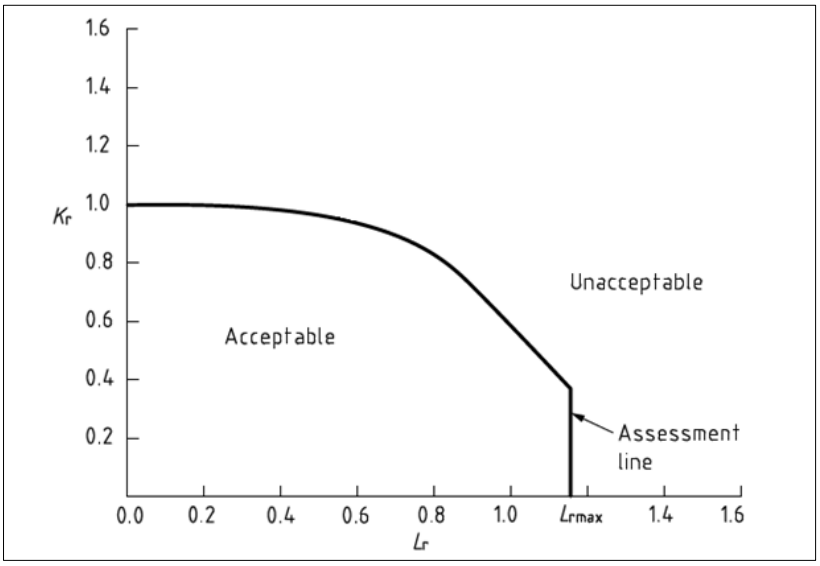

Figure 7.3 – Failure criteria according to BS7910:2013 [BS7910, 2013]

The load ratio is defined as:

$$L_r = \frac{\sigma_{eq}}{\sigma_Y(T_{shell})} \tag{7.19}$$

Where the equivalent stress can be evaluated with the Von Mises criteria and it is divided by the yield strength at the temperature of the material. The maximum value of the loading rate:

$$L_{r,max} = \frac{\sigma_u + \sigma_Y}{2\sigma_Y} \tag{7.20}$$

Where σ_u is the ultimate tensile strength of the material. If no material data is available it can be conservatively considered 1.

The fracture ratio is calculated as:

$$K_r = \frac{K_1}{K_{mat}} \tag{7.21}$$

Where K_1 is the stress intensity factor for the crack and K_{mat} is the material toughness. For the penny shaped crack, considered in RADMOD model:

$$K_1 = 2\sigma_{\max,\mathrm{Mohr}}\sqrt{\frac{a}{\pi}} \tag{7.22}$$

a is the radius of the crack with a set value of 2.5 mm, $\sigma_{\max,\mathrm{Mohr}}$ is the maximum stress obtained by the Mohr circle which corresponds to the circumferential stress σ_{circ} in this case. K_{mat} derives from material information and for the analysis of steel structures can be settled to 50 Mpa $m^{0.5}$.

Knowing K_r and L_r at every iteration it is possible to enter the graph and check if the shell can hold the pressure or it is expected to fail. For level 1 assessment the curve can be numerically evaluated as follows:

- $L_r \leq 1 \quad \rightarrow \quad f(L_r) = (1 + 0.5L_r^2)^{-\frac{1}{2}}[0.3 + 0.7e^{-\mu L_r^6}]$ (7.23a)
- $1 < L_r < L_{r,max} \quad \rightarrow \quad f(L_r) = f(1)L_r^{\frac{N-1}{2N}}$ (7.23b)
- $L_r \geq L_{r,max} \quad \rightarrow \quad f(L_r) = 0$ (7.23c)

Where $\mu = \min(0.001\frac{E}{\sigma_Y}; 0.6)$ and $N = 0.3\left(1 - \frac{\sigma_U}{\sigma_Y}\right)$ with E the Young module of material and for steel ASTM-A36 it is around 200Gpa [Engineering ToolBox, 2016].

7.2.5 Simplified stratification sub-models

Three simplified stratification sub-models are available in the RADMOD code, two of which are from literature and the third one is developed and tuned also on Computational Fluid Dynamics (CFD) calculations. Basically, the stratification sub-models split the liquid into two or three nodes individuating a liquid bulk at constant temperature and one or two nodes which are responsible for all the heat exchange and thus their temperature results altered. For all the theoretical consideration on the stratification and, in particular, on the effect on it of the PRV opening, see section 5.3. The latter effects are implemented in the model stopping the stratification sub-model at the first PRV opening, switching to the Baseline RADMOD model.

Generally, all the stratification sub-models are not good for coated tank as the time scale is longer and it is not reasonable that the bulk keeps the initial temperature with no heat exchange for the whole process. [Bazzocchi, 2014] For this reason, in this work only the third stratification sub-model (called *Strat 3*) is implemented in order to upgrade it with the novel parameters tuned by A. Rum [Rum, 2015] so for details and equations on the other two models (called *Strat 1* and *Strat 2*) refer to [Bazzocchi, 2014].

Strat 3

This approach is proposed by Bazzocchi [Bazzocchi, 2014] and further tuned in CFD simulations by Rum [Rum, 2015]. The version proposed in this work implements the upgrade obtained by Rum's CFD simulations, in the lumped RADMOD model.

The approach is similar to the *Strat 1* proposed by Birk [Birk, 2013], it is based on simplifying assumptions that do not involve the resolution of equations of motion. The liquid is split into two nodes considering that all the input heat is received by an upper stratified layer, laying above the bulk phase at constant temperature (see Figure 7.4).

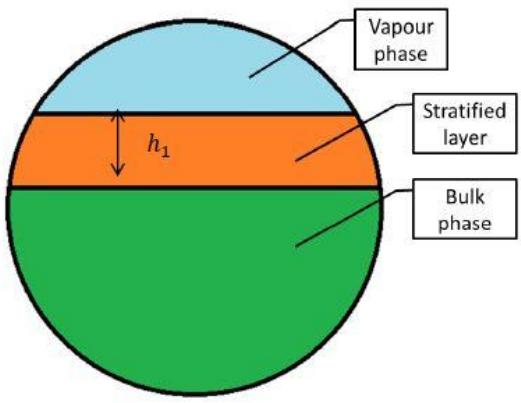

Figure 7.4 – Lading nodes according to the Strat 3 model [Bazzocchi, 2014]

The equations system is the same as in the Baseline RADMOD, the only difference is in the liquid mass, where instead of the whole liquid mass there is just the stratified layer part. Since all the heat received by the liquid goes to the stratified layer, to solve the system of equation a novel fitting parameter has to be entered: the height of the stratified layer h1. *Strat 1* model just assumed a constant thickness for the boundary layer used as fitting parameter that is difficult to tune and adapt to different geometries and was derived only for large scale configurations. Instead, as discussed on the following, the parameter was subjected to extended validation based first on experimental results [Bazzocchi, 2014] and then results of detailed CFD modelling. [Rum, 2015]

The previously prediction of the value of h_1 is found by comparison of several RADMOD simulations against experimental data, changing the value to perfectly match the the time to open of the PRV, it results in the following correlation:

$$\frac{h_1}{D_i} = 0.0861\sqrt{\frac{P_{open,PRV} - P_{in}}{D_i FD}} \tag{7.24}$$

Where D_i is the inner diameter of the tank (in m), the pressure difference (in bar) is given by the opening pressure of the PRV and the initial pressure of the tank and FD is the initial volumetric filling level as a fraction, empty is 0 and full is 1.

The novel correlation for the evaluation of the height of the stratified layer is reported below in equation (7.25) and the relative coefficient values are reported in Table 7.3:

$$\frac{h_1}{D_i} = a_1 + a_2 \cdot FD + a_3 \cdot Heat\ Flux + a_4 \cdot (P_{open,PRV} - P_{in}) \tag{7.25}$$

Where the not-already defined variable is the $Heat\ Flux$ expressed in W/m^2, this parameter is calcuted through equation (7.8) setting the value of T_{wall} equal to the initial temperature T_{in}, int his way the maximum heat flux over the external wall is evaluated and thus a maximum value of h_1 is obtained.

Table 7.3 – Coefficient values for the evaluation of h_1 in the novel implementation of Strat 3 model [Rum, 2015]

coefficient	value
a1	-0.1042
a2	0.3027
a3	$1.2 \cdot 10^{-6}$
a4	$-8 \cdot 10^{-9}$

Quite clearly, the value of h_1 cannot exceed the level in the tank. In case the correlation results in values of h_1 higher than the actual height occupied by the liquid, it means the stratification phenomenon is not relevant. This usually occurs for low values of volumetric filling level, as documented by experimental observations [Heymes et al. 2013]. The MatLab code checks this and in the case of no stratification it just runs the Baseline RADMOD.

Once it is known the value of h_1, the mass of the liquid going into the equations system is simply derived; it is possible to evaluate the 'level' of the bulk (L_{bulk}) as:

$$L_{bulk} = L - h_1 \tag{7.26}$$

So the mass of the bulk and of the stratified layer are:

$$m_{bulk} = \rho_L R_i^2 W \left(\cos^{-1}\left(\frac{R_i - L_{bulk}}{R_i}\right) - \sin\left(\frac{R_i - L_{bulk}}{R_i}\right)\left(\frac{R_i - L_{bulk}}{R_i}\right)\right) \quad (7.27)$$

$$m_{Strat.L.} = m_{tot,liquid} - m_{bulk} \quad (7.28)$$

This model is active only before the opening of the PRV and the evaporated part is small, the bulk layer is considered at constant mass and temperature so all the heat and mass exchange is happening with the stratified liquid layer. At the opening of the PRV an instant mixing occurs, so to evaluate the average liquid temperature it is possible to do an energy balance to a perfect mixer:

$$m_L cp_L (T_L - T_{bulk}) = m_{boundary\ layer} cp_L (T_{boundary\ layer} - T_{bulk}) \quad (7.29)$$

Where m_L is the total liquid mass and cp_L is the specific heat of the liquid evaluated at an average temperature of the temperature difference multiplying it.

Since all the heat received by the liquid goes to the stratified layer, the equations system is the same as in the Baseline RADMOD, the only difference is in the liquid mass, where instead of the whole liquid mass there is just the stratified layer part.

7.3 Upgrade of the lumped model: simulation of defective coatings

The RADMOD model described in the previously section allows the prediction of the behaviour of unprotected and coated tanks, in this thesis work it is implemented a thermal sub-model able to predict the response of the coating in presence of defects in itself. Chapter 3 is aimed to characterize this thermal insulation defects, there can be seen that the defects in insulation systems considered in this work are air gaps formed between the external steel jacket and the shell of the vessel. The phenomena taking place in this enclosure are described in paragraph 6.1.1.

For the implementation of the sub-model, first the nodes division is revised through a geometrical analysis of the problem, then the heat exchanges between the nodes are modified to add the terms related to the novel nodes. The model is validated against experimental data explained in section 3.4, and the validation results are discussed in section 9.3. Due to the particular conditions used in the experimental tests used for the model validation another sub-model is needed, this is reported in paragraph 7.3.2. Both the Baseline and the Strat 3 RADMOD models are enhanced for the simulation of defective coatings and are implemented in the RADMOD sub-model.

7.3.1 Thermal sub-model for defects on thermal insulation system

RADMOD nodes

The nodes division of the Baseline code is modified and four new nodes are individuated for the defective zone, a sketch of the section of the tank and the related division in nodes are shown in Figure 7.5 and 7.8.

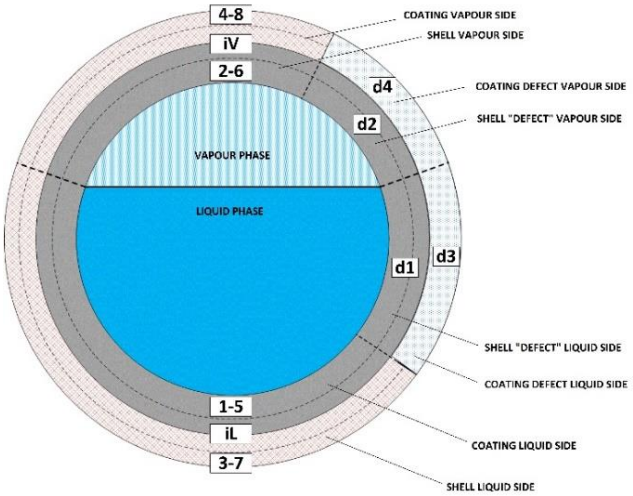

Figure 7.5 – Sketch of the vessel and the related node division in the novel RADMOD model for defective coatings

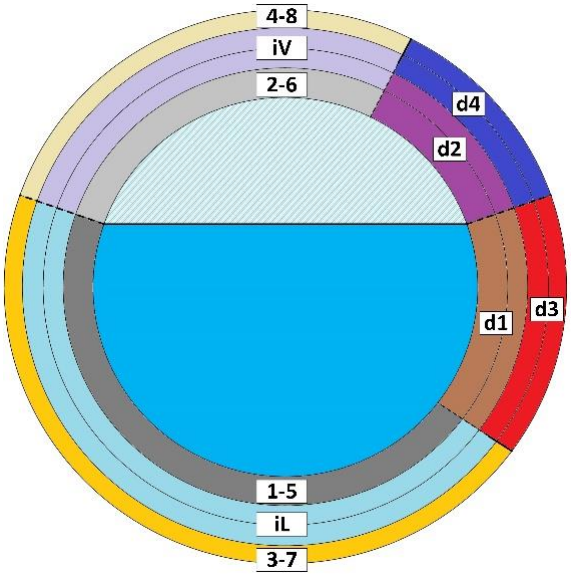

Figure 7.6 – Node division in the novel RADMOD model for defective coatings

The nodes considered in Section 7.2.2 are the same in this novel sub-model, with the addition of four new nodes:

- Node d1 → Shell wall in contact with the liquid and with the air gap
- Node d2 → Shell wall in contact with the vapour and with the air gap
- Node d3 → Coating defect of liquid side (air gap)
- Node d4 → Coating defect of vapour side (air gap)

The input data required in this thermal sub-model are reported below and can be seen in Figure 7.7:

- Defect top height (H_{top})
- Defect bottom height (H_{btm})
- Defect length (L_{def})

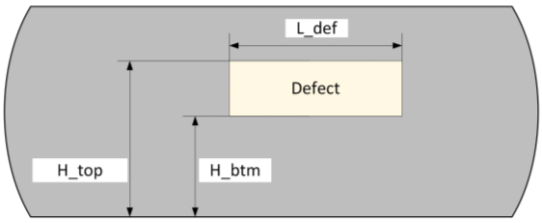

Figure 7.7 – Required input defect data in the novel RADMOD model for defective coatings

Knowing the liquid level in every iteration the code estimates the defect area in the vapour or in the liquid space. The greatest difficulty was to define the novel exchange areas and upgrade the existing ones, as mentioned in the previously section, the definition of three areas for each nodes could be reviewed to make the model easier to handle.

Defective areas definition

First the angles formed by the top and bottom heights of the defect are calculated through the equations set (7.30) and the angles sketch is shown in Figure 7.8.

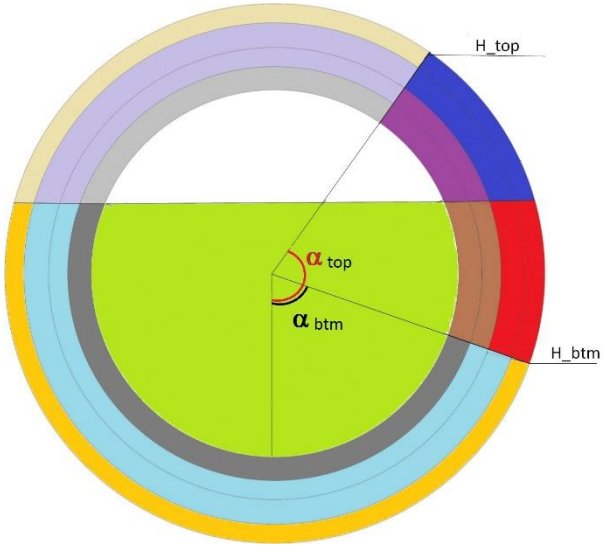

Figure 7.8 – Definition of defect angles in the novel RADMOD model

$$\alpha_{top} = \text{acos}\left(\frac{(R_e+s_i)-H_{top}}{R_e+s_i}\right) \quad (7.30a)$$

$$\alpha_{top} = \text{acos}\left(\frac{(R_e+s_i)-H_{btm}}{R_e+s_i}\right) \quad (7.30b)$$

Where R_e is the external radius of the vessel and s_i is the thermal insulation thickness.

Now, three cases are possible: the defect is both in liquid and vapour space or the defect is only in one phase space, liquid or vapour. The model checks this condition comparing the height of defect with the liquid level, in every iteration. Thus the areas can be defines as shown in equations (7.31a-7.38a). Whereas the averaged value of the nodal defect areas is expressed in general form in equation (7.39):

Defect in both liquid and vapour space

$$A_{d1,int} = L_{def} R_i \left(\text{acos}\left(\frac{R_i - L}{R_i}\right) - \alpha_{btm}\right) \quad (7.31a)$$

$$A_{d1,ext} = L_{def} R_e \left(\text{acos}\left(\frac{R_e - L}{R_e}\right) - \alpha_{btm}\right) \quad (7.32a)$$

$$A_{d2,int} = L_{def} R_i \left(\alpha_{top} - \text{acos}\left(\frac{R_i - L}{R_i}\right)\right) \quad (7.33a)$$

$$A_{d2,ext} = L_{def} R_e \left(\alpha_{top} - \text{acos}\left(\frac{R_e - L}{R_e}\right)\right) \quad (7.34a)$$

$$A_{d3,int} = A_{d1,ext} \quad (7.35a)$$

$$A_{d3,ext} = L_{def}(R_e + s_i)\left(\text{acos}\left(\frac{(R_e + s_i) - L}{R_e + s_i}\right) - \alpha_{btm}\right) \quad (7.36a)$$

$$A_{d4,int} = A_{d2,ext} \quad (7.37a)$$

$$A_{d4,ext} = L_{def}(R_e + s_i)\left(\alpha_{top} - \text{acos}\left(\frac{(R_e + s_i) - L}{R_e + s_i}\right)\right) \quad (7.38a)$$

$$\overline{A_d} = \frac{A_{d,int} + A_{d,ext}}{2} \quad (7.39)$$

Where R_i is the internal radius of the vessel and L is the liquid level, thus $\text{acos}\left(\frac{R-L}{R}\right)$ represents the angle formed by the liquid level defined in the same way as α_{top} and α_{btm} are defined in equations set (7.30).

The case in which the defect is only on the liquid side can happen only if the initial value of H_{top} results lower that the liquid level. Whereas the other case, defect in vapour side only, corresponds to H_{btm} greater than L and it can also take place during the simulation due to level falls below the defect lower height H_{btm}. In these cases one side (liquid or vapour) has no "defective" nodes, so, to keep the model simple, rather than define another set of equations for each case, the areas corresponding to the nodes no more present are set to zero. Thus the areas definitions reported in sets (7.31a – 7.38a) are modified in the equations (7-31b – 7.38b) and (7-37c – 7.38c) for defect only in liquid and vapour side, respectively, as follows:

Defect in liquid side only

$$A_{d1,int} = L_{def} R_i \left(\alpha_{top} - \alpha_{btm}\right) \quad (7.31b)$$

$$A_{d1,ext} = L_{def} R_e \left(\alpha_{top} - \alpha_{btm}\right) \quad (7.32b)$$

$$A_{d2,int} = 0 \quad (7.33b)$$

$$A_{d2,ext} = 0 \quad (7.34b)$$

$$A_{d3,int} = A_{d1,ext} \quad (7.35b)$$

$$A_{d3,ext} = L_{def}(R_e + s_i)\left(\alpha_{top} - \alpha_{btm}\right) \quad (7.36b)$$

$$A_{d4,int} = 0 \quad (7.37b)$$

$$A_{d4,ext} = 0 \quad (7.38b)$$

Defect in vapour side only

$$A_{d1,int} = 0 \quad (7.31c)$$

$$A_{d1,ext} = 0 \quad (7.32c)$$

$$A_{d2,int} = L_{def} R_i \left(\alpha_{top} - \alpha_{btm}\right) \quad (7.33c)$$

$$A_{d2,ext} = L_{def} R_e \left(\alpha_{top} - \alpha_{btm}\right) \quad (7.34c)$$

$$A_{d3,int} = 0 \quad (7.35c)$$

$$A_{d3,ext} = 0 \quad (7.36b)$$

$$A_{d4,int} = A_{d2,ext} \quad (7.37c)$$

$$A_{d4,ext} = L_{def}(R_e + s_i)\left(\alpha_{top} - \alpha_{btm}\right) \quad (7.38c)$$

In both cases the average area of the not-present nodes cannot be calculated as the mean of internal and external areas, because the heat exchange equations between the nodes are not changed and thus an averaged value of the nodal area equal to zero generates an indeterminate form in the resolution of the equation. For these reason, in case of defect only in one of the fluid-phase side, the averaged defect nodal areas are set to unit for the not-present nodes, the equations results do not change because all the other related areas are set to zero but it avoids the inseminate form. Thus, equation (7.39a) is valid for the existing nodes, while for the other nodes it is defined as in equation (7.39b):

If $A_{d,int/ext} \neq 0$

$$\overline{A_d} = \frac{A_{d,int} + A_{d,ext}}{2} \quad (7.39a)$$

If $A_{d,int/ext} = 0$

$$\overline{A_d} = 1 \quad (7.39b)$$

Now that the defect nodal areas are defined they are subtracted from the surfaces defined in the Baseline RADMOD model, following the schematization reported in Figure 7.6.

With the configuration reported above, the defect can cover a maximum of half total insulation surface and in case of half engulfed tank the defect is assumed to be on the engulfed side. The validation model (see paragraph 7.3.2) has a different configuration that may be used for implementation of a defect on both tank sides.

RADMOD equations in presence of defective coatings

Since all the nodal are are modified with respect the defect position, which changes in function of the liquid level during the simulation, and since no conduction through the shell is considered in the RADMOD model, the heat exchange equations defined for the Baseline RADMOD are valid and untouched with the exception of the liquid and vapour ones. This equations are the same as in the Baseline but with the addition of the exchanging terms with the defective nodes. At the variables defined for the Baseline RADMOD model are added four new variables and related equations for the defective nodes:

- Temperature of shell in contact with the liquid and defect T_{d1}
- Temperature of shell in contact with the vapour and defect T_{d2}
- Temperature of defect in contact with the flame on liquid side T_{d3}
- Temperature of defect in contact with the flame on vapour side T_{d4}

For the heat exchange phenomena taking place inside the defect enclosure, refer to paragraph 6.1.1. For what concerns the fundamental equations implemented in the RADMOD Baseline and in the novel sub-models for defective coating, the summaries are reported in appendix A.

A schematisation of all the exchanges tanking pace in this problem is reported in Figure 7.9 where the nodes shown in Figure 7.5 are exploded in single blocks. The radiative fluxes are indicated with the red arrows, the convective heat transport with the green ones and the conductive exchanges are the blue arrows. The flame, and the ambient air exchanges in case of partially engulfed tank, are graphically on the left side.

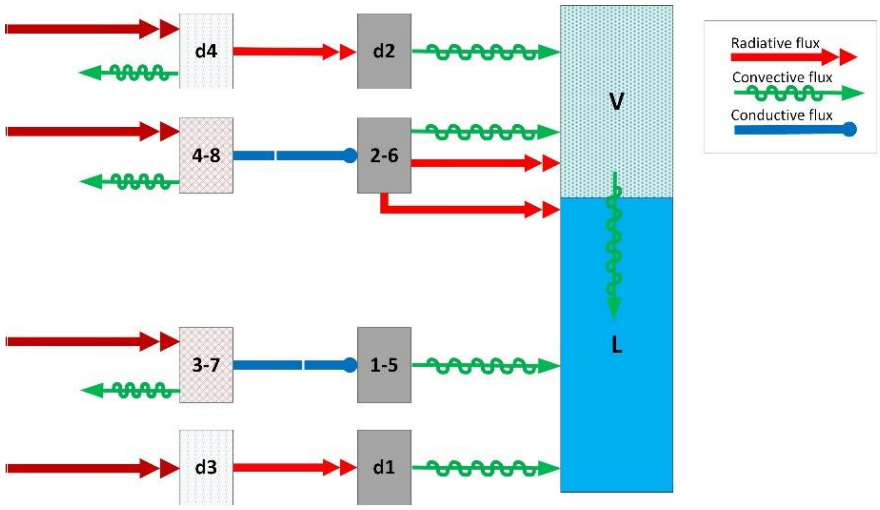

Figure 7.9 – Schematization of the nodes and the exchanges between them of the novel RADMOD sub-model for defective coatings

Temperature of shell under defect in contact with liquid phase (T_{d1})

$$d_s cp_{sL} s_s \overline{A_{d1}} \frac{dT_{d1}}{dt} = A_{d1ext} q_{d3,rad} - q_{d1,L} \quad (7.40)$$

Where d_s, cp_{sL} and s_s are the density, heat capacity and thickness of the carbon steel shell. The heat capacity of the shell (cp_{sL}) is calculated as a function of the temperature, $s_s\overline{A_{d1}}$ represents the volume of the material to be heated. $q_{d3,rad}$ is the radiative heat power recived by the shell from the surrounding air gap, expressed by equation (7.59) and $q_{d1,L}$ is the convective heat transmitted from the shell to the liquid node and it is estimated through the equation (7.47).

Temperature of shell under defect in contact with vapour phase (T_{d2})

$$d_s cp_{sV} s_s \overline{A_{d2}} \frac{dT_{d2}}{dt} = A_{d2ext} q_{d4,rad} - q_{d2,V} \quad (7.41)$$

Where $s_s\overline{A_{d2}}$ is the nodal volume, $q_{d3,rad}$ is the radiative heat power defined by equation (7.59) and $q_{d2,V}$ is the convective and radiative heat transmitted from the shell to the vapour node and it is estimated through equation (7.55).

Temperature of defect air gap in liquid side in contact with the flame (T_{d3})

$$d_a cp_a s_i \overline{A_{d3}} \frac{dT_{d3}}{dt} = A_{d3ext} I_{ext} - A_{d1ext} q_{d3,rad} \quad (7.42)$$

Where d_a and cp_a are respectively the density and the heat capacity of the air inside the enclosure defined in equation (7.60) and (7.61) respectively. I_{ext} is the radiative and convective heat load from the flame to the external nodal surface, it is calculated with the equation (7.8) defined for the Baseline RADMOD with adequate value of variables. $s_i\overline{A_{d3}}$ represent the nodal volume.

Temperature of defect air gap in liquid side in contact with the flame (T_{d4})

$$d_a cp_a s_i \overline{A_{d4}} \frac{dT_{d3}}{dt} = A_{d4ext} I_{ext} - A_{d2ext} q_{d4,rad} \quad (7.43)$$

In the same way in which the balance of external node in liquid side is defined, also the equation for the vapour side external node is defined as shown in equation (7.43).

Liquid temperature upgrades

Equation (7.1) for the evaluation of the liquid temperature in case of not boiling liquid is valid because the fluid still receives the same heat powers from the pre-existent nodes. Since the radiative flux from the node$_{d2}$ is currently neglected, only one term is added to this equation: the convective contribute from the inner wall of node$_{d1}$. Equation (7.2) relative at the liquid temperature in case of boiling liquid is clearly untouched, since the variation of the liquid temperature in this case is zero. The novel equation for the not boiling liquid is:

$$m_L cv_L \frac{dT_L}{dt} = \left[q_{L,boil} + q_{L,rad} + q_{LV}\right] + q_{d1,L} \quad (7.44)$$

The unchanged terms are in square bracket, and the only term in more than (7.1) is $q_{d1,L}$ which is defined in equation (7.47) with the appropriate parameters reported before.

Vapour temperature upgrades

The equations (7.6) and (7.7) for the vapour temperature evaluation, respectively for not boiling and boiling liquid, both have in this sub-model one more term, which corresponds to the convective exchange with node$_{d2}$ inner surface defined as $q_{d2,V}$ and calculated from equation (7.55) with the appropriate parameters. The equations implemented in the RADMOD model for defective coating are:

Not boiling liquid:

$$m_V cv_V \frac{dT_V}{dt} = \left[q_V + q_{V,rad} - q_{LV} - zz\phi \frac{RT_V}{MW}\right] + q_{d2,V} \quad (7.45)$$

Boiling liquid:

$$m_V cv_V \frac{dT_V}{dt} = \left[q_L + q_{V,rad} - q_{LV} - zz\phi \frac{RT_V}{MW} + \frac{dm_L}{dt}\left(cv_V(T_V - T_L) - zz\frac{RT_L}{MW}\right)\right] + q_{d2,V} \quad (7.46)$$

Heat power to the liquid from "defective" liquid-space wall (node$_{d1}$)

The heat power received through convection by the liquid from node$_{d1}$ walls, is expressed as:

$$q_{d1,L} = A_{d1int} h_L (T_{d1} - T_L) \quad (7.47)$$

Where h_L is the convective heat transfer coefficient and it depends on the pool boiling regime (see chapter 5). Two cases are possible:

- Interface evaporation $T_{d1} < T_{boil} + 2℃$ → Natural convection

- Nucleate boiling $T_{d1} \geq T_{boil} + 2℃$

For natural convection, the coefficient is obtained defining first the dimensionless numbers Prandtl, Grashof and Rayleigh, for liquid properties (subscript L) and for the hot horizontal flat surfaces facing upward, as reported in [Perry & Green, 1997], as:

$$Pr_L = \frac{\mu_L cp_L}{k_L} \tag{7.48a}$$

$$Gr_L = \frac{x_i^3 \rho_L^2 g(T_{d1} - T_L)\beta_L}{\mu_L^2} \tag{7.48b}$$

$$Ra_L = Gr_L Pr_L \tag{7.48c}$$

Where g is the gravitational acceleration and β_L the compressibility of liquid and x_i is the characteristic length and it is calculated as ratio of four times the surface and the wetted perimeter involved in the phenomenon:

$$x_i = \frac{4A_{d1int}}{2\left(W + {}^{A_{d1int}}/_{W}\right)} \tag{7.49}$$

Where W is the tank length.

Then the coefficient h_L is calculated through the Nusselt number, as follows:

$$Nu_L = f(Ra_L) = \frac{h_L x_i}{k_L} \tag{7.50}$$

Where the function which links Nu_L to Ra_L, depends on the value of the latter dimensionless number (Ra_L).

In the case of nucleate boiling, there are several possible formulations for this phenomenon which have been included in the Matlab code following the design correlations of evaporators. Here it is reported one of the equation suggested in [Perry & Green, 1997]:

$$h_L = 3.75 * 10^{-5} P_c^{0.69} q^{"0.7} \left[1.8\left(\frac{P}{P_c}\right)^{0.17} + 4\left(\frac{P}{P_c}\right)^{1.2} + 18\left(\frac{P}{P_c}\right)^{10}\right] \tag{7.51}$$

Where P_c is the critical pressure and $q^{"} = h_L(T_{15} - T_L)$.

The critical flux (see chapter 5) is reached when the inequality (7.54) by [Perry & Green, 1997] is not more verified:

$$q^{"}_{max} = 0.18\rho_V \Lambda \left(\frac{(\rho_L - \rho_V)\sigma g}{\rho_V^2}\right)^{1/4} > h_L(T_{d1} - T_L) \tag{7.52}$$

Where ρ_L and ρ_V are the density of the liquid and the vapour of the fluid calculated at T_L.

Heat power to the vapour from "defective" vapour-space wall (node$_{d2}$)

The total heat entering the vapour node is the sum of a convective contribution $q_{V,conv}$ and a radiative contribution $q_{V,rad}$:

$$q_{d2,V} = q_{V,conv} + q_{V,rad} = A_{d2int} h_{V,c}(T_{d2} - T_V) + A_{d2int} h_{V,r}(T_{d2} - T_V) \tag{7.53}$$

The radiative heat transfer coefficient $h_{V,r}$ is currently set equal to zero, for further evaluation. Whereas, the convective coefficient is calculate with the equations (7.56) or with equation (7.58) depending on the PRV function.

If the PRV is closed, defining the dimensionless key parameters of equations set (7.48) but with the subscript V and changing the characteristic length as shown in equation (7.57), the convective coefficient is [Perry & Green, 1997]:

$$Nu = \frac{h_{V,c}\, xi}{k_V} = 0.27Ra^{1/4} \tag{7.54}$$

$$x_i = \frac{4A_{d2int}}{2\left(W + {}^{A_{d2int}}/_{W}\right)} \tag{7.55}$$

If the PRV is opened, forced convection is also considered ($h_{V,forced}$) and added to the natural convection coefficient.

$$Nu = \frac{h_{V,forced}\, xi}{k_V} = 0.0243Re^{0.8}Pr^{0.4} \tag{7.56}$$

Where:

$$Pr = \frac{\mu_V cp_V}{k_V} \;;\; Re = \frac{4\phi}{p\mu_V} \tag{7.57}$$

Where ϕ is the mass flow throughout the PRV and characteristic length (x_i) is given by the ratio of the section of vapour phase and the wetted perimeter according to:

$$x_i = \frac{4A_{vap}}{p_{wetted}} = \frac{R_i^2\left(cos^{-1}\left(\frac{L-R_i}{R_i}\right) - sin\left(\frac{L-R_i}{R_i}\right)\left(\frac{L-R_i}{R_i}\right)\right)}{2\pi cos^{-1}\left(\frac{L-R_i}{R_i}\right)} \tag{7.58}$$

Heat exchange inside the defect

The mechanisms of heat transport in the enclosure are discussed in paragraph 6.1.1, where is assessed that the radiation is the main mechanism in the air gap. Thus the two terms of radiative transport $q_{d3,rad}$ and $q_{d4,rad}$ can be the defined as:

$$q_{d,rad} = \sigma\varepsilon_s\left(T_{d,ext}^4 - T_{d,int}^4\right) \tag{7.59}$$

Where $T_{d,ext}$ is the temperature of the external node which irradiates the internal node at temperature $T_{d,int}$.

Air properties inside the enclosure

The density of the air is calculated through the ideal gas law:

$$d_a = \frac{P\, Mw_a}{R\, T} \tag{7.60}$$

Mw_a is the molecular weight of air, P and T are the pressure inside the enclosure, the pressure is set equal to the atmospheric value and the temperature is the mean between the temperature of the defect nodes ($node_{d3}$ and $node_{d4}$).

The heat capacity of the air inside the enclosure is estimated as a function of the temperature, defined as the mean of the defect nodes temperatures. The correlation is from [Knudsen et al. 1999b]. The equation for the air heat capacity is:

$$cp_a = \left(cv_1 + cv_2 \left(\frac{cv_3}{T \sinh\left(\frac{cv_3}{T}\right)} \right)^2 + cv_4 \left(\frac{cv_5}{T \cosh\left(\frac{cv_5}{T}\right)} \right)^2 \right) \quad (7.61)$$

Where cv_{1-5} are constant relative to the gas.

7.3.2 Validation thermal sub-model for defects on thermal insulation system

The data used for the validation of the sub-model for defective coating and the tests conditions are described in Section 3.4. The node division are defined in order to recreate the tests conditions, and this is shown in Figure 7.10.

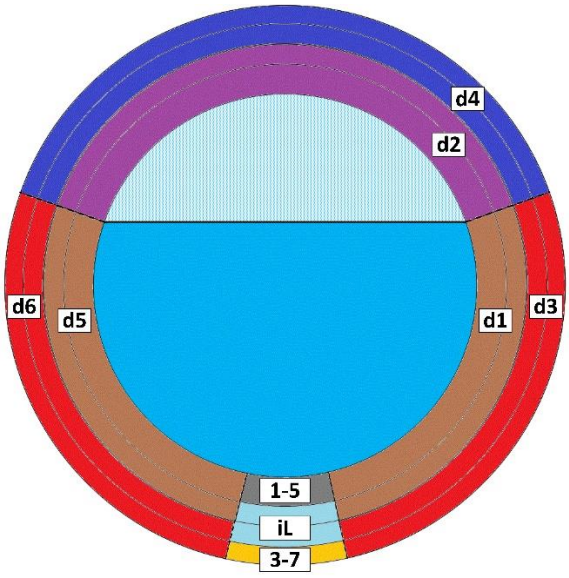

Figure 7.10 – Tank central section schematised of the nodes for the validation sub-model of the RADMOD for defective coatings

It should be reminded that in the tests the fire engulfs only half of the tank which corresponds at the right side of the schematisation reported above (Figure 7.10), the nodes corresponding to the not-defective insulation cannot be see in this sketch, but there are already present (see Figure 3.6 in Section 3.4). Compared with the previously division, (see Figure 7.6) two more nodes are added:

- Node d5 → Shell wall in contact with the liquid and with the not engulfed defect node$_{d6}$
- Node d6 → Not engulfed coating defect of liquid side (air gap)

Areas definition

For what concerns the engulfed nodes on the liquid side (node$_{d1}$ and node$_{d3}$) the areas defined in the equations sets (7.31-32) and (7.35-36) remain untouched. While node$_{d2}$ and node$_{d4}$ are now extended to the left side of the tank and they are partially engulfed. The areas definition, also in this case, remain unchanged and when the validation sub-model is activated the only measure to adopt is to set the top height of the defect equal to the external diameter, including the insulation thickness, of the tank. In fact the validation sub-model doubling the values of the nodal areas obtained with the equations sets (7.33-34) and (7.37) corresponding to internal and external surfaces of node$_{d2}$ and the internal surface of node$_{d4}$, but not the external surface of the latter node. In fact, node$_{d4}$ is now engulfed partially, so half of its external area exchanges with the flame

and the other half with the ambient air, for this reason equation (7.38) is still used for determination of the external surface of node$_{d4}$ and the area thus obtained is used for both the flame and the ambient air exchanges, see equation (7.70).

The surfaces of the two novel nodes on liquid side are set equal to the surfaces of the liquid side nodes already present, since the problem results to be symmetrical:

$$A_{d5} = A_{d1} \tag{7.62}$$

$$A_{d6} = A_{d2} \tag{7.63}$$

Equations (7.62) and (7.63) are valid for the internal, external and averaged surfaces of the new nodes (node$_{d5}$ and node$_{d6}$).

Equations definition in the RADMOD validation sub-model

Two more variables and thus two more equations are added in this sub-model. The new variables are:

- Temperature of shell in contact with the liquid and the not-engulfed defect T_{d5}
- Temperature of not-engulfed defect in contact with ambient air on liquid side T_{d4}

Figure 7.11 is the upgraded Figure 7.9 which report the nodes as a blocks and the interaction between each other.

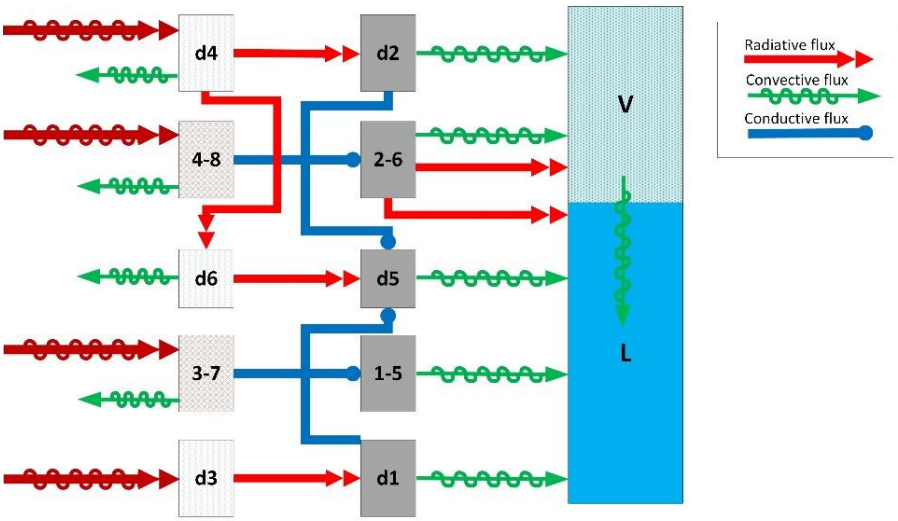

Figure 7.11 – Schematization of the nodes and the exchanges between them of the RADMOD validation sub-model for defective coatings

As can be seen in Figure 7.11, the only equations changed in the validation sub-model are the ones corresponding to the nodes which exchange with the novel node (node$_{d5}$ and node$_{d6}$).

Temperature of not-engulfed shell in contact with liquid (T_{d5})

This node is on the not-engulfed side of the tank, the entering heat powers come from the defective air gap radiating the node and it is assumed that also the conduction mechanism from the adjacent nodes goes to heat up the node, as shown in equation (7.64):

$$d_s cp_{sL} s_s \overline{A_{d5}} \frac{dT_{d5}}{dt} = A_{d5ext} q_{d6,rad} + A_{d2d5} q_{d2,cond} - A_{d5int} q_{d5,L} + A_{d1d5} q_{d1,cond} \quad (7.64)$$

The heat capacity of the steel shell (cp_{sL}) is calculated as a function of the temperature of the node. $s_s\overline{A_{d5}}$ is the nodal volume and $\overline{A_{d5}}$, A_{d5ext} and A_{d5int} are obtained through the equation (7.62), $q_{d6,rad}$ is the heat flux entering the node by radiation from the surrounding node$_{d6}$, it is evaluated as shown in equation (7.71). $q_{d5,L}$ is the convective heat from the shell to the liquid, as for the evaluation of $q_{d1,L}$, it is estimated through the equation (7.47) with appropriate value of area (A_{d5int}) and temperature difference ($T_{d5} - T_L$). Two conduction terms are present in equation (7.64) one from the vapour side node ($q_{d2,cond}$) and the other one from the liquid engulfed side ($q_{d1,cond}$), they are introducted to increase the heat load reached by this node and are respectively defined in equations (7.72) and (7.73). The exchanging area associated with the conduction terms are:

$$A_{d2d5} = A_{d1d5} = L_{def} s_s \quad (7.65)$$

There are the orthogonal surfaces to the cylinder axis, in the interface of node$_{d2}$ - node$_{d5}$ and node$_{d1}$ - node$_{d5}$, respectively.

Temperature of not-engulfed defect of liquid in contact with the ambient air (T_{d6})

This node receives heat from the above node$_{d4}$ and removes the heat away from node$_{d5}$ through radiation and from external ambient air:

$$d_a cp_a s_i \overline{A_{d6}} \frac{dT_{d6}}{dt} = A_{d4d6} q_{d4,rad} - A_{d5ext} q_{d6,rad} - A_{d6ext} I_{amb} \quad (7.66)$$

The air properties d_a and cp_a are respectively calculated by equations (7.60) and (7.61), the volume of the air in the node is expressed by $s_i\overline{A_{d6}}$ and $q_{d4,rad}$ is the radiative power from node$_{d6}$,defined in equation (7.78), its exchange surface is defined as:

$$A_{d4d6} = L_{def} s_i \quad (7.67)$$

The latter equation is the same as those defined for the conductive exchange in equation (7.65), thus it is the interface between the two nodes (node$_{d4}$ and node$_{d6}$). Further investigation on this area definition should be considered. The other areas A_{d6ext} and $\overline{A_{d6}}$ follow the equation (7.63).

I_{amb} is the exchange by radiative and convective mechanisms from the node external surface to the ambient air.

Equations upgrade

The equations used for the implementation of the thermal sub-model for defective coating are the same in the validation model with the addition of the terms of exchange with node$_{d5}$ and node$_{d6}$, the modified equations are reported below with the unchanged terms in square bracket:

Temperature of node$_{d1}$ (T_{d1})

$$d_s cp_{sL} s_s \overline{A_{d1}} \frac{dT_{d1}}{dt} = \left[A_{d1ext} q_{d3,rad} - q_{d1,L}\right] - A_{d1d5} q_{d1,cond} \quad (7.68)$$

Temperature of node$_{d2}$ (T_{d2})

$$d_s cp_{sV} s_s \overline{A_{d2}} \frac{dT_{d2}}{dt} = \left[A_{d2ext} q_{d4,rad} - q_{d2,V}\right] - A_{d2d5} q_{d2,cond} \quad (7.69)$$

Temperature of node$_{d4}$ (T_{d4})

$$d_a cp_a s_i \overline{A_{d4}} \frac{dT_{d4}}{dt} = \left[A_{d4ext} I_{ext} - A_{d2ext} q_{d4,rad}\right] - A_{d4ext} I_{amb} - A_{d4d6} q_{d4,rad} \quad (7.70)$$

Temperature of liquid (T_L)

$$m_L cv_L \frac{dT_L}{dt} = \left[q_L + q_{LV} + q_{d1,L}\right] + A_{d5int} q_{d5,L} \quad (7.71)$$

Heat load from the flame

The radiative part of heat that from the flame reaches the external steel jacket, expressed through equation (7.8) in the validation model is modified in order to set the black body temperature as input instead of the flame temperature. The two temperatures are linked together through the flame emissivity as: $\varepsilon_f \cdot T_f^4 = T_{BB}^4$ [Modest, 2003], thus, replacing the term $(\varepsilon_f \cdot T_f^4)$ in equation (7.8), the latter becomes:

$$I_{ext} = \sigma\varepsilon_s\left(T_{BB}^4 + \left(1 - \varepsilon_f\right)T_{amb}^4\right) - \left(\sigma\varepsilon_s T_w^4\right) \quad (7.72)$$

Heat loads to the shell node of not-engulfed liquid side (node$_{d5}$)

The radiant flux at input of the node is written as:

$$q_{d6,rad} = \sigma\varepsilon_s(T_{d6}^4 - T_{d5}^4) \quad (7.73)$$

Equation (7.73) corresponds to the equation (7.59), with the adequate parameters, used for the evaluation of the heat transported by radiation inside the enclosure.

The other two thermal inputs at the shell node are both conductive from the engulfed shell nodes:

$$q_{d1,cond} = \frac{k_{sL}}{d_{condL}}(T_{d1} - T_{d5}) \quad (7.74)$$

$$q_{d2,cond} = \frac{k_{sV}}{d_{condV}}(T_{d2} - T_{d5}) \quad (7.75)$$

The thermal conductivities k_{sL} and k_{sV} are estimating as functions of the temperature of each node. The term d_{cond} is the distance between the node through which the conductive exchange takes place. It is assumed equal to the circumferential arc from the higher point of the heating node, to the start of the node to be heat, that are:

$$d_{condL} = \frac{R_i}{2}\mathrm{acos}\left(\frac{R_i - L}{R_i}\right) \quad (7.76)$$

$$d_{condV} = \left(R_i + \frac{s_s}{2}\right)\alpha_{top} \quad (7.77)$$

The subscript (L) is associated to the conduction from the engulfed liquid side node (node$_{d1}$) and the subscript (V) indicates the conduction from the engulfed, even if partially, vapour side node (node$_{d2}$). Two of the test used for the validation have the defect covering all the circumference of the vessel, while one test has the configuration shown in Figure 7.10, where the "defective" shell node on the liquid side are not in direct contact, thus the term $q_{d1,cond}$ should not be present or at least should be referred to the node in real contact with the defect (node$_{15}$), but in the code this term is left unchanged since the difference between the temperature of the real-contact node (node$_{15}$) and the implemented node (node$_{d1}$) is not so relevant (about 10°C).

Heat loads to the not-engulfed defect node of liquid side ($node_{d6}$)

The only term entering the node is from the surrounding air gap ($node_{d4}$) which radiates $node_{d4}$, the equation for the evaluation of this radiative flux is defined in the same way as for the radiative exchange inside the enclosure, equation (7.59), by including the appropriate temperature, as shown in equation (7.78):

$$q_{d4,rad} = \sigma \varepsilon_s (T_{d4}^4 - T_{d6}^4) \quad (7.78)$$

Validation set-up

The RADMOD validation sub-model described in this paragraph (7.3.2) is used considering also the stratification sub-model (strat3). During the validation a tuning factor is introduced for the height of the stratified layer, its value is set equal to 2. The doubled height of the stratified layer resulted to be around 60% of the total liquid filling level, such value of stratified depth, imposed in the stratification sub-model, represents a halfway between the Baseline and the stratified RADMOD models, respectively advised for unprotected and coated tanks, just as the problem implemented was. Moreover, the heat exchanges between the not engulfed defect ($node_{d4}$) and ambient air was overestimated by 3 times.

7.3.3 Software implementation

There are five main MatLab codes developed, four of which are pre-existing codes and they consider the baseline and the three stratification sub-models version of RADMOD. They are called *RADMOD_Baseline.m* , *RADMOD_Strat1.m*, *RADMOD_Strat2.m* and *RADMOD_Strat3.m*. The fifth main code is called *RADMOD_defect* and considers both the Baseline and the Strat3 version. Other than these core files there are several functions for external evaluation, like for the thermodynamic properties of lading and wall material and for the heat-transfer coefficients. Each function can be called up within the main code to calculate the variation of these parameters with the time.

Three Excel files are included, two for the initial data set-up: *InitialData.xlsx* for the pre-existing main codes and *InitialData_def.xlsx* for the novel implementation of the code for defective coatings (*RADMOD_defect.m*); and a third Excel file for reporting results (*Results.xlsx*). The two files for the input set-up are identical except for the section dedicated to the defect, which it was not present in the previously version of the code, and for the position of the cell. The first recommendation is to use the appropriate input file with the appropriate .m file or MatLab cannot read correctly the cell, so with respect to the model version that has to be run choose the appropriate input Excel file following the Table 7.4.

Table 7.4 – Summary of the MatLab code available associated with the appropriates input Excel file

MatLab code	Input Excel file	Model Version
RADMOD_defect.m	InitialData_def.xlsx	Baseline
		Strat3
RADMOD_Baseline.m	InitialData.xlsx	Baseline
RADMOD_Strat1.m	InitialData.xlsx	Strat1
RADMOD_Strat2.m	InitialData.xlsx	Strat2
RADMOD_Strat3.m	InitialData.xlsx	Strat3

Once the MatLab code and the input file are chosen, to run a simulation it is possible to follow the simple instructions:

1. INPUT DATA: Open the InitialData.xlsx file and add all the inputs required (geometrical features, fire conditions, PRV dimension, etc.…). The only recommendation to follow is that of keeping the same format not moving the cells. Once this step has been completed, all data must be saved like first sheet. It is possible to create new copies of sheets to keep more initial data saved, just moving them away from the first position.

2. CODE SELECTION: Chose the code to run among the five main Matlab codes. Open the selected one and start the simulation pressing the Run bottom on the Editor page. The defect file is the most developed code so more results are provided, it is possible to select, in the input data file, what model version to run, it is advised to select the Baseline model for coated and defective tanks and the Strat3 model for uncoated tanks. If the defect file is running the MatLab window reports a message showing what model version is running.

3. SIMULATION END: Wait until the end of simulation which can lasts a few minutes, from 2 to 5 min. depending the number of numerical iterations. It might happen that an error message could be displayed and it can be explained to the oversize of time step. If for some reason the simulation must be stopped manually it is possible to do that by pressing Ctrl+C in Matlab window.

4. RESULTS: On Matlab screen are reported the time to failure (ttf_conservative and ttf) and, the time of the opening of PRV. The other parameters (fluid temperature, pressure and so on) can be seen in the plots as time function, while if it is necessary to have their numerical values the Results.xlsx file can be open. It is important to remember that the Results.xlsx must not be open during the simulation otherwise Matlab will not not able to write the output data as it cannot get access to the file giving an error.

8 Definition of sensitivity analysis and case studies

Two modelling approaches are adopted in this thesis work: an advanced finite elements method (FEM) model and a simplified lumped parameters model, both are aimed to assess the performance of insulated tanks exposed to fire in presence of defects in their thermal insulation system. A sensitivity analysis is performed on the FEM model, the parameters to vary and their values are discussed in this chapter in the following section 8.1. Whereas the lumped model is applied to real-scale case studies, section 8.2 is dedicated to the definition of variables and geometries individuated for the simulations. The results of the sensitivity analysis and case studies are reported and discussed in chapter 9.

8.1 Sensitivity analysis

In order to provide a sensitivity analysis for the FEM model, a series of variables are selected, in order to assess the effect of their variation. The implementation of a model, in general, requires several guesses and approximations of the realty. In the specific case of a model for tanks engulfed in fires, the assumptions made, especially in the approximation of flame conditions, may lead to relevant modification in the final results [Birk, 1995].

This part of the thesis work is aimed to understand how each assumption adopted in the model influences the simulation results, in order to assess which parameters should be modelled more accurately and which not significantly influence the response. This is aimed at determining the uncertainties affecting the model and the reliability of computer simulations.

he mesh and time step implemented in the analysis are described in chapter 6, where it is also assessed the mesh independency (see section 6.3.3). The geometries and the boundary conditions implemented are the same used for the validation of the FEM model. As in the validation, the geometry is a quarter portion of a tank equipped with a coating blanket of ceramic fibre to which a square portion (15.2x15.2 mm^2) of insulation is removed. Both the external steel jacket and the shell wall are made of carbon steel. The internal shell wall surface is supposed to be in contact with ambient air while the flame engulfs the complete external surface of the jacket.

Three model geometries are simulated, each varying five variables related both to the flame and to the steel, as follows:

Geometries

- Fully protected
- Sealed
- Defect 15.2

Falme parameters:

- T_{BB} → 3 values of black body temperature
- h_{fl} → 3 values of convective heat coefficient between the flame and the steel jacket
- ε_f → 3 values of emissivity

Steel parameters:

- h_f → 3 values of convective heat coefficient between the tank shell and ambient air
- ε_s → 3 values of emessivity of the steel exposed to fire

A total of thirty-three simulations are performed, eleven for each geometry, i.e. a baseline simulation and ten sensitivity simulations, as summarized in Table 8.1, the modelling approach with which the parameters are defined please refer to chapter 6.

Table 8.1 – Summary of the parameters varied for each geometry in the sensitivity analysis performed on the FEM model

		Baseline	Minimum value	Maximum value
Flame	T_{BB} °C	871	815	927
	h_{fl} W/m^2K	25	20	30
	ε_f	0.8	0.7	0.9
Steel	h_f W/m^2K	10	5	15
	ε_s	0.8	0.85	0.95

The models are described in section 6.3.1, a schematisation of the geometry for the case "Defect 15.2" is shown in Figure 8.1. The materials properties implemented in the FEM model for the carbon steel are summarized in Table 8.2 whereas Table 8.3 shows the insulation specifications.

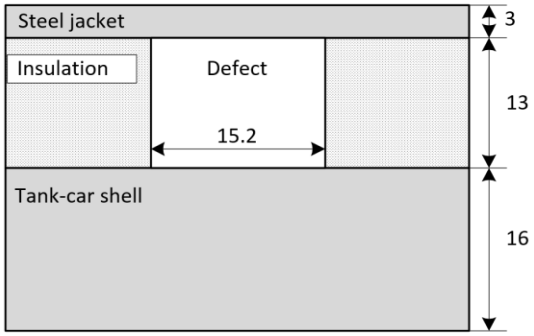

Figure 8.1 – Schematisation of geometry ID "Defect 15.2" implemented in the FEM model, lengths in mm

Table 8.2 – Material properties implemented in the FEM simulations, related to carbon steel with density equal to 7850 kg/m^3 [Scarponi et al. 2016]

Temperature $°C$	**Heat capacity** $j/kg\ K$	**Thermal conductivity** $W/m\ K$
100	487.6	50.7
300	564.7	44.0
500	666.5	37.4
700	1008.2	30.7
900	650.4	24.0

Table 8.3 – Material properties implemented in the FEM simulations, related to thermal protection coating with density 72 kg/m^3 and specific heat 1130 $j/kg\ K$ [Scarponi et al. 2016]

Temperature $°C$	**Thermal conductivity** $W/m\ K$
200	0.06
400	0.11
600	0.18
800	0.28

8.2 Case studies

Once the lumped RADMOD model is validated against experimental data of bonfire small-scale tanks with defective coating, (see specific results in section 9.3) the model is extended to several case studies increasing the scale of both tank and defect.

For the simulations of unprotected tanks the RADMOD stratification (Strat 3) sub-model is used, whereas in all the other cases (fully protected and defective coatings) the baseline model is selected for simulations of this case studies, as suggested by [Nigro, 2015] .

The various cases of interest differ each other for the geometry, filling level and ratio of tank surface not covered by thermal protection due to the defect. The total number of simulations and the details of each ones are collected in Table 8.5. For all cases the propane contained inside the tank is a saturated liquid. The bonfire tests used for model validation were performed in North America, and the initial condition of saturated propane is mostly taken to 9 or 12 degree, here it is assumed equal to 10°C. Moreover, the fire apparatus used in this tests is similar to the one used for the bonfire tests on the quarter cylinder tank (see section 3.3 and 3.4) on which an accurate evaluation of the flame properties is available [VanderSteen, Birk, 2003] following this data the flame emissivity (ε_f) is assumed equal to 0.45 and the black body temperature (T_{BB}) is set to 871°C. With this specifications the flame temperature (T_f) is obtaneid through equation (8.1) [Modest, 2003] and it is set to 1120°C. For environmental requirement it can be assumed that the wind velocity is of 1 m/s and the environment temperature is equal to 20°C.

$$\varepsilon_f \cdot T_f^4 = T_{BB}^4 \quad (8.1)$$

For the selection of horizontal pressurized vessels, the geometrical sizing was derived from vessels typically used for the applications of interest, which were reported in [Landucci et al. 2014], individuating a medium- and a large-scale tank. For every tank the PRV was designed according to API RP-520 and its behaviour was assumed relay opening at design pressure. The PRV cross area designed in such way is then oversized by 30%, further details in [Nigro, 2015]. The dimensions related to the tank are summarized in Table 8.4.

Table 8.4 – Geometrical details related to tanks for case studies implemented with the RADMOD model [Landucci et al. 2013; Nigro, 2015]

Tank scale	**Tank ID**	**Design pressure**	**Volume**	**Diameter**	**Length**	**Shell thickness**	**PRV area**
		bar	m^3	mm	mm	mm	cm^2
Medium	M	15	25	1700	10500	15	80
Large	L	15	50	2100	13200	18	32.5

Table 8.5 – Summary of the case studies implemented with the RADMOD model

Case ID	**A_{def}/A_{tank}**	**A_{def}**	**H_{top}**	**H_{btm}**	**L_{def}**	**Filling**
	%	m^2	m	m	m	% v/v
$M_{8\%def}$	**8**	4.5	1.7	1.23	9.45	70
$M_{15\%def}$	**15**	8.4	" [a]	0.85	" [a]	70
$M_{30\%def}$	**30**	16.8	" [a]	0.23	" [a]	70
$M_{40\%def}$	**40**	22.4	" [a]	0.03	" [a]	70
$M_{45\%fill}$	15	8.4	" [a]	0.85	" [a]	**45**
$M_{70\%fill}$	15	" [a]	" [a]	" [a]	" [a]	**70**
$M_{95\%fill}$	15	" [a]	" [a]	" [a]	" [a]	**95**
$L_{8\%def}$	**8**	7.0	2.1	1.52	11.9	70
$L_{15\%def}$	**15**	13.1	" [a]	1.05	" [a]	70
$L_{30\%def}$	**30**	26.1	" [a]	0.28	" [a]	70
$L_{40\%def}$	**40**	34.8	" [a]	0.03	" [a]	70
$L_{45\%fill}$	15	13.1	" [a]	1.05	" [a]	**45**
$L_{70\%fill}$	15	" [a]	" [a]	" [a]	" [a]	**70**
$L_{95\%fill}$	15	" [a]	" [a]	" [a]	" [a]	**95**

" [a] : as above

The case studies identificated with the subscript *45%fill* are the same as *15%def* , in fact this percentace of defective insulation area is chosen for the evaluation of the effect of initial liquid filling level variation. The top height of the defect is set equal to the tank diameter in each simulation, the defect wideness corresponds to the 90% of the tank length. The bottom height of defect is obtained from the other parameters through equation 8.2.

$$H_{btm} = H_{top} - D_{tank} \sin\left(\frac{A_{def}}{L_{def}\, D_{tank}}\right) \qquad (8.2)$$

The insulation system implemented in the case studies is the the same as in the FEM model, thus the properties of this materials collected in Table 8.3 are used for the RADOMOD simulations. The steel jacket and the tank shell are both made of carbon steel, as in the FEM model, but in this code the specific heat and thermal conductivity are not function of the temperature, thus their averaged value in the range of temperature of interest are set in the case studies. The specific heat is set equal to 490 $j/kg\ K$, while thermal conductivity is assumed to be 44 $W/m\ K$. The density value is left to 7850 kg/m^3 and the yield strength used for the evaluation of the time to failure of the tank is 480 MPa. [Engineering ToolBox, 2016]

9 Results and discussion

9.1 FEM validation results

The validation of the FEM model was carried out against the experimental data described in section 3.3. Several squared defects on a quarter portion of tank were bonfire tested and thus the geometries implemented for the validation aimed to reproduce them. The geometries implemented were specified according to Section 6.3 and the boundary conditions were modelled as reported in section 6.2. For further details on the FEM model validation refer to [Scarponi et al. 2016].

9.2 Sensitivity analysis results

In this section are reported the results of the sensitivity analysis performed on the FEM model. The aim of this analysis is understanding which of the several parameters implemented in the model, have significant influence on the results obtained. The geometries, the parameters and the boundary conditions of the simulations performed during the sensitivity analysis are reported in section 8.1. The results are collected in Figures 9.3 and Figures 9.4, where the curves are obtained setting-up a baseline simulation, taking its parameters value as a reference to the comparison with the results of the sensitivity simulations, in which only one parameter value differs from the baseline.

The sensitivity analysis was performed on three different geometries: with coating, completely without coating and with coating in presence of defect; in this section are shown only the results of the latter geometry since it involved more phenomena and thus it can be considers the completest-case examined.

9.2.1 Dynamic analysis of temperature in the center of defect

Figures 9.3 (a, b, c, d, e) show the dynamic temperature behaviour of the central point of the defect in function of the time. In particular each figure shows the results obtained changing one parameter: (a) black body temperature of the flame, (b) emissivity of the flame, (c) emissivity of the steel exposed to fire, convective heat coefficient between the flame and external steel jacket (d) or between the internal shell and ambient air (e). The baseline simulation is indicated as “Base_” followed by the reference-value of the parameters on which the sensitivity analysis is performed, the results of the other simulations are identified specifying the variable name and its associated value implemented in the model. The results are summarized in Table 9.1 reporting the relative error of each simulation with respect the baseline temperature.

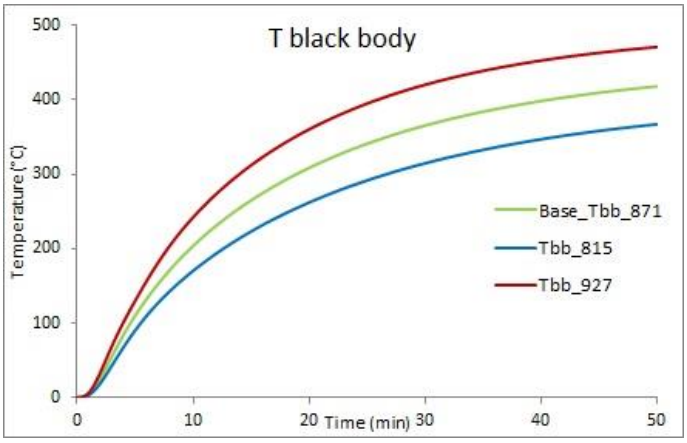

Figure 9.1a – Sensitivity analysis results, dynamic defect center temperature, influence of the black body temperature (T_{BB} in °C)

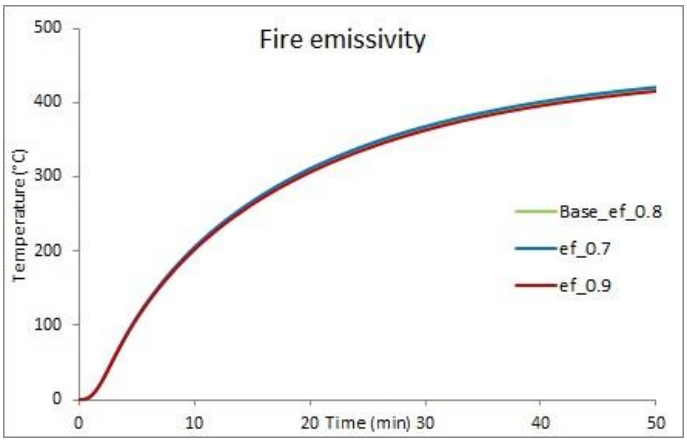

Figure 9.1b – Sensitivity analysis results, dynamic defect center temperature, influence of flame emissivity (ε_f)

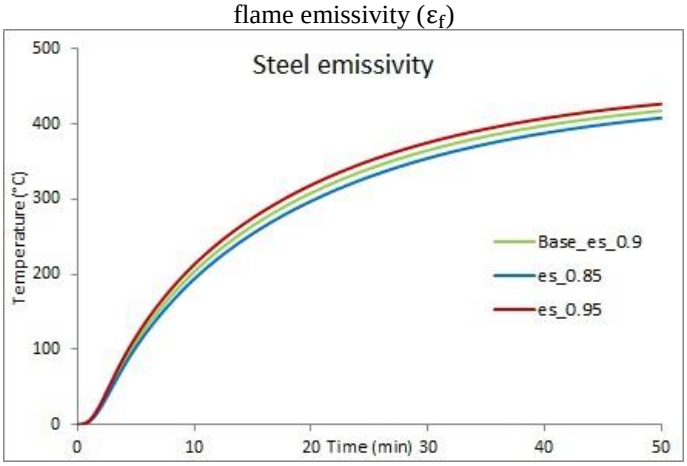

Figure 9.1c – Sensitivity analysis results, dynamic defect center temperature, influence of exposed steel emissivity (ε_s)

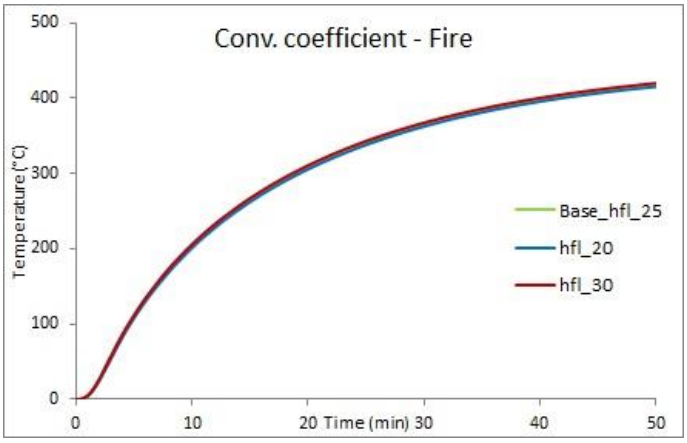

Figure 9.1d – Sensitivity analysis results, dynamic defect center temperature, influence of convective coefficient between the flame and the external jacket (h_{fl} $in\ W/m^2K$)

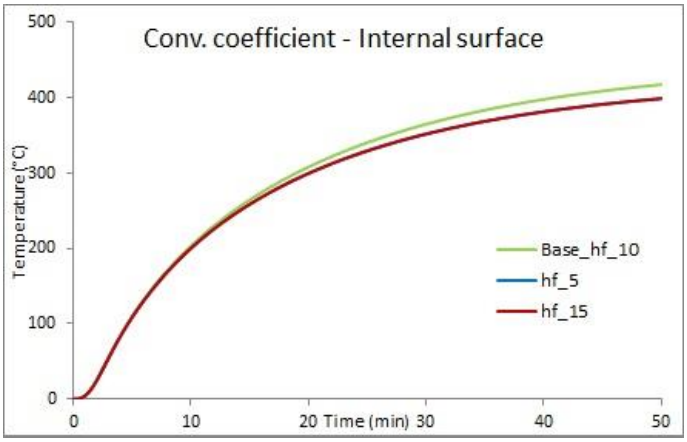

Figure 9.1b – Sensitivity analysis results, dynamic defect center temperature, influence of convective coefficient between the internal steel and ambient air (h_f $in\ W/m^2K$)

The relative error of each simulation with respect the baseline temperature is calculated as shown in equation (9.1):

$$\Delta T\% = \frac{T_{simulation} - T_{baseline}}{T_{baseline}} \cdot 100 \qquad (9.1)$$

Table 9.1 – Relative errors obtained from the sensitivity analysis, results obtained for the temperature at the center of defect

$\Delta T\%$	T_{BB}		ε_f		ε_s		h_{fl}		h_f	
	min	**max**	**min**	**max**	**min**	**max**	**min**	**max**	**min**	**max**
start	-22%	28%	1%	-1%	-11%	14%	-6%	6%	0%	0%
end	-12%	13%	1%	-1%	-2%	2%	-1%	1%	5%	-4%
averaged	-15%	17%	1%	-1%	-4%	4%	-1%	1%	3%	-3%

9.2.2 Temperature profile along the defect

Whereas in Figure 9.4 (a, b, c, d, e) are plotted the temperature profile along the defect at 20 minutes from the starting of simulation. The results are summarized in Table 9.2 where the relative errors obtained through equation (9.1) are collected. The normalized distance from the defect central point is reported in abscissas.

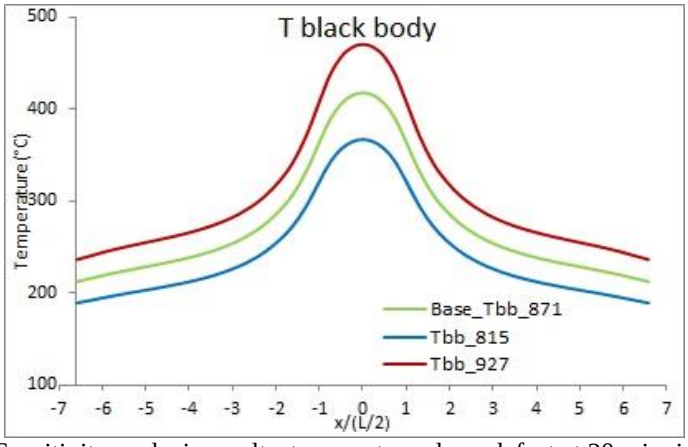

Figure 9.2a – Sensitivity analysis results, temperature along defect at 20 min, influence of the black body temperature (T_{BB} in °C)

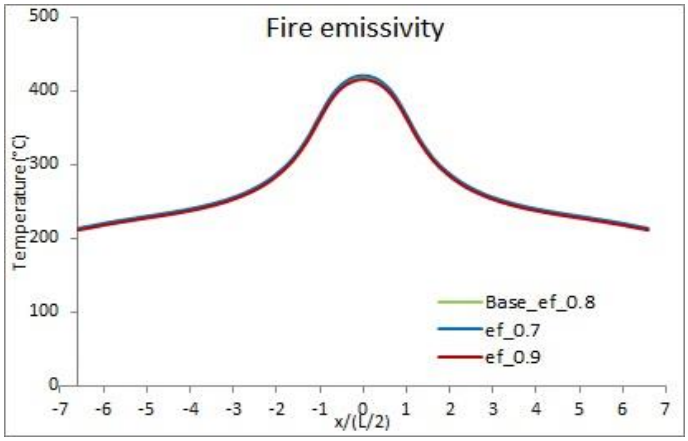

Figure 9.2b – Sensitivity analysis results, temperature along defect at 20 min, influence of flame emissivity (ε_f)

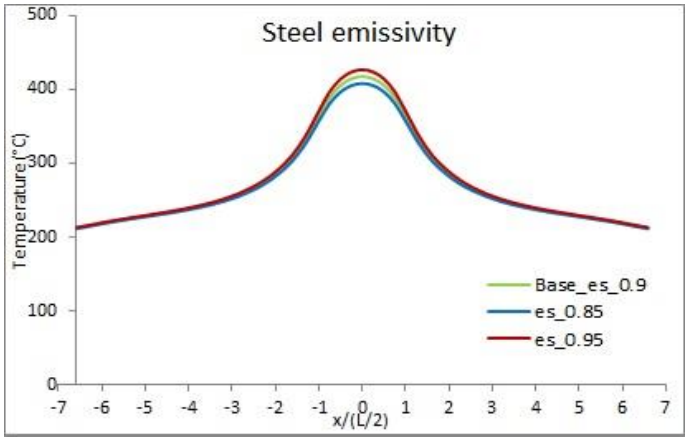

Figure 9.2c – Sensitivity analysis results, temperature along defect at 20 min, influence of exposed steel emissivity (ε_s)

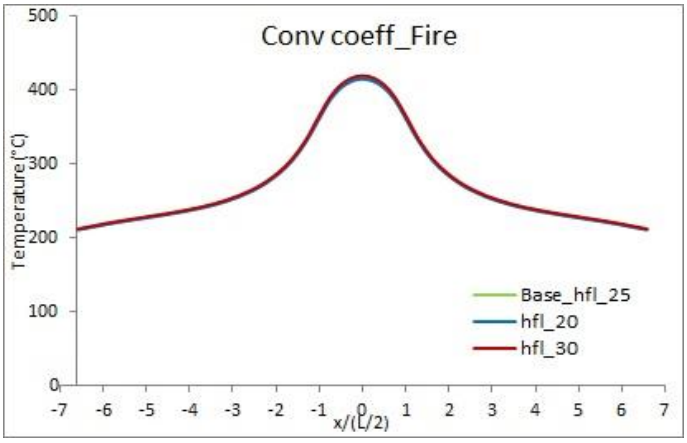

Figure 9.2d – Sensitivity analysis results, temperature along defect at 20 min, influence of convective coefficient between the flame and the external jacket (h_{fl} $in\ W/m^2K$)

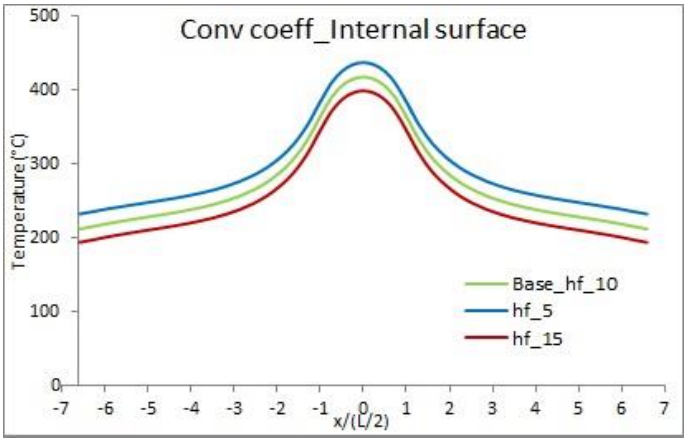

Figure 9.2e – Sensitivity analysis results, temperature along defect at 20 min, influence of convective coefficient between the internal steel and ambient air (h_f $in\ W/m^2K$)

In the following Table 9.2 the results of the analysis are summarized reporting the relative error of each simulation with respect the baseline temperature, calculated as shown in equation (9.1). In this case the relative error committed in the central point and in the external points are reported.

Table 9.2 – Relative errors obtained from the sensitivity analysis, results obtained for the temperature along the defect at 20 minutes for central point and external points

$\Delta T\%$	T_{BB}		ε_f		ε_s		h_{fl}		h_f	
	min	**max**	**min**	**max**	**min**	**max**	**min**	**max**	**min**	**max**
central	-11%	11%	1%	-1%	0%	0%	0%	0%	10%	-9%
external	-12%	13%	1%	-1%	-2%	2%	-1%	1%	5%	-4%

9.2.3 Discussion on the sensitivity analysis results

The sensibility analysis highlights that the results are main influenced by the flame black body temperature amongst other parameters. This results was expected since the radiative heat power received by the system from the flame is a function of the temperature raised to the fourth power, thus a variation in the flame temperature should significantly affect the thermal behaviour of the system. The results of the implementation supports the previously assumption, different black body temperatures show variation from the baseline of about 30% in the dynamic analysis and a little bit more than the 10% in the defect temperature profile at 20 minutes. Clearly, a black body temperature increase leads to an increase of the temperature reached in the defect, and vice versa.

The other parameter which was expected to influence the thermal behaviour of the system was the flame emissivity, it determines, in this case, the temperature of convective exchange of the flame. In fact in this model the black body temperature and the flame emissivity are set as input data and the flame temperature (T_f) is obtained from this two parameters, as equation (9.2) shows.

$$\varepsilon_f \cdot T_f^4 = T_{BB}^4 \qquad (9.2)$$

Nevertheless, the results of this analysis point out that changing the emissivity of the flame a maximum of 1% error can be reached. This is probably due to the few contribution of the convective heat transfer mechanism compared to the radiative one, this can be see also in the results obtained changing the emissivity of the steel exposed to fire and the convective heat exchange from the flame and the jacket. Changing the steel emissivity the results get far from the baseline ones of a 5% and in fact, the it regulates the radiative exchange between the flame and the external jacket. Whereas different value of the convective heat exchange of the flame do not affect the temperature reached in the defect.

The last variable analysed is the convective heat transport coefficient of the inner tank wall in contact with ambient air. Its influence can be seen in the temperature profile along the defect at 20 minutes (Figure 9.3e), if the coefficient increases the dissipative power from the wall increases and thus the temperature in the defect results to be lower, and vice versa.

The sensitivity analysis highlights the importance of modelling the parameters linked to the radiative exchange between the flame and the jacket. In particular the main variable able to affect significantly the results is the black body temperature of the flame.

9.4 RADMOD validation

The lumped parameters model (RADMOD) was enhanced for the simulation of coated tanks exposed to fire in presence of defect in their insulation system. In order to assess the credibility of the results obtained with the novel RADMOD model, a validation against experimental data was needed. The validation of the model was carried out by comparison the results obtained with the RADMOD model and the results of the bonfire tests described in section 3.4.

The boundary conditions were set-up according to section 7.4. The geometries and the insulation properties were implemented in order to recreate the same conditions of the bonfire tests, thus all details are specified in section 3.4, with the exception of the tank length, which value was set to 2.12 m neglecting the heads of the tank. The steel properties are reported in section 8.2 as they were also used for the case-studies simulations.

The experimental available data concern: the temperature of the lading (vapour and liquid phase), the temperature of the wall exposed to fire and the pressure reached inside the tank. Three bonfire tests were carried out and thus three set of data were available for the validation of the model, some specifications on the set-up related to the three cases are summarized in table 9.3.

Table 9.3 – Information on the input data used in the RADMOD validation

Bonfire test ID	**04-03**	**04-04**	**04-05**
A_{def}/A_{tank} (%)	15%	15%	8%
Filling degree (%)	71%	78%	71%
Time step (s)	1	1	1
Initial lading pressure (bar)	6.6	8.9	6.6
PRV opening P (bar)	26.26	21.2	26.26
PRV closing P (bar)	23.85	19.3	23.85

The PRV behaviour was assumed to be relay and the discharge area was set to 1.8 cm^2 . The ambient temperature was estimated to be 18°C with a wind velocity of 1 m/s. The time checked for each simulation was choose equal to the time at which the tanks failed during the bonfire tests. The black body temperature of the flame was set equal to 871°C with an emissivity of 0.45.

9.4.1 Validation results – Pressure prediction

Figure 9.4 shows the pressure results obtained with the RADMOD model compared with the results of the experimental tests, in particular: (a) test 04-03, (b) test 04-04 and (c) test 04-05. It is reported also the time to failure predicted by the model with the two different criteria explained in paragraph 7.2.4 and the experimental ones estimated by Birk [Birk et al. 2006], more details in section 3.4.

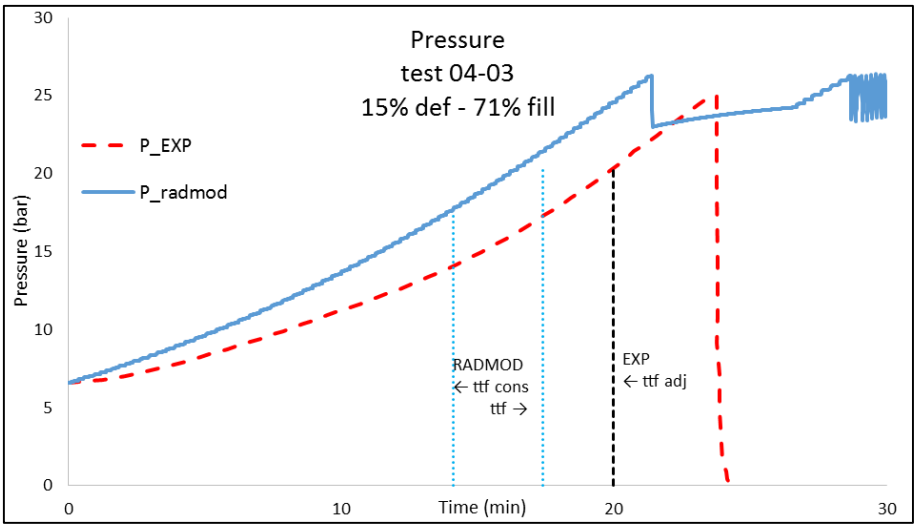

Figure 9.3a – RADMOD validation results, pressure comparison of experimental test 04-03

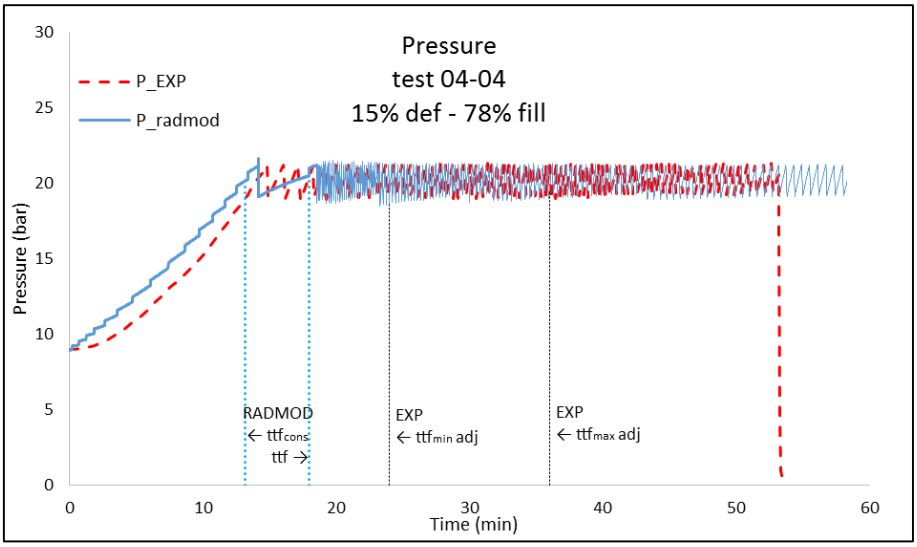

Figure 9.3b – RADMOD validation results, pressure comparison of experimental test 04-04

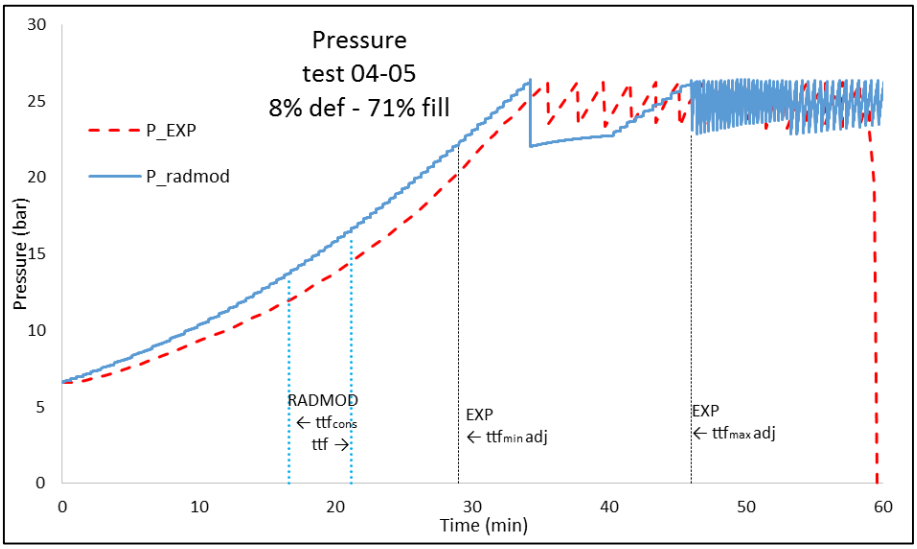

Figure 9.3c – RADMOD validation results, pressure comparison of experimental test 04-05

9.4.2 Validation results – Lading temperature prediction

The experimental data on the lading temperature were available only for test 04-03 and 04-04 (both with 15% A_{def}), thus, no validation on the lading temperature prediction was performed on the small-defect simulation. The results are shown in Figures 9.5, (a) for test 04-03 and (b) test 04-04, where the temperatures obtained by the thermocouples are compared with the results obtained with the RADMOD model. The position of the thermocouples and their ID number is also shown in Figures 9.5, where are reported the central bundle of thermocouples (see section 3.4) used in the validation. The temperature obtained with the model are the temperature of the vapour node and the averaged liquid temperature between the bulk (at constant temperature) and the stratified liquid layer (with altered temperature).

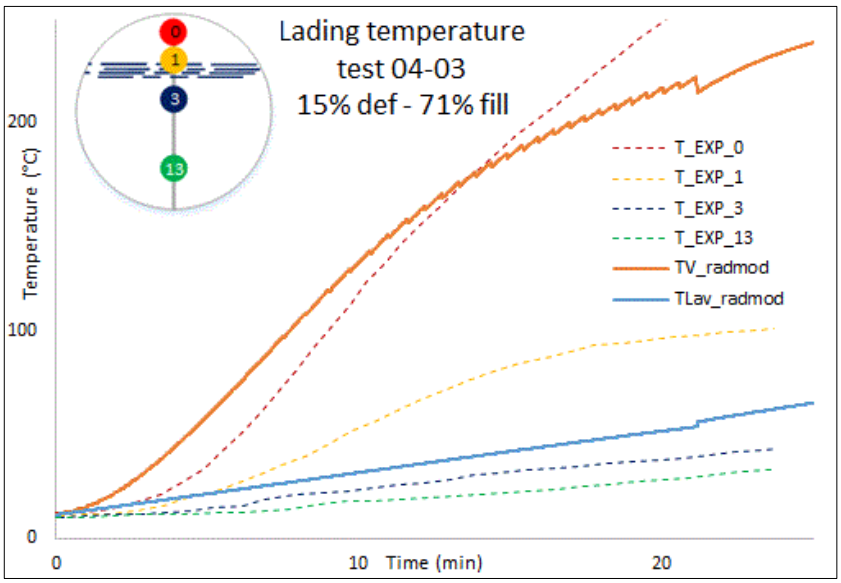

Figure 9.4a – RADMOD validation results, lading temperature comparison, experimental test 04-03. A sketch of vessel section and thermocouples bundle are reported in the upper left

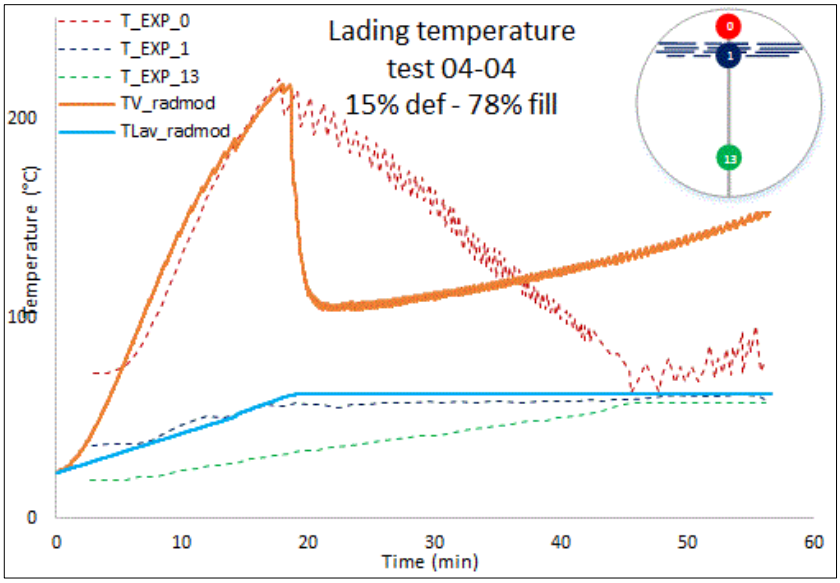

Figure 9.4b - RADMOD validation results, lading temperature comparison, experimental test 04-04. A sketch of vessel section and thermocouples bundle are reported in the upper right

9.4.2 Validation results – Wall temperature prediction

The last step of the validation was aimed to evaluate the ability of the model to predict the temperature of the tank walls. This parameter determines the time to failure of the tank calculated by the model, since the estimation of the yield strength of the material depends on the maximum temperature reached by the steel walls (see paragraph 7.2.4). The walls in contact with the vapour phase have higher temperatures and in particular the shell between the vapour and the engulfed defect has the highest one (T_{d2}).

The temperature comparison shown in Figures 9.7 is between the temperature read from the wall thermocouple and the temperature of the shell nodes under the exposed defect ($node_{d1}$ and $node_{d2}$ respectively in contact with the liquid and the vapour phase) calculated by the model. The thermocouples position during the experiments is shown in Figures 9.6 where the instrumented wall under the defect wideness is reported, for a complete sketch of the instrumentation see section 3.4. In Figures 9.6 it is also shown, by the blue dotted lines, the indicative level reached by liquid during the tests.

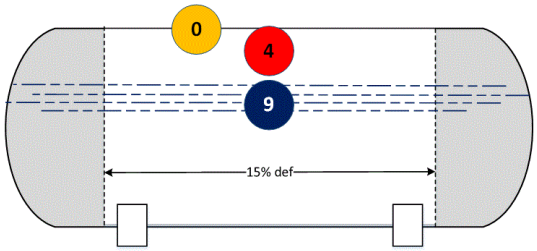

Figure 9.5a – Sketch of vessel and wall thermocouples position, experimental test 04-03

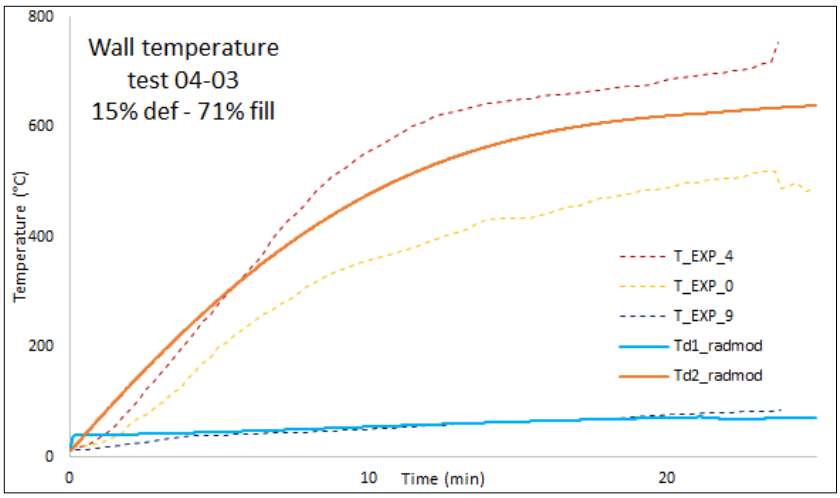

Figure 9.6a – RADMOD validation results, wall temperature comparison, experimental test 04-03

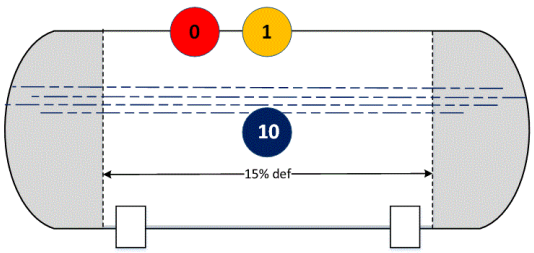

Figure 9.5b – Sketch of vessel and wall thermocouples position, experimental test 04-04

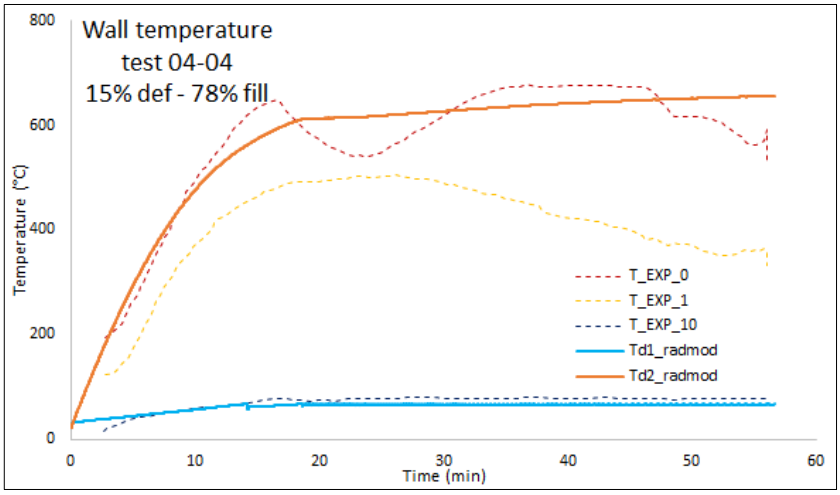

Figure 9.6b – RADMOD validation results, wall temperature comparison, experimental test 04-04

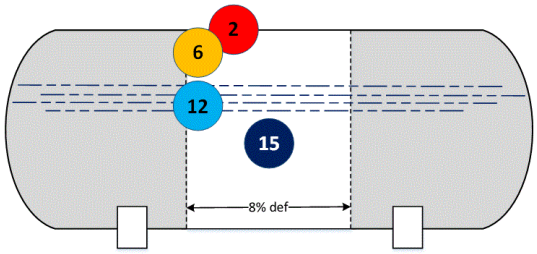

Figure 9.5c – Sketch of vessel and wall thermocouples position, experimental test 04-05

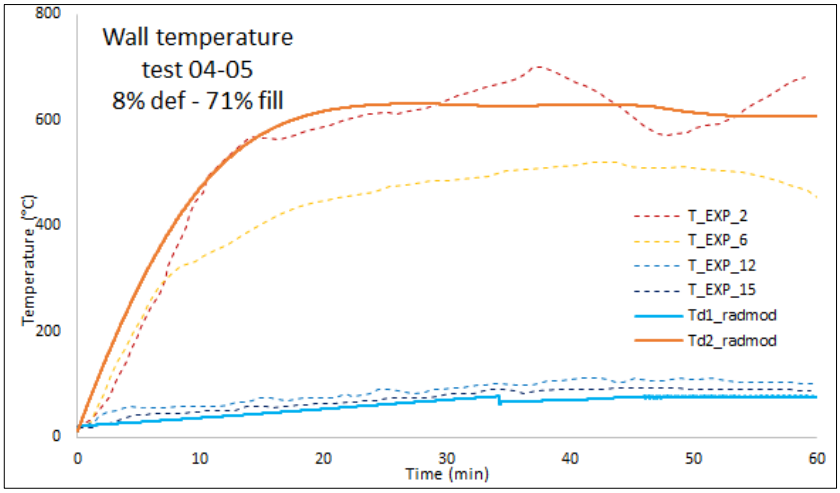

Figure 9.6c – RADMOD validation results, wall temperature comparison, experimental test 04-05

9.4.3 Discussion on the RADMOD model for defective coatings validation results

Generally, the model shows to be able to predict the behaviour of the three parameters analysed during the validation. The few experiments available permit to validate the model by the introduction of two tuning factor, one for the stratified layer depth and one for the dissipative term of the system to ambient air. It would be interesting to establish the performance of the code compared with medium- and large-scale experimental data. The variables compared during the validation are discussed in this section, in relation to the results previously shown.

Pressure

The model shows a good prediction of the pressure behaviour inside the tank, the simulated pressure curves result to be conservative compared to the real pressure registered during the tests. Changing the value of the tuning factor the pressure turns out to increase both with the lower depth of the stratified layer and with the flame emissivity increases. In the latter case also the temperature reached by the walls is higher leading to an early time to failure of the tank. Another point to consider is that up to the opening time of PRV, the pressure profiles are close to the experimental ones, whereas, as explained in section 7.2.5, at the opening of the PRV an ideal mixing occurs between the liquid bulk and the liquid in the stratified layer, resulting in a vapour pressure lower than the real one. Thus, after the PRV opening the pressure profiles deviates from the experimental curves up to the second opening of the PRV.

In the end, the model reproduces the first opening of the PRV well, the pressure calculated in this point is overestimated by 5% for the simulations of test 04-04 and 04-05, whereas for the first test (04-03) it around 20%. Coming closer to the uniform liquid bulk temperature, the pressure profile approaches the experimental one.

Lading temperature

From the results shown in Figures 9.5, the behaviour of both liquid and vapour phase obtained with the model, is close to the experimental profiles. In the first test (04-03) the PRV never opens and the vapour temperature is good predicted by the model. Also the liquid averaged temperature profile conservatively follows the experimental data. In the second test (04-04) the vapour temperature profile is well predicted up to the PRV opening, then, for the same considerations made above on pressure underestimation after the first material discharge, also the vapour temperature undergo a lowering greater than the experimental one after the PRV opening. Whereas, the liquid averaged temperature remains close to its real behaviour also after the PRV opening.

Wall temperature

The thermocouples on the tank shell collect bundles of temperature profiles, of which in Figures 9.7 are shown the higher curve and a representative profile of the other data. This experimental curves result well predicted by the model, which calculates an averaged temperature close to the higher reached during experiments, for the wall in contact with the vapour phase. On the other hand the temperature of the walls in contact with the liquid phase results to be slightly underestimated.

9.5 Results of the case studies

In this section, the results of medium- and large-scale tanks implemented as case-studies are reported and discussed. The results are obtained through the implementation of the RADMOD model for defective real-scale defects, which boundary conditions are described in paragraph 7.3.1, while the case-studies definition is reported in section 8.2.

In this paragraph results of different defect areas simulations are compared, varying both the initial liquid filing level and the tank scale. The analysed cases are: the presence or not of insulation system and its integrity, the different ratio of defective insulation area and different initial filling level. The effect of changing this parameters is analysed on three variables: the pressure inside the tank, the temperature of the lading, in particular the vapour phase, and the time to failure of the tank, thus the maximum temperature reached by shell walls. The time scale of the following graphs is cut after the prediction of time to failure.

9.5.1 Pressure

In Figure 9.8 are shown the pressure results of the medium- (a) and large-scale (b) tanks, in the case of unprotected, fully protected and with 30% of defective insulation area. Whereas in Figure 9.9 is reported the pressure profile with different defective areas compared between each other and with the fully protected case. The pressure profiles obtained implementing different filling level are reported in Figure 9.10.

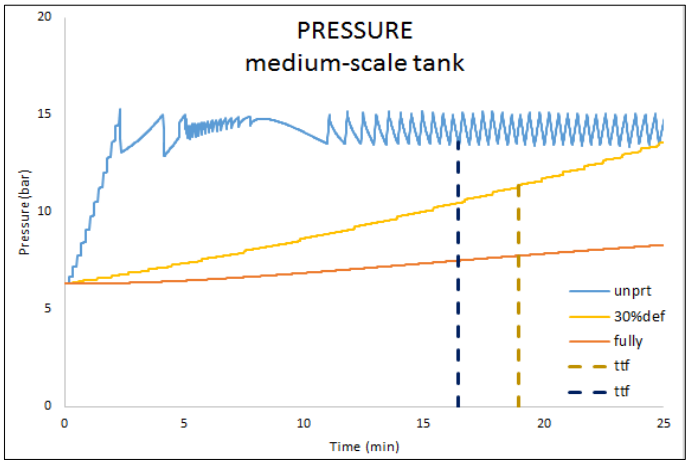

Figure 9.7a – Medium scale case study, pressure comparison between unprotected, fully protected and 30% defective insulation area

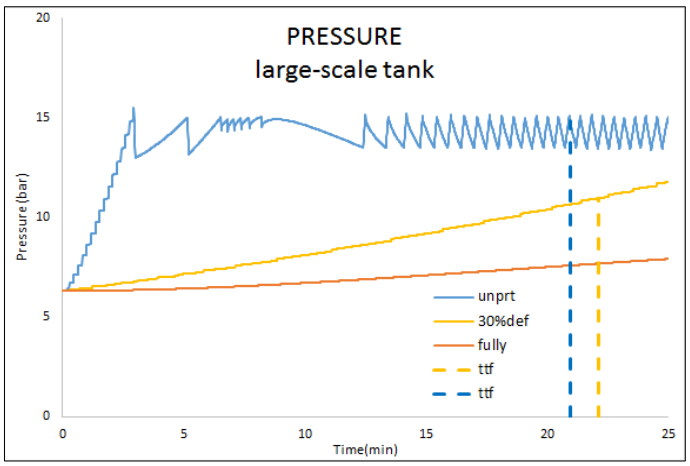

Figure 9.7b – Large scale case study, pressure comparison between unprotected, fully protected and 30% defective insulation area

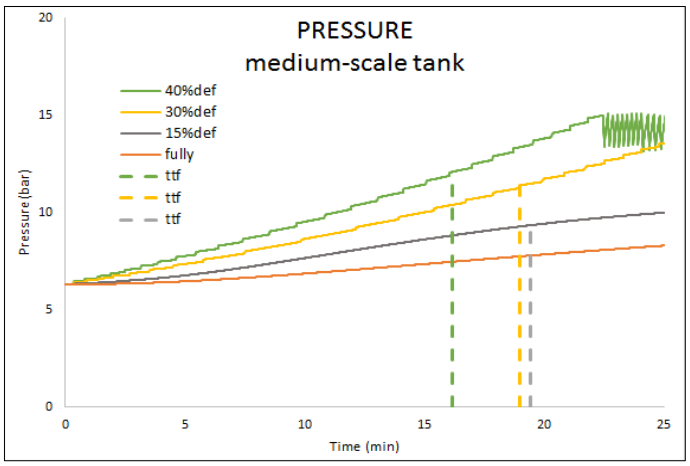

Figure 9.8a – Medium scale case study, pressure comparison between different ratio of defective area (fully protected, 15%, 30% and 40% of defective area)

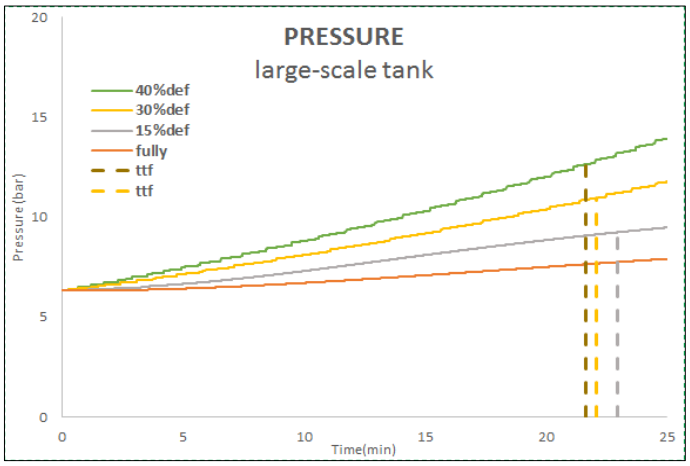

Figure 9.8b – Large scale case study, pressure comparison between different ratio of defective area (fully protected, 15%, 30% and 40% of defective area)

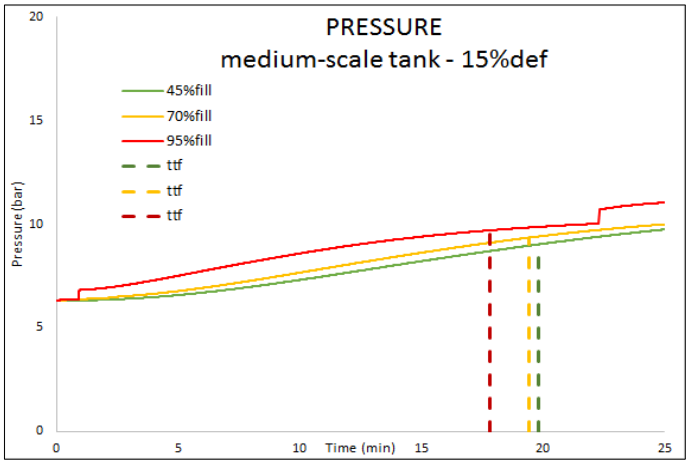

Figure 9.9a – Medium scale case study, pressure comparison between different initial filling level (45%, 70% and 95% filling; 15% defective area)

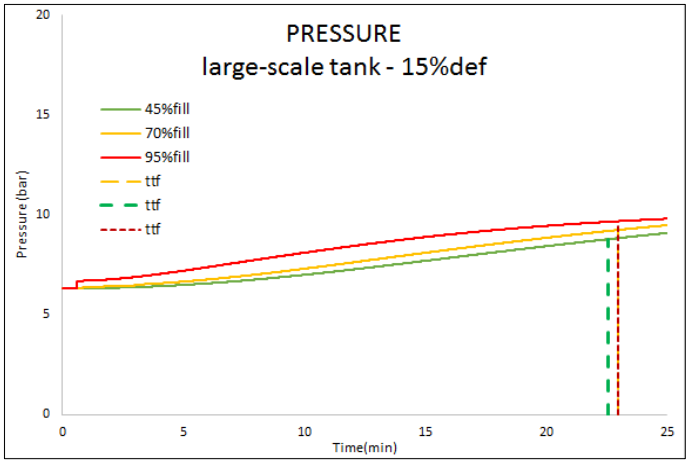

Figure 9.9b – Large scale case study, pressure comparison between different initial filling level (45%, 70% and 95% filling; 15% defective area)

9.5.2 Lading temperature

The vapour temperature results are shown in Figure 9.11 for the insulation presence and in Figure 9.12 with respect different defective areas, each Figure shows in (a) the medium-scale results and in (b) the large-scale ones. The results of the simulation with different initial liquid filling are collected in Figure 9.13. Whereas the comparison between the tank scales is shown in Figure 9.14.

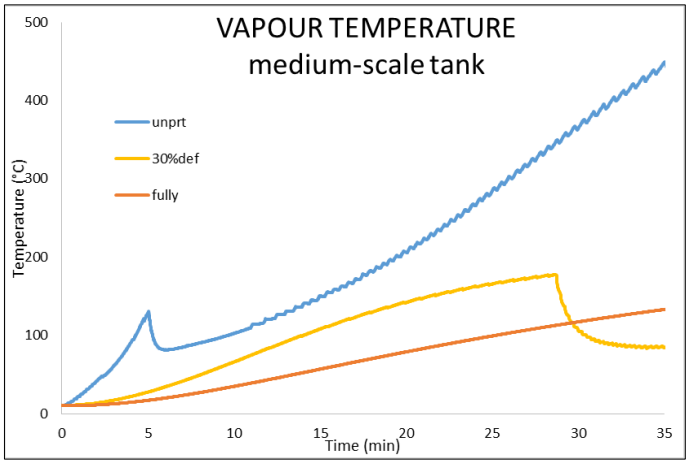

Figure 9.10a – Medium scale case study, vapour temperature comparison between unprotected, fully protected and 15% defective insulation area

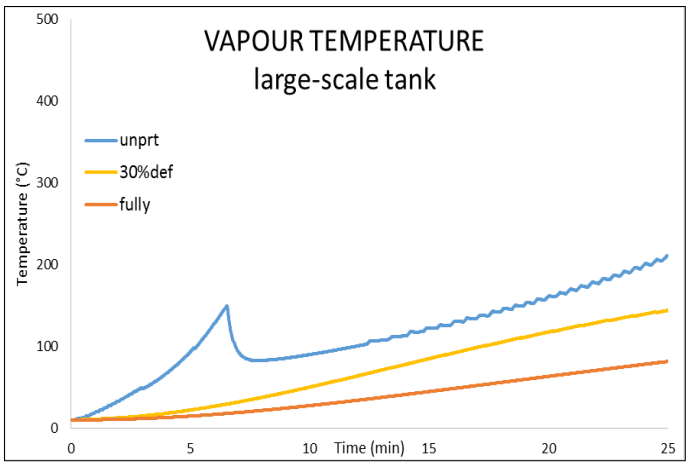

Figure 9.10b – Large scale case study, vapour temperature comparison between unprotected, fully protected and 15% defective insulation area

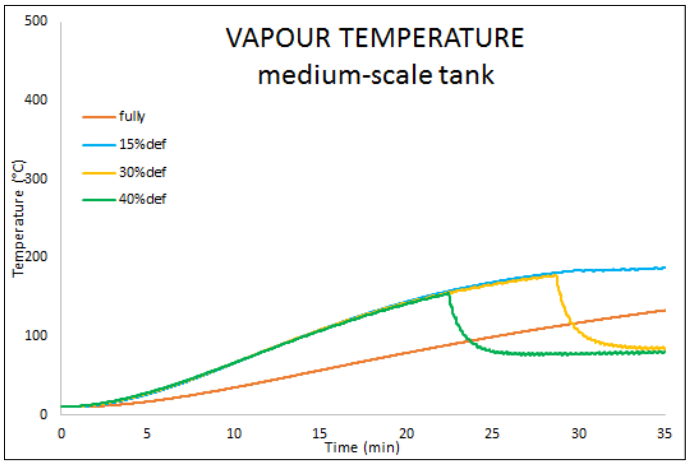

Figure 9.11a – Medium scale case study, vapour temperature comparison between different ratio of defective area (fully protected, 15%, 30% and 40% of defective area)

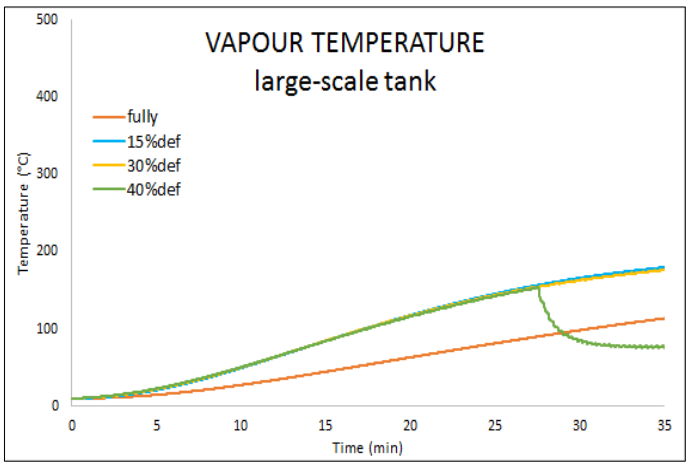

Figure 9.11b – Large scale case study, vapour temperature comparison between different ratio of defective area (fully protected, 15%, 30% and 40% of defective area)

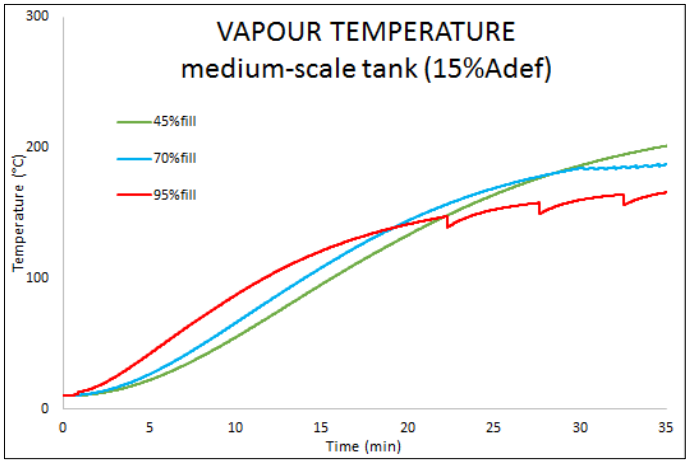

Figure 9.12a – Medium scale case study, vapour temperature comparison between different initial filling level (45%, 70% and 95% filling; 15% defective area)

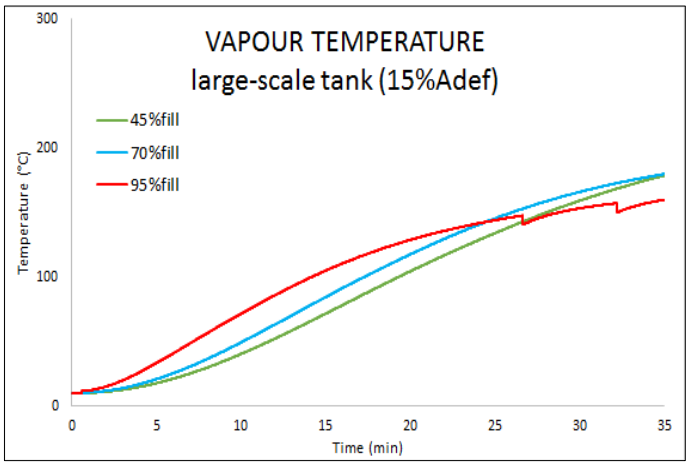

Figure 9.12b – Large scale case study, vapour temperature comparison between different initial filling level (45%, 70% and 95% filling; 15% defective area)

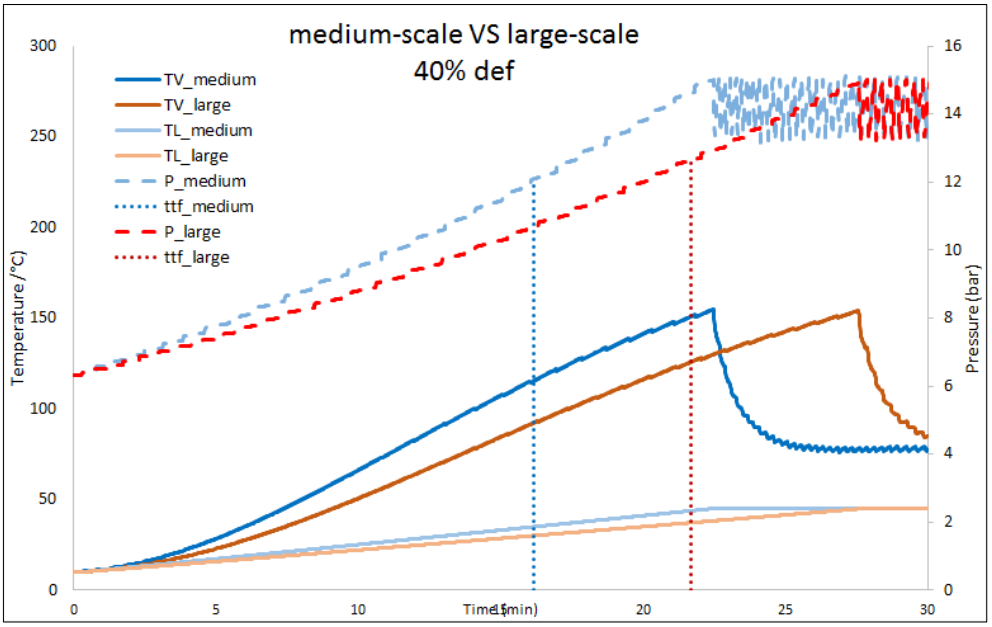

Figure 9.13 – Different tank scale results comparison, liquid and vapour temperatures are reported jointly the pressure inside the tank

9.5.3 Discussion

Pressure

It was expected that the tank with 30% of defective insulation area has a pressure profile intermediated between the fully protected and the fully unprotected tank, Figures 9.8 confirm this assumption. The defective area increase leads to a higher pressure inside the tank, as well as the liquid filling increase. In this case, the top volume of vessel available for the vapour phase filling, decreases and the system responds with a faster pressurization.

Lading temperature

The behaviour of the vapour temperature follows the same consideration done for the pressure, about the intermediate behaviour of the defective coating-case and the unprotected or fully protected ones. Up to the first opening of the PRV the curves relative to different defect areas appears superimposed. Whereas the comparison between the different initial filling level turns out in a vapour temperature altered, for higher liquid filling the resulting vapour temperature is higher.

Wall temperature and time to failure of the tank

The maximum wall temperature reached by the shell wall in contact with the defective air gap and the vapour phase has no noticeable changes between the case-studies. This supports the hypothesis of the existence of a critical defect size exceeding which the temperature reached in the defect is not correlated to the defect size. Thus, also the time to failure calculated with the model, according to section 7.2.4, are not much influenced by the defect area increase. The conservative times to failure of the tank obtained with the model, relative at different defective area are summarized in Table 9.4 for the medium-scale and in Table 9.5 for the large-scale, the fully protected tank never fails during the simulations.

Table 9.4 – Summary of the time to failure results of the medium-scale case-studies

$A_{def}/A_{coating}$	%	**8%**	15%	**15%**	15%	**30%**	**40%**	**unprot.**
Filling level	%	70%	**45%**	**70%**	**95%**	70%	70%	70%
$ttf_{conservative}$	min	18	18	17	16	17	16	11
ttf_{BS7910}	min	20	20	19	18	19	20	16
emptying	min							60

Table 9.5 – Summary of the time to failure results of the large-scale case-studies

$A_{def}/A_{coating}$	%	15%	**15%**	15%	**30%**	**40%**	**unprot.**
Filling level	%	**45%**	**70%**	**95%**	70%	70%	70%
$ttf_{conservative}$	min	20	20	18	19	19	14
ttf_{BS7910}	min	23	23	21	22	22	19
emptying	min						68

Tank scale

The results of the simulation with 40% of defective area and 70% of initial filling, is used for the comparison of the medium- and large-scale of tank. As it was expected to be, the smaller tank pressurizes earlier, and both the liquid and the vapour temperatures follow this profile.

10 Conclusions and future works

Starting from the data analysis of past accidents occurred in road and rail hazmat transportation, the main causes and consequences of accidents involving LPG were identified. Accidental fire exposures emerged among causes of LPG tankers failure, in this scenario the BLEVEs are the worst case occurrence. Thus, the analysis raised the question of the need of passive fire protection systems able to avoid, or at least delay, the BLEVEs, since ADR and RID regulations do not require any PFP on LPG tankers. The matter with the implementation of such protections on tankers is that thermal coatings undergo defects, as discovered by thermographic inspection of tank-cars [Birk & Cunningham, 2000], thus the action of thermal protection may be compromised. To assess the performance of defective insulation systems, overcoming real-scale bonfire tests, the implementation of simulation tools was considered. Thus, the issues concerning insulated tanks exposed to fire with defective insulation system were characterized first through the analysis of available bonfire experiments [Birk et al. 2006; VanderSteen & Birk, 2003] and then through the analysis of literature studies [Scarponi et al. 2016].

With this basis, an advanced FEM model was presented. The model was implemented and validated by [Scarponi et al. 2016] and then it was applied to a sensitivity analysis, to assess the influence of several parameters on the behaviour of a quarter cylinder tank exposed to fire, with different deficiencies configuration. The FEM model requires and provides detailed information on the problem, allowing the use of a correct failure criteria to evaluate the time to failure of the tank. This analysis has very high computational time, a way to reduce it is to skip the computing of pressure and lading temperature providing these data as external boundary conditions.

Thus, a simplified lumped parameters model was implemented to assess the performance of defective coatings, in order to save computation time and requiring less detailed information in input. The RADMOD model was improved for the simulation of defective coatings with respect to a previously work [Landucci et al. 2013] which was developed only for unprotected and completely insulated tanks. The model validation was performed against available experimental data [Birk et al. 2006] on small-scale tanks. Then the model was extended to the simulation of medium- and large-scale tanks through the definition of several case-studies.

The results obtained with the RADMOD code have showed that the model generally realizes a conservative analysis of the thermal behaviour of LPG tanks, providing credible temperatures and pressure profiles and also computing a conservative time to failure, which anyway gives an idea of tank behaviour. However, some keys improvements could be considered in the development of the work as discussed in the following:

- Add extra nodes
- Partial engulfment enhancement
- Heat transfer coefficients detailed correlations
- Vapour transparency detailed analysis
- Itemized studies on PRV opening effect
- De-stratification sub-model

- Widening type of substances implemented
- Software lightening and speeding up

Introducing extra nodes, generally, could be a good improvement of the code. Firstly, the steel jacket could also be considered adding the associated nodes, whereas more nodes in the shell could bring more detailed maximum temperature of the shell. Farther, the current version of the model considers the partial engulfment of the tank only dividing the external surfaces, thus the computed temperature is averaged on the node. Add extra nodes, with respect the engulfment, could allow the simulation of different flame impingements and it would be interesting especially for the analysis in the first time step when the fire is not usually fully propagated.

For what concerns the heat transfer modelling and balances, the evaluation of heat-transfer coefficients affects the temperature profiles, thus, many simplified correlations were adopted and more detailed correlation could be considered. Moreover, for the heat transfer by radiation between the shell walls and vapour-phase, an improvement was already done not considering the vapour as completely transparent, but a detailed analysis could be done considering three quantities; gas emissivity, gas absorptivity and gas transmissivity among which the first one is a function of the gas temperature, while the others are functions of both gas and surface radiation temperatures. Moreover, a conductive contribution through the liquid side shell and the vapour side shell could be considered.

A limit of the model is in the vapour temperature after the opening of the PRV, now there is already a heat transfer coefficient boost considering a forced convective contribution after PRV opening, anyway some extra studies could be done on that. Actually, the vapour is also considered as a pure gas, it is reasonable to believe that some liquid droplets could be present in the gas bulk as the consequence of boiling process and it has a 2-phases venting through PRV. Another improvement related to the PRV could be the implementation of a de-stratification sub-model, since at the PRV opening the model considers the immediate mixing of the stratified layer and this, clearly, needs further improvement to model the real behaviour of the liquid-phase inside the tank.

The model could be also extended to other substances like pure compound or mixture. In latter case also the mixing rule could be considered, which requires quite more efforts.

Also the software code could be improved, first rewriting it from brand new to make the simulation faster and to add less approximation in the mathematical calculation, and then checking the analytical stability of the model.

The defect sub-model could be modified allowing setting the percentage of defective area in each side, vapour or liquid. This action requires a geometrical analysis of the problem which is complicated if different fire impingement want to be simulated.

In conclusion, when experimental data will be available for medium- and large-scale tanks some validation studies have to be carried to verify the ability of the defective RADMOD sub-model.

References

- *Rum, Modeling the behaviour of pressurized vessels exposed to fires through Computational Fluid Dynamics, Master's Degree Thesis in Chemical Engineering at University of Pisa, Pisa, 2015*
- *A.M. Birk, Analysis of a Propane Sphere Bleve, CEt - AIDIC 31, 2013*
- *A.M. Birk, Modelling the response of tankers exposed to external fire impingement, J. Hazard. Mater. 20 (1988) 197-225*
- *A.M. Birk, Scae effects with fire exposure of pressure-liquefied gas tanks, J. Loss Prev. Process Ind. Vol. 8 No. 5. pp. 275-290, 1995*
- *ADR, European Agreement, Concerning the International Carriage of Dangerous Good by Road, Volume I and II, United Nations, 2014*
- *ANSYS inc, ANSYS Mechanical APDL Theory Reference (R. 14.5), ANSYS Inc, Canonsburg, PA, 2013*
- *API Standard 520, Sizing, Selection, and Installation of Pressure-relieving Devices - Part 1 Sizing and selection, 2014*
- *API Standard 520, Sizing, Selection, and Installation of Pressure-relieving Devices - Part 1 Sizing and selection, 2014*
- *API Standard 527, Seat Tightness of Pressure Relief Valves, 2014*
- *ARIA database, Web Site, Home Page, Accessed in January 2016, Available to: www.aria.developpement-durable.gouv.fr*
- *ASME, Boiler and Pressure Vessel Code, Section VIII, Division 1, Rules for Construction of Pressure Vessels, 2015*
- *Hemmatian, E. Planas, J. Casal, On BLEVE definition, the significance of superheat limit temperature (Tsl) and LNG BLEVE's, J. Loss Prev. Process Ind., 40 (2016) 81, 2015*
- *BAM - Federal Institute for Materials Research and Testing, BLEVE (Boiling Liquid Expanding Vapour Explosion) in dangerous goods tanks - investigation into the performance of tank constructions and equipment, particularly thermal and fire protection insulation in the event of fire, 2012*
- *Birk A.M., Cunningham M.H., Thermographic inspection of rail-car thermal insulation, S0094-9930(00)01104-5*
- *Birk A.M., Cunningham M.H., Thermographic Inspection of Rail-Car Thermal Insulation,J. Pressure Vessel Technol 122(4), 494-501, 2000*
- *Birk, A.M, Poirier, D., Davison, C., On the thermal rupture of 1.9 m3 propane pressure vessels with defects in their thermal protection system, Journal of Loss Prevention in the Process Industries 19 (2006) 582-597*
- *Birk, A.M., A.M. Birk Engineering, Tank-car insulation defect assessment criteria: thermal analysis of defects, Transportation development centre, TP 13518E, October 1999*
- *Birk, A.M., and M.H. Cunningham. Liquid temperature stratification and its effect on BLEVEs and their hazards. Journal of Hazardous Material, 1996: 219-237.*
- *Birk, A.M., Cunningham, M.H.,The boiling liquid expanding vapor explosion, J. Loss Prev. Process Ind., 7 (1994), pp. 474–480*
- *Birk, A.M., Development and validation of a mathematical model of a rail tank-car engulfed in fire, PhD Thesis, Queen's University, Ontario, Canada, 1983*
- *BS7910, Guide to methods for assessing the acceptability of flaws in metallic structures, 2013*
- *Butler, C.J., M.A. Persaud, T.A. Roberts, L.C. Shirvill, and S. Wright. "Heat-up and failure of Liquefied Petroleum Gas storage vessel exposed to a jet-fire." In Loss Prevention in the Process Industries, 1069-1106. Stockholm, 2001.*
- *Canadian General Standards Board Standard CAN/CGSB 43.147-2002*
- *CCPS; Guidelines for pressure relief and effluent handling system, March 1998*
- *Center for Chemical Process Safety (CCPS), Vapour Cloud Explosion, Pressure Vessel Burst, BLEVE and Flash Fire Hazards, 2nd ed., Hoboken, NJ: John Wiley and Sons, 2010*
- *CFR Code of Federal Regulation, 49 CFR Part 179 "specification for tankwagons" U.S. Government Publishing Office, Washington, DC, 2015. https://www.law.cornell.edu/cfr/text/49/part-179/appendix-B*
- *CGSB - Canadian General Standards Board Standard, Ottawa, Ontario, Canada, CAN/CGSB 43.147-97, 1997*
- *COUNCIL DIRECTIVE 94/55/EC of 21 November 1994 on the approximation of the laws of the Member States with regard to the transport of dangerous goods by road*
- *Crowl, S. A. Tipler, Sizing Pressure-Relief Devices, AIChE, October 2013*
- *D.W. Sallet, Pressure relief valve sizing for vessels containing compressed liquefied gases. I.Mech.E.Symp. Paper No C274/79, 1979*

- *D'Aulisa A., Tugnoli A., Cozzani V., Landucci G. & Birk A. (2014). CFD Modeling of LPG essels Under Fire Exposure Conditions. AIChe Journal, pp. 4292-4305.*
- *"Decreto Ministeriale 4 settembre 1996 - Attuazione della direttiva 94/55/CE del Consiglio concernente il*
- *ravvicinamento delle legislazioni degli Stati membri relative al trasporto di merci pericolose su strada"*
- *Droste, B., Schoen, W., Full scale fire tests with unprotected and thermal insulated LPG storage tanks, Journal of Hazardous Materials, 20 (1988) 41-53*
- *1993-1-2, Eurocode 1: Action on structures - Part 1-2: General actions - Actions on structures exposed to fire , 2005*
- *Elastic Properties and Young Modulus for some Materials, The Engineering ToolBox, Accessed in January 2016, Available to: www.engineeringtoolbox.com*
- *Emrys Scarponi, G., Landucci, G., Tugnoli, A., Cozzani, V., Birk, A.M., International Journal of Themal Sciences, 2016*
- *Heymes, L. Aprin, A.M. Birk, P. Slangen, J.B. Jarry, H. François, G. Dusserre, An experimental study of an LPG tank at low filling level heated by a remote wall fire, J. Loss Prev. Process Ind. 26 (2013) 1484-1491*
- *Forrest, H.S., Emergency relief vent sizing for fire exposure when teo-phase flows must be considered, Proceeding of the 19th Loss Prevention Symposium. American Institute of Chemical Engineers, Houston*
- *"G. Gubinelli, Models for the Assessment of Domino Accidents in the*
- *Process Industry, Ph.D. thesis in Chemical*
- *Engineering. University of Pisa, Pisa, 2006"*
- *Landucci et al., Reliability Engineering and System Safety 132(2014)125–145, 2014*
- *Landucci, A. Tugnoli, V. Busini, M. Derudi, R. Rota, V. Cozzani, The Viareggio LPG accident: Lessons learnt, J. Of Loss Prev. In the Process Ind., 24 (2011) 466-476*
- *Landucci, Development and Modelling of Passive Fire Protection Systems, Ph.D. thesis in Chemical Engineering. University of Pisa, Pisa, 2008*
- *G. Landucci, et al., Modeling heat transfer and pressure build-up in LPG vessels exposed to fire, International Journal of Thermal Science, 2016*
- *"G. Landucci, G. Gubinelli, G. Antonioni, V. Cozzani, The assessment of the damage probability of storage tanks in domino events*
- *triggered by fire, Accident Analysis and Prevention 41 (2009) 1206-1215, 2009"*
- *G. Landucci, M. Molag, J. Reinders, V. Cozzani, Experimental and analytical investigation of thermal coating effectiveness for 3m3 LPG tanks engulfed by fire, J. Hazard. Mater. 161 (2009) 1182-1192, 2009*
- *"G. Zuccaro, A Case of Choice of Passive Fire Protection (PFP) in an*
- *Oil & Gas EPC Project, AIDIC DOI: 10.3303/CET1226053, 2012"*
- *International Standard EN ISO 13702:1999, Petroleum and natural gas industries - Control and mitigation of fire and explosions on oggshore production installations - Requirements and Guidelines, 1999*
- *J.E.S. Venart, Boiling liquid expanding vapour explosions (BLEVE): possibe failure mechanisms and their consequences, papaer 10 in Harzards XV, Volume 1, 2000*
- *J.G. Knudsen, H.C. Hottel, A.F. Sarofim, P.C. Wankat, K.S. Knaebel, Heat and mass transfer, Section 5, in: M. Hill (Ed.), Perry's Chem. Eng. Handb., 7th ed., McGraw Hill, New York, NY, 1999*
- *J.G. Knudsen, H.C. Hottel, A.F. Sarofim, P.C. Wankat, K.S. Knaebel, PHYSICAL AND CHEMICAL DATA, Section 2, in: M: Hill (Ed.), Perry's Chem. Eng. Handb., 7th ed., McGraw Hill, New York, NY, 1999*
- *Johnson M.R., Tank car thermal analysus, Volume 1 and 2, DOT/FRA/ORD-98/09A and DOT/FRA/ORD-98/09B, November 1998*
- *Johnson M.R., TCFIRE: A model for prediction of fire effects on tank cars, AAR Publucation SD-053, 1995*
- *K. Moodie, Experiments and modelling: an overview with particular reference to fire engulfment, J. Hazard. Mater. 20 (1988) 149-175*
- *Keltner, N. R., Nicolette, V. F., Brown, N. N. and Bainbridge, B. L. J. Hazard. Mater. 1990, 25, 33-47*
- *Kern, Process heat transfer, McGraw-Hill book company, International edition, 1965.*
- *L. Nigro, Analysis And Simulation Of The Thermal Behaviour Of Lpg Tankers Exposed To Fire, Master's Degree Thesis in "Progettazione Di Apparecchiature E Impianti M", Alma Mater Studiorum - University of Bologna, Bologna, 2015*
- *Landucci G., Cozzani V., Birk M., Heat Radiation Effects in Domino Effects in the Process Industries, Cozzani V. and Reniers G. Amsterdam-Elsevier, 2013: 70-115.*
- *Landucci G., Tugnoli A., Cozzani V., Analysis of fired coated vessels in presence of defects in the thermal protection, 2011*

- *Lees, F.P., Loss Prevention in the Process Industries-Hazard Identification, Assessment, and Control, vols. 1–3, Butterworth-Heinemann, Oxford, 1996*
- *Legge 12 agosto 1962 n.1839*
- *Leung and Epstein, A generalized correlation for two-phase non-flashing homogeneous chocked flow, Trans. ASME J. Heat Tranfer 112 (May), pp. 528-530, 1990*
- *Leung and Epstein, A generalized critical flow model for non-ideal gases, AIChe J. 34(9), pp. 1568-1572, 1988*
- *Leung and Nazario, Sizing pressure relief valves in flashing, two-phase service: an alternative procedure, J. Loss Prev. Process Ind. 5 (5), pp. 263-269, 1992*
- *M. Bazzocchi, Evaluation Of The Pressure Build Up In Pressurized Tankers Exposed To Fire, Master's Degree Thesis in "Progettazione Di Apparecchiature E Impianti M", Alma Mater Studiorum - University of Bologna, Bologna, 2014*
- *M. Molag, A. Kruithof, BLEVE prevention of a LPG tank vehicle or a LPG tank wagon, report R2005/364, Netherlands Organisation for Applied Scientific Research – TNO, Apeldoorn, 2005*
- *M.F. Modest, Radiative Heat Transfer, Academic Press, New York, NY, 2003*
- *Ministero delle Infrastrutture e dei Trasporti, Conto Nazionale delle Infrastrutture e dei Trasporti, Anni 2012-2013*
- *Moodie, K., Cowley, L.T., Denny, R.B., Small, L.M., Williams, I., Fire engulfment tests on a 5 tonne LPG tank, Journal of Hazardous Materials, 20 (1988) 55-71*
- *N.U. Aydemir, V.K. Magapu, A.C.M. Souse and J.E.S. Venart, Thermal response analysis of LPG tanks exposed to fire, J. Hazard. Mater. 20 (1988) 239-262*
- *Paltrinieri, N. et al., Risk reduction in road and rail LPG transportation by passive fire protection, J. Hazard. Mater. (2009), doi: 10.1016/j.jhazmat.2008.12.122*
- *Perry, R. H., and D. W. Green, Eds., "Process Safety" Chapter 23, in Perry's Chemical Engineers' Handbook, 8th ed., McGraw-Hill, New York (1984)*
- *Peter M. Maitlis, A. de Klerk, Greener Fischer-Tropsch Processes for Fuels and Feedstocks, Februar 2013*
- *R. Mauri, Elementi di Fenomeni di Trasporto (II ed.). PLUS, Pisa University Press, 2012*
- *R.C. Reid. Possible mechanism for pressurized-liquid tank explosions or BLEVE's. Science 1979;203:1263-1265*
- *R.K. Eckhoff, Boiling liquid expanding vapour explosions (BLEVEs): A brief review, J. Loss Prev. Process Ind. 32 (2014) 30-43, 2014*
- *R.W. Prugh, Quantify BLEVE hazards, Chem. Eng. Prog. 87 (2) (1991) 66–71.*
- *Recommendations on the transport of dangerous goods, Model Regulations, Volume I, UN, ST/SG/AC.10/1/Rev.18 (Vol.I), 2013*
- *S.K.S. Boetcher, Natural convection from circular cylinders, Springer, Heidelberg, Germany, 2014*
- *S.W. Churchill, H.H.S. Chu, Correlating equations for laminar and turbolent free convection from vertical plate, Int. J. Heat Mass Transf. 18 (1975) 1323-1329*
- *Smith J.M, Van Ness H.C., Abbot M.M. In "Introduction to chemical engineering thermodynamics". 7th Revised edition 2004*
- *"T. A. Roberts, I. Buckland, L. C. Shirvill, B. J. Lowesmith And P. Salater, Design And Protection Of Pressure Systems To Withstand Severe Fires, Trans IChemE, Part B, March 2004*
- *Process Safety and Environmental Protection, 82(B2): 89–96"*
- *TNO Methods for the calculation of Physical Effects -due to releases of hazardous materials (liquids and gases)-Yellow Book, 3th ed., 2005*
- *Townsend, W., Anderson, C., Zook, J., Cowgill, G., Comparison of thermally coated and uninsulated rail tank-cars filled with LPG subjected to a fire environment, US Department of Transportation, Washington DC, 1974*
- *TSO, Fire and Rescue Service, Operational guidance - Incidents involving hazardous materials, ID2511951 C5 11/12, 2012*
- *UNECE Official Web Site, in Transport – Areas of work – Dangerous Goods, Accessed in January 2016 , Available to: www.unece.org*
- *VanderSteen, J.D.J., Birk, A.M., Fire tests on defective tank-car thermal protection systems, Journal of Loss Prevention in the Process Industries 16 (2003) 417-425*
- *W.J. King, The basic laws and data of heat transmission, American Society of Mechanical Engineers, 1932*
- *Walls W.L., The BLEVE - Part 1, Fire Command, vol. 17, 1979*
- *Walls W.L., What is BLEVE?, Fire Journal, vol. 31, 1978*
- *Yu, C.M., N.U. Aydemir, e J.E.S. Venart. «Transient Free Convection and Thermal Stratification in Uniformly-Heated Partially-Filled Horizontal Cylindical and Spherical Vessels.» Journal of Thermal Science 1, n. 2, 1992*
- *Zografos, K.G., Androutsopoulos, K.N., 2004. A heuristic algorithm for solving hazardous materials distribution problems. European Journal of Operations Research 152, 507–519, 2004*

Appendix A

Additional information about the modelling of heat and mass balances in the RADMOD Baseline code are reported in this appendix. First are explained the equations related to the variables, then the heat loads and heat exchange coefficients are defined. and in the end the nodal area are determinate.

The summary of the equations implemented in the RADMOD Baseline is reported in Table A.1 and A.2. While, the equations set implemented in the novel version of the code are collected in Table A.2 and A.3 for the defective sub-model and in Table A.4 and A.5 for the validation sub-model.

Pressure

The equation to describe the pressure trend comes directly from the ideal gas law:

$$PV_V = zz\frac{m_V}{MW}RT_V \tag{A.1}$$

Where V_V is the gas volume. Considering the differentiate with constant zz and doing the mathematical rearrangements, a general formula for both thermodynamic systems is:

$$\frac{dP}{dt} = \frac{zz\rho_V}{m_V}\left(\frac{P}{\rho_L}\frac{dm_L}{dt} + \frac{RT_V}{MW}\frac{dm_V}{dt} + \frac{Rm_V}{MW}\frac{dT_V}{dt}\right) \tag{A.2}$$

Where ρ_V and $\rho_L$are the vapour and liquid densities. Including the other equation of liquid and vapour mass, the equation (A.2) will become specific for the case of sub-cooled or boiling liquid.

Liquid mass and Level

The liquid level inside the tank has an important role to define the surface for heat exchange for each node and consequently the correct thermal response of the tank.

Not boiling liquid:

$$\frac{dm_L}{dt} = 0 \tag{A.3}$$

$$\frac{dL}{dt} = 0 \tag{A.4}$$

Boiling liquid:

$$\frac{dm_L}{dt} = -\frac{(q_L + q_{LV})}{\Lambda} \tag{A.5}$$

$$\frac{dL}{dt} = \frac{1}{2\rho_L W\sqrt{R_i^2 - (R_i - L)^2}}\frac{dm_L}{dt} \tag{A.6}$$

Where Λ is the heat of vaporization, W is the length of the tank and, R_i is the inner radius of cylindrical container.

Vapour mass

To evaluate the vapour mass it is possible to take into account of the variation of total mass ($m_{tot} = m_L + m_V$) that is equal to the mass flow entering the system (none) less the mass flow discharged through the PRV:

$$\frac{dm_V}{dt} = -\frac{dm_L}{\mathrm{dt}} - \phi \qquad \text{(A.7)}$$

Including the other balance of liquid mass it is possible to obtain the two simple specific equations for the vapour in the case of sub-cooled and boiling liquid.

Temperature of the shell in contact with the liquid (T_{15})

$$d_s cp_{sL} \frac{s_s}{2} \overline{A_{15}} \frac{dT_{15}}{dt} = A_{15ext} \frac{k_{sL}}{s_s} (T_{iL} - T_{15}) - q_{L,boil} \qquad \text{(A.8)}$$

Where d_s is the density of shell material, cp_{sL} (eq. A.30) and k_{sL} (eq. A.31) are respectively the heat capacity and the thermal conductivity of wall in contact with the liquid, s_s is the shell thickness, $\overline{A_{15}}$ and A_{15ext} are the node averaged and external surface, respectively formulated as shown in equations (A.36c) and (A.36b). Considering the node division, $\frac{s_s}{2}\overline{A_{15}}$ gives the volume of the node$_{15}$, $A_{15ext}\frac{k_{sL}}{s_s}(T_{iL} - T_{15})$ is the conductive heat power entering the system on the liquid side. $q_{L,boil}$ is the heat power transferred from the wall in contact with the liquid to the liquid amount, and it is different if the liquid system is sub-cooled or boiling. The formulation of energy balance does not consider the conductive heat flux due to the circular pattern; this is negligible because the thickness is small.

Temperature of the shell in contact with the vapour (T_{26})

$$d_s cp_{sV} \frac{s_s}{2} \overline{A_{26}} \frac{dT_{26}}{dt} = A_{26ext} \frac{k_{sV}}{s_s} (T_{iV} - T_{26}) - q_V - q_{L,rad} \qquad \text{(A.9)}$$

Where cp_{sV} and k_{sV} are respectively the heat capacity and the thermal conductivity of shell on vapour side as a function of temperature. As in the case of the liquid-space wall, $\frac{s_s}{2}\overline{A_{26}}$ gives the volume of the node$_{26}$, $A_{26ext}\frac{k_{sV}}{s_s}(T_{iV} - T_{26})$ is the conductive heat power entering the system on the vapour side. While q_V is the heat power transferred from the wall to the vapour phase, it consists of both radiative and convective contribution. Term $q_{L,rad}$ is the heat power transferred from wall on vapour side to the liquid by radiation.

Temperature of the intermediate nodes iL and iV (T_{iL} and T_{iV})

Unprotected:

$$d_s cp_{sL} \frac{s_s}{2} \overline{A_{iL}} \frac{dT_{iL}}{dt} = A_{iL,F} I_{ext,L} - A_{iL,A} I_{amb,L} - A_{15ext} \frac{k_{sL}}{s_s} (T_{iL} - T_{15}) \qquad \text{(A.10)}$$

$$d_s cp_{sV} \frac{s_s}{2} \overline{A_{iV}} \frac{dT_{iV}}{dt} = A_{iV,F} I_{ext,V} - A_{iV,A} I_{amb,V} - A_{26ext} \frac{k_{sV}}{s_s} (T_{iV} - T_{26}) \qquad \text{(A.11)}$$

Coated:

$$\left(d_s cp_{sL} \frac{s_s}{2} \overline{A_{\imath L \imath nt}} + d_i cp_i \frac{s_i}{2} \overline{A_{\imath L ext}}\right) \frac{dT_{iL}}{dt} = A_{37int} \frac{k_i}{s_i} (T_{37} - T_{iL}) - A_{15ext} \frac{k_{sL}}{s_s} (T_{iL} - T_{15}) \quad \text{(A.12)}$$

$$\left(d_s cp_{sV} \frac{s_s}{2} \overline{A_{\imath V \imath nt}} + d_i cp_i \frac{s_i}{2} \overline{A_{\imath V ext}}\right) \frac{dT_{iV}}{dt} = A_{48int} \frac{k_i}{s_i} (T_{48} - T_{iL}) - A_{26ext} \frac{k_{sV}}{s_s} (T_{iV} - T_{26}) \quad \text{(A.13)}$$

Where d_i , cp_i , k_i and s_i are respectively the density, the heat capacity, the thermal conductivity and the thickness of the coating. For the determination of all the nodal areas related to A_{iL}, A_{iV}, A_{48}, A_{37}, $A_{15}$and A_{26} see equations (A.36-A.41).

The heat leaving the systems to the inner nodes remains unchanged from the two cases, it is expressed as $A_{15ext} \frac{k_{sL}}{s_s} (T_{iL} - T_{15})$ and $A_{26ext} \frac{k_{sV}}{s_s} (T_{iV} - T_{26})$, for node$_{iL}$ and node$_{iV}$ respectively, and represents the power heat transferred by conduction from the intermediate nodes to the internal node$_{15}$ and node$_{26}$.

Temperature of the external coating nodes 48 and 37 ($T_{48}$and T_{37})

As already said, this nodes are present only in case of coated tank and the equations are the same as the intermediate nodes for unprotected tanks. The temperature of the nodes on liquid side (T_{37}) and on vapour side (T_{48}) are calculated as:

$$d_i cp_i \frac{s_i}{2} \overline{A_{37}} \frac{dT_{37}}{dt} = A_{37,F} I_{ext,L} - A_{37,A} I_{amb,L} - A_{37int} \frac{k_i}{s_i} (T_{37} - T_{iL}) \quad \text{(A.14)}$$

$$d_i cp_i \frac{s_i}{2} \overline{A_{48}} \frac{dT_{48}}{dt} = A_{48,F} I_{ext,V} - A_{48,A} I_{amb,V} - A_{48int} \frac{k_i}{s_i} (T_{48} - T_{iV}) \quad \text{(A.15)}$$

Heat loads from external nodes to ambient

In case of partial engulfment the heat flux from the shell surface to the ambient air is both convective and radiative:

$$I_{amb} = h_a (T_w - T_{amb}) + \sigma \varepsilon_s \left(T_w^4 - T_{amb}^4\right) \quad \text{(A.16)}$$

Where T_w is, the generic wall temperature to change with the specific nodal temperature, T_{amb} is the ambient temperature and $h_a$is the convective heat-transfer coefficient to evaluate the heat exchange between the shell and the air at the temperature T_{amb}. As suggested in [Kern, 1965]:

$$h_a = 0.3 * 5.678 (T_{wall} - T_{amb})^{0.25} \quad \text{(A.17)}$$

Heat loads to the liquid from the internal shell nodes

The heat load received by the liquid $q_L$is defined as the sum of a convective and a radiative contribution ($q_L = q_{L,boil} + q_{L,rad}$). The convective term is expressed as:

$$q_{L,boil} = A_{15int} h_L (T_{15} - T_L) \quad \text{(A.18)}$$

Where h_L is the convective heat transfer coefficient and it depends on the pool boiling regime. The two cases and the relative correlation for the estimation of h_L are the same

used in the novel RADMOD version and described in paragraph 7.3.1 for the two cases of interface evaporation or nucleate boiling.

Regarding the radiative heat transfer between the vapour-space internal surface and the liquid, in the novel implementation of the code, see paragraph 7.3.1.

Heat loads to the liquid from the vapour phase

$$q_{LV} = A_{LV} h_{LV} (T_V - T_L) \quad \text{(A.19)}$$

A_{LV} is surface of the liquid-vapour interface calculated throught equation (A.42). The heat-transfer coefficient h_{LV} is consist of two terms, a natural convective coefficient and other radiative. For convective contribution the correlation of hot horizontal plate facing downward are adopted as suggested in [Perry & Green, 1997]. Defining the same dimensionless key parameter of (7.28 , paragraph 7.3.1), but with the subscript V and the characteristic length defined as in equation (A.21) , the heat coefficient $h_{LV,conv}$ is derived from:

$$Nu = \frac{h_{LV} xi}{k_V} = 0.27 Ra^{1/4} \quad \text{(A.20)}$$

$$x_i = \frac{4A_{LV}}{2\left(W + {}^{A_{LV}}/_{W}\right)} \quad \text{(A.21)}$$

Whereas the radiative heat-transfer coefficient from vapour to liquid is calculate by the empirical correlation [Perry & Green, 1997]:

$$h_{LV,rad} = 5.6783 \frac{\left[\left(\frac{T_V}{100}\right)^4 - \left(\frac{T_L}{100}\right)^4\right] 0.173}{(T_V - T_L)} \quad \text{(A.22)}$$

Heat loads to the vapour from the internal shell nodes

The total heat entering the vapour node is the sum of a convective contribution $q_{V,conv}$ and a radiative contrivution $q_{V,rad}$:

$$q_V = q_{V,conv} + q_{V,rad} = A_{26int} h_{V,c} (T_{26} - T_V) + A_{26int} h_{V,r} (T_{26} - T_V) \quad \text{(A.23)}$$

The convective coefficient is calculate with the equations (A.24) or with equation (A.26) depending on the PRV function.

If PRV is closed:

Defining the dimensionless key parameters of (7.48, paragraph 7.3.1) but with the subscript V and characteristic length defined as shown in equation (A.25), the convective coefficient is:

$$Nu = \frac{h_{V,c}\, xi}{k_V} = 0.27 Ra^{1/4} \quad \text{(A.24)}$$

$$x_i = \frac{4A_{26int}}{2\left(W + {}^{A_{26int}}/_{W}\right)} \quad \text{(A.25)}$$

If PRV is opened:

Forced convection is also considered and added to the natural convection coefficient.

$$Nu = \frac{h_{V,forced}\, xi}{k_V} = 0.0243 Re^{0.8} Pr^{0.4} \quad \text{(A.26)}$$

Where:

$$Pr = \frac{\mu_V cp_V}{k_V} \;;\; Re = \frac{4\phi}{p\mu_V} \quad \text{(A.27)}$$

Where ϕ is the mass flow throughout the PRV derived with equation (A.35) Characteristic length x_i is given by the ratio of the section of vapour phase and the wetted perimeter according to:

$$x_i = \frac{4A_{vap}}{p_{wetted}} = \frac{R_i^2\left(cos^{-1}\left(\frac{L-R_i}{R_i}\right) - sin\left(\frac{L-R_i}{R_i}\right)\left(\frac{L-R_i}{R_i}\right)\right)}{2\pi cos^{-1}\left(\frac{L-R_i}{R_i}\right)} \quad \text{(A.28)}$$

The radiative coefficient $h_{V,rad}$ is calculated as follow:

$$h_{V,r} = 5.6783 \frac{\left[\left(\frac{T_{26}}{100}\right)^4 - \left(\frac{T_V}{100}\right)^4\right] 0.173}{(T_{26} - T_V)} \quad \text{(A.29)}$$

Thermal properties of wall material

The thermodynamic properties of the steel wall (stainless and carbon steel) are dependent of the temperature of the wall. Properties of interest are the heat capacity, and the conductive heat transfer coefficient.

The specific heat of carbon steel (subscript CS) is a fit of the properties for steel taken from Eurocode [Eurocode 1, 2005] as seen in equation set (A.30), where cp is calculated in J/kgK and the steel temperature T is in°C.

- $20 \leq T(°C) < 600$

$$cp_{CS} = 425 + 0.773 \cdot T - 0.00168 \cdot T^2 + 2.22 \cdot 10^{-6} \cdot T^3 \quad \text{(A.30a)}$$

- $600 \leq T(°C) < 735$

$$cp_{CS} = 666 + \frac{13002}{738 - T} \quad \text{(A.30b)}$$

- $735 \leq T(°C) < 900$

$$cp_{CS} = 545 + \frac{17820}{T - 731} \quad \text{(A.30c)}$$

- $900 \leq T(°C) < 1200$

$$cp_{CS} = 650 \quad \text{(A.30d)}$$

The thermal conductivity (k_{CS}) is modelled from equation set (A.31), as found by Eurocode [Eurocode 1, 2005]. It is estimated as W/mK.

- $20 \leq T(°C) < 800$

$$k_{CS} = 54 - 0.0333 \cdot T \quad \text{(A.31a)}$$

- $800 \leq T(°C) < 1200$

$$k_{CS} = 27.3 \quad \text{(A.31b)}$$

The same approach is considered for the stainless steel (subscript SS). The specific heat of stainless steel may be determined from the following equation (A.32), whereas the conductive heat transfer coefficient follows the equation (A.33). Both correlations are found by Eurocode [Eurocode 1, 2005].

- $20 \leq T(°C) < 1200$

$$cp_{SS} = 450 + 0.280 \cdot T - 2.91 \cdot 10^{-4} \cdot T^2 + 1.34 \cdot 10^{-7} \cdot T^3 \quad \text{(A.32)}$$

- $20 \leq T(°C) < 1200$

$$k_{SS} = 14.6 - 0.0127 \cdot T \quad \text{(A.33)}$$

Mass flow through PRV

The general equation for determination of the mass flow discharged through he PRV is defined as: $\phi = \rho_v u A_{cross}$. The density of the vapour ρ_v is calculated through the ideal gas law, and for considering the real gas behaviour the compressibility factor (zz) is inserted in the equation. The cross-sectional area (A_{cross}) is the area of valve through which the fluid has the efflux velocity u. Making use of Mach number definition (eqation A.34) for a subsritical flow (more detail in Chapter 5), the mass flow is calculated with hypothesis of a isentropic process and, considering that the internal dissipative phenomena (wall friction) and the heat exchanges with the external environment are negligible.

$$Ma = \sqrt{\frac{\left(\frac{P}{P_{disc}}\right)^{\frac{\gamma-1}{\gamma}} - 1}{\frac{\gamma-1}{2}}} \quad \text{(A.34)}$$

$$\phi = c_D A_{PRV} \frac{P}{zz} \sqrt{\frac{\gamma MW}{RT_V}} \frac{Ma}{\left(1+\frac{\gamma-1}{2}Ma^2\right)^{\frac{\gamma+1}{2(\gamma-1)}}} \quad \text{(A.35)}$$

Nodal areas

The nodal areas are calculated in function of the liquid level, which determines the surfaces in the liquid space and the ones in the vapour space. The the definition of three exchanging areas for each node, specifically: internal, external and averaged area, is complex and the difference between the three surfaces on the same node is not that significative. The internal and the external areas are are the surfaces through with the heat powers passing through, whereas the averaged areas are used for the volumes evaluation. A simplification is advisable in the future works, by the definition of one area of exchange for each node. Starting the inner nodes, the different nodal areas are defined as follow, subscripts i or s means that the variables are referred to the insulation or to the steel walls, L is the liquid level and W is the tank length:

Liquid side inner node (node$_{15}$)

$$A_{15int} = 2WR_i cos^{-1}\left(\frac{R_i - L}{R_i}\right) \quad \text{(A.36a)}$$

$$A_{15ext} = \frac{A_{15int}+\overline{A_{iL}}}{2} \quad \text{(A.36b)}$$

$$\overline{A_{15}} = \frac{A_{15int}+A_{15ext}}{2} \quad \text{(A.36c)}$$

Vapour side inner node (node$_{26}$)

$$A_{26int} = 2\pi W R_i - A_{15int} \quad \text{(A.37a)}$$

$$A_{26ext} = \frac{A_{26int}+\overline{A_{iV}}}{2} \quad \text{(A.37b)}$$

$$\overline{A_{26}} = \frac{A_{26int}+A_{26ext}}{2} \quad \text{(A.37c)}$$

Liquid side intermediate node (node$_{iL}$)

$$\overline{A_{iLint}} = \frac{\overline{A_{iL}}+A_{15ext}}{2} \quad \text{(A.38a)}$$

$$\overline{A_{iLext}} = \frac{\overline{A_{iL}}+A_{37int}}{2} \quad \text{(A.38b)}$$

$$\overline{A_{iL}} = 2WR_e cos^{-1}\left(\frac{R_e-L}{R_e}\right) \quad \text{(A.38c)}$$

Vapour side intermediate node (node$_{iV}$)

$$\overline{A_{iVint}} = \frac{\overline{A_{iV}}+A_{26ext}}{2} \quad \text{(A.39a)}$$

$$\overline{A_{iVext}} = \frac{\overline{A_{iV}}+A_{48int}}{2} \quad \text{(A.39b)}$$

$$\overline{A_{iV}} = 2\pi W R_e - \overline{A_{iL}} \quad \text{(A.39c)}$$

Liquid side external node (node$_{37}$)

$$A_{37int} = \frac{\overline{A_{iL}}+A_{37ext}}{2} \quad \text{(A.40a)}$$

$$A_{37ext} = 2W(R_e + s_i)cos^{-1}\left(\frac{R_e+s_i-L}{R_e+s_i}\right) \quad \text{(A.40b)}$$

$$\overline{A_{37}} = \frac{A_{37int}+A_{37ext}}{2} \quad \text{(A.40c)}$$

Vapour side external node (node$_{48}$)

$$A_{48int} = \frac{\overline{A_{iV}}+A_{48ext}}{2} \quad \text{(A.41a)}$$

$$A_{48ext} = 2W(R_e + s_i) - A_{37ext} \quad \text{(A.41b)}$$

$$\overline{A_{48}} = \frac{A_{48int}+A_{48ext}}{2} \quad \text{(A.41c)}$$

Liquid-vapour interface

$$A_{LV} = WD_i sin\left(cos^{-1}\left|\frac{L-R_i}{R_i}\right|\right) \quad \text{(A.42)}$$

Summary of equations system in the RADMOD code

RADMOD code – Equations set

The equations set defined for the Baseline RADMOD model are 12 for a coated tank, whereas 10 variables are defined for unprotected tanks. The equations set is shown in Table A.1 and A.2 , in case of unprotected tanks the last two equations are not solved. If RADMOD_Strat1.m or RADMOD_Strat3.m the equations set is valid, with the appropriate definition of m_L.

Table A.1 – Summary of the RADMOD code equations set for the Sub-Cooled liquid condition, $P > P_{sat}(T_L)$

T_L	$m_L cp_L \frac{dT_L}{dt} = q_{L,boil} + q_{Lrad} + q_{LV}$
T_V	$m_V cv_V \frac{dT_V}{dt} = q_V - q_{LV} - zz\,\phi \frac{RT_V}{M_W}$
P	$\frac{dP}{dt} = zz \frac{\rho_V R}{M_W} \frac{dT_V}{dt} - zz\phi \frac{\rho_V R T_V}{m_V M_W}$
L	$\frac{dL}{dt} = 0$
m_L	$\frac{dm_L}{dt} = 0$
m_V	$\frac{dm_V}{dt} = -\phi$
T_{15}	$d_s cp_s \frac{s_s}{2}\left(\frac{A_{15int} + A_{15av}}{2}\right)\frac{dT_{15}}{dt} = A_{15av}\frac{k_s}{s_s}(T_{iL} - T_{15}) - q_{L,boil}$
T_{26}	$d_s cp_s \frac{s_s}{2}\left(\frac{A_{26int} + A_{26av}}{2}\right)\frac{dT_{26}}{dt} = A_{26av}\frac{k_s}{s_s}(T_{iV} - T_{26}) - A_{26int} h_V (T_{26} - T_V) - q_{L,rad}$
T_{iL}	$\left(d_i cp_i \frac{s_i}{2}\left(\frac{\overline{A_{iL}} + A_{37int}}{2}\right) + d_s cp_s \frac{s_s}{2}\left(\frac{\overline{A_{iL}} + A_{15ext}}{2}\right)\right)\frac{dT_{iL}}{dt} = A_{37int}\frac{k_i}{s_i}(T_{37} - T_{iL}) - A_{15ext}\frac{k_s}{s_s}(T_{iL} - T_{15})$
T_{iV}	$\left(d_i cp_i \frac{s_i}{2}\left(\frac{\overline{A_{iV}} + A_{48int}}{2}\right) + d_s cp_s \frac{s_s}{2}\left(\frac{\overline{A_{iV}} + A_{26ext}}{2}\right)\right)\frac{dT_{iV}}{dt} = A_{48int}\frac{k_i}{s_i}(T_{48} - T_{iV}) - A_{26ext}\frac{k_s}{s_s}(T_{iV} - T_{26})$
T_{37}	$d_i cp_i \frac{s_i}{2}\left(\frac{A_{37int} + A_{37ext}}{2}\right)\frac{dT_{37}}{dt} = A_{37F} I_{extL} - A_{37A} I_{extL} - A_{37int}\frac{k_i}{s_i}(T_{37} - T_{iL})$
T_{48}	$d_i cp_i \frac{s_i}{2}\left(\frac{A_{48int} + A_{48ext}}{2}\right)\frac{dT_{48}}{dt} = A_{48F} I_{extV} - A_{48A} I_{extV} - A_{48int}\frac{k_i}{s_i}(T_{48} - T_{iV})$

Table A.2 – Summary of the RADMOD code equations set for the boiling liquid condition, $P \leq P_{sat}(T_L)$.

T_L	$\frac{dT_L}{dt} = 0$
T_V	$m_V cv_V \frac{dT_V}{dt} = q_V - q_{LV} - zz\,\phi \frac{RT_V}{M_W} + \frac{dm_L}{dt}\left(cv_V(T_V - T_L) - \frac{R}{M_W}T_L\right)$
P	$\frac{dP}{dt} = zz\frac{\rho_V}{m_V}\left(\frac{P}{\rho_L}\frac{dm_L}{dt} + \frac{RT_V}{M_W}\frac{dm_V}{dt} + \frac{Rm_V}{M_W}\frac{dT_V}{dt}\right)$
L	$\frac{dL}{dt} = \frac{1}{2\rho_L W\sqrt{R^2 - (R-L)^2}}\frac{dm_L}{dt}$
m_L	$\frac{dm_L}{dt} = -\frac{(q_L + q_{LV})}{\Lambda}$
m_V	$\frac{dm_V}{dt} = \frac{(q_L + q_{LV})}{\Lambda} - \phi$
T_5	$d_s cp_s \frac{s_s}{2}\left(\frac{A_{15ext} + A_{15int}}{2}\right)\frac{dT_{15}}{dt} = A_{15ext}\frac{k_s}{s_s}(T_{iL} - T_{15}) - q_{L,boil}$
T_{26}	$d_s cp_s \frac{s_s}{2}\left(\frac{A_{26ext} + A_{26int}}{2}\right)\frac{dT_{26}}{dt} = A_{26ext}\frac{k_s}{s_s}(T_{iV} - T_{26}) - A_{26int}h_V(T_{26} - T_V) - q_{V,rad}$
T_{iL}	$\left(d_i cp_i \frac{s_i}{2}\left(\frac{\overline{A_{iL}} + A_{37int}}{2}\right) + d_s cp_s \frac{s_s}{2}\left(\frac{\overline{A_{iL}} + A_{15ext}}{2}\right)\right)\frac{dT_{iL}}{dt} = A_{37int}\frac{k_i}{s_i}(T_{37} - T_{iL}) - A_{15ext}\frac{k_s}{s_s}(T_{iL} - T_{15})$
T_{iV}	$\left(d_i cp_i \frac{s_i}{2}\left(\frac{\overline{A_{iV}} + A_{48int}}{2}\right) + d_s cp_s \frac{s_s}{2}\left(\frac{\overline{A_{iV}} + A_{26ext}}{2}\right)\right)\frac{dT_{iV}}{dt} = A_{48int}\frac{k_i}{s_i}(T_{48} - T_{iV}) - A_{26ext}\frac{k_s}{s_s}(T_{iV} - T_{26})$
T_{37}	$d_i cp_i \frac{s_i}{2}\left(\frac{A_{37int} + A_{37ext}}{2}\right)\frac{dT_{37}}{dt} = A_{37F}I_{extL} - A_{37A}I_{extL} - A_{37int}\frac{k_i}{s_i}(T_{37} - T_{iL})$
T_{48}	$d_i cp_i \frac{s_i}{2}\left(\frac{A_{48int} + A_{48ext}}{2}\right)\frac{dT_{48}}{dt} = A_{48F}I_{extV} - A_{48A}I_{extV} - A_{48int}\frac{k_i}{s_i}(T_{48} - T_{iV})$

Novel RADMOD sub-model for defective coatings – Equations set

The novel RADMOD model for the presence of defect in the thermal insulation system required the definition of 16 variable and the associated equations. The equations set for the RADMOD_defect.m are summarized in Table A.3 and A.4 for sub-cooled and boiling liquid conditions, respectively. If the Strat3 is selected in the input data file, the equations set is valid, with the appropriate definition of m_L.

Table A.3 – Summary of equations set of the novel RADMOD code for defective coatings, for the boiling liquid condition, $P > P_{sat}(T_L)$.

T_L	$m_L cp_L \frac{dT_L}{dt} = q_{L,boil} + q_{Lrad} + q_{LV} + q_{d1,L}$
T_V	$m_V cv_V \frac{dT_V}{dt} = q_V - q_{LV} - zz\,\phi \frac{RT_V}{M_W} + q_{d2,V}$
P	$\frac{dP}{dt} = zz \frac{\rho_V R}{M_W} \frac{dT_V}{dt} - zz\,\phi \frac{\rho_V R T_V}{m_V M_W}$
L	$\frac{dL}{dt} = 0$
m_L	$\frac{dm_L}{dt} = 0$
m_V	$\frac{dm_V}{dt} = -\phi$
T_{15}	$d_s cp_s \frac{s_s}{2}\left(\frac{A_{15ext} + A_{15int}}{2}\right)\frac{dT_{15}}{dt} = A_{15ext}\frac{k_s}{s_s}(T_{iL} - T_{15}) - q_{L,boil}$
T_{26}	$d_s cp_s \frac{s_s}{2}\left(\frac{A_{26ext} + A_{26int}}{2}\right)\frac{dT_{26}}{dt} = A_{26ext}\frac{k_s}{s_s}(T_{iV} - T_{26}) - A_{26int} h_V (T_{26} - T_V) - q_{L,rad}$
T_{iL}	$\left(d_i cp_i \frac{s_i}{2}\left(\frac{\overline{A_{iL}} + A_{37int}}{2}\right) + d_s cp_s \frac{s_s}{2}\left(\frac{\overline{A_{iL}} + A_{15ext}}{2}\right)\right)\frac{dT_{iL}}{dt} = A_{37int}\frac{k_i}{s_i}(T_{37} - T_{iL}) - A_{15ext}\frac{k_s}{s_s}(T_{iL} - T_{15})$
T_{iV}	$\left(d_i cp_i \frac{s_i}{2}\left(\frac{\overline{A_{iV}} + A_{48int}}{2}\right) + d_s cp_s \frac{s_s}{2}\left(\frac{\overline{A_{iV}} + A_{26ext}}{2}\right)\right)\frac{dT_{iV}}{dt} = A_{48int}\frac{k_i}{s_i}(T_{48} - T_{iV}) - A_{26ext}\frac{k_s}{s_s}(T_{iV} - T_{26})$
T_{37}	$d_i cp_i \frac{s_i}{2}\left(\frac{A_{37int} + A_{37ext}}{2}\right)\frac{dT_{37}}{dt} = A_{37F} I_{extL} - A_{37A} I_{extL} - A_{37int}\frac{k_i}{s_i}(T_{37} - T_{iL})$
T_{48}	$d_i cp_i \frac{s_i}{2}\left(\frac{A_{48int} + A_{48ext}}{2}\right)\frac{dT_{48}}{dt} = A_{48F} I_{extV} - A_{48A} I_{extV} - A_{48int}\frac{k_i}{s_i}(T_{48} - T_{iV})$
T_{d1}	$d_s cp_{sL} s_s \overline{A_{d1}} \frac{dT_{d1}}{dt} = A_{d1ext} q_{d3,rad} - q_{d1,L}$
T_{d2}	$d_s cp_{sV} s_s \overline{A_{d2}} \frac{dT_{d2}}{dt} = A_{d2ext} q_{d4,rad} - q_{d2,V}$
T_{d3}	$d_a cp_a s_i \overline{A_{d3}} \frac{dT_{d3}}{dt} = A_{d3ext} I_{ext} - A_{d1ext} q_{d3,rad}$
T_{d4}	$d_a cp_a s_i \overline{A_{d4}} \frac{dT_{d3}}{dt} = A_{d4ext} I_{ext} - A_{d2ext} q_{d4,rad}$

Table A.4 – Summary of equations set of the novel RADMOD code for defective coatings, for the boiling liquid condition, $P \leq P_{sat}(T_L)$.

T_L	$\frac{dT_L}{dt} = 0$
T_V	$m_V cv_V \frac{dT_V}{dt} = q_V - q_{LV} - zz\phi \frac{RT_V}{M_W} + \frac{dm_L}{dt}\left(cv_V(T_V - T_L) - \frac{R}{M_W}T_L\right) + q_{d2,V}$
P	$\frac{dP}{dt} = zz\frac{\rho_V}{m_V}\left(\frac{P}{\rho_L}\frac{dm_L}{dt} + \frac{RT_V}{M_W}\frac{dm_V}{dt} + \frac{Rm_V}{M_W}\frac{dT_V}{dt}\right)$
L	$\frac{dL}{dt} = \frac{1}{2\rho_L W\sqrt{R^2 - (R-L)^2}}\frac{dm_L}{dt}$
m_L	$\frac{dm_L}{dt} = -\frac{(q_L + q_{LV})}{\Lambda}$
m_V	$\frac{dm_V}{dt} = \frac{(q_L + q_{LV})}{\Lambda} - \phi$
T_{15}	$d_s cp_s \frac{s_s}{2}\left(\frac{A_{15ext} + A_{15int}}{2}\right)\frac{dT_{15}}{dt} = A_{15ext}\frac{k_s}{s_s}(T_{iL} - T_{15}) - q_{L,boil}$
T_{26}	$d_s cp_s \frac{s_s}{2}\left(\frac{A_{26ext} + A_{26int}}{2}\right)\frac{dT_{26}}{dt} = A_{26ext}\frac{k_s}{s_s}(T_{iV} - T_{26}) - A_{26int}h_V(T_{26} - T_V) - q_{L,rad}$
T_{iL}	$\left(d_i cp_i \frac{s_i}{2}\left(\frac{\overline{A_{iL}} + A_{37int}}{2}\right) + d_s cp_s \frac{s_s}{2}\left(\frac{\overline{A_{iL}} + A_{15ext}}{2}\right)\right)\frac{dT_{iL}}{dt} = A_{37int}\frac{k_i}{s_i}(T_{37} - T_{iL}) - A_{15ext}\frac{k_s}{s_s}(T_{iL} - T_{15})$
T_{iV}	$\left(d_i cp_i \frac{s_i}{2}\left(\frac{\overline{A_{iV}} + A_{48int}}{2}\right) + d_s cp_s \frac{s_s}{2}\left(\frac{\overline{A_{iV}} + A_{26ext}}{2}\right)\right)\frac{dT_{iV}}{dt} = A_{48int}\frac{k_i}{s_i}(T_{48} - T_{iV}) - A_{26ext}\frac{k_s}{s_s}(T_{iV} - T_{26})$
T_{37}	$d_i cp_i \frac{s_i}{2}\left(\frac{A_{37int} + A_{37ext}}{2}\right)\frac{dT_{37}}{dt} = A_{37F}I_{extL} - A_{37A}I_{extL} - A_{37int}\frac{k_i}{s_i}(T_{37} - T_{iL})$
T_{48}	$d_i cp_i \frac{s_i}{2}\left(\frac{A_{48int} + A_{48ext}}{2}\right)\frac{dT_{48}}{dt} = A_{48F}I_{extV} - A_{48A}I_{extV} - A_{48int}\frac{k_i}{s_i}(T_{48} - T_{iV})$
T_{d1}	$d_s cp_{sL} s_s \overline{A_{d1}}\frac{dT_{d1}}{dt} = A_{d1ext}q_{d3,rad} - q_{d1,L}$
T_{d2}	$d_s cp_{sV} s_s \overline{A_{d2}}\frac{dT_{d2}}{dt} = A_{d2ext}q_{d4,rad} - q_{d2,V}$
T_{d3}	$d_a cp_a s_i \overline{A_{d3}}\frac{dT_{d3}}{dt} = A_{d3ext}I_{ext} - A_{d1ext}q_{d3,rad}$
T_{d4}	$d_a cp_a s_i \overline{A_{d4}}\frac{dT_{d3}}{dt} = A_{d4ext}I_{ext} - A_{d2ext}q_{d4,rad}$

RADMOD validation sub-model for defective coatings – Equations set

Table A.5 – Summary of equations set of the novel RADMOD validation sub-model for defective coatings, for the boiling liquid condition, $P > P_{sat}(T_L)$.

T_L	$m_L cp_L \frac{dT_L}{dt} = q_{L,boil} + q_{Lrad} + q_{LV} + q_{d1,L} + A_{d5int} q_{d5,L}$
T_V	$m_V cv_V \frac{dT_V}{dt} = q_V - q_{LV} - zz\phi \frac{RT_V}{M_W} + q_{d2,V}$
P	$\frac{dP}{dt} = zz \frac{\rho_V R}{M_W} \frac{dT_V}{dt} - zz\,\phi \frac{\rho_V R T_V}{m_V M_W}$
L	$\frac{dL}{dt} = 0$
m_L	$\frac{dm_L}{dt} = 0$
m_V	$\frac{dm_V}{dt} = -\phi$
T_{15}	$d_s cp_s \frac{s_s}{2} \left(\frac{A_{15ext} + A_{15int}}{2} \right) \frac{dT_{15}}{dt} = A_{15ext} \frac{k_s}{s_s} (T_{iL} - T_{15}) - q_{L,boil}$
T_{26}	$d_s cp_s \frac{s_s}{2} \left(\frac{A_{26ext} + A_{26int}}{2} \right) \frac{dT_{26}}{dt} = A_{26ext} \frac{k_s}{s_s} (T_{iV} - T_{26}) - A_{26int} h_V (T_{26} - T_V) - q_{L,rad}$
T_{iL}	$\left(d_i cp_i \frac{s_i}{2} \left(\frac{\overline{A_{iL}} + A_{37int}}{2} \right) + d_s cp_s \frac{s_s}{2} \left(\frac{\overline{A_{iL}} + A_{15ext}}{2} \right) \right) \frac{dT_{iL}}{dt} = A_{37int} \frac{k_i}{s_i} (T_{37} - T_{iL}) - A_{15ext} \frac{k_s}{s_s} (T_{iL} - T_{15})$
T_{iV}	$\left(d_i cp_i \frac{s_i}{2} \left(\frac{\overline{A_{iV}} + A_{48int}}{2} \right) + d_s cp_s \frac{s_s}{2} \left(\frac{\overline{A_{iV}} + A_{26ext}}{2} \right) \right) \frac{dT_{iV}}{dt} = A_{48int} \frac{k_i}{s_i} (T_{48} - T_{iV}) - A_{26ext} \frac{k_s}{s_s} (T_{iV} - T_{26})$
T_{37}	$d_i cp_i \frac{s_i}{2} \left(\frac{A_{37int} + A_{37ext}}{2} \right) \frac{dT_{37}}{dt} = A_{37F} I_{extL} - A_{37A} I_{extL} - A_{37int} \frac{k_i}{s_i} (T_{37} - T_{iL})$
T_{48}	$d_i cp_i \frac{s_i}{2} \left(\frac{A_{48int} + A_{48ext}}{2} \right) \frac{dT_{48}}{dt} = A_{48F} I_{extV} - A_{48A} I_{extV} - A_{48int} \frac{k_i}{s_i} (T_{48} - T_{iV})$
T_{d1}	$d_s cp_{sL} s_s \overline{A_{d1}} \frac{dT_{d1}}{dt} = A_{d1ext} q_{d3,rad} - q_{d1,L} - A_{d1d5} q_{d1,cond}$
T_{d2}	$d_s cp_{sV} s_s \overline{A_{d2}} \frac{dT_{d2}}{dt} = A_{d2ext} q_{d4,rad} - q_{d2,V} - A_{d2d5} q_{d2,cond}$
T_{d3}	$d_a cp_a s_i \overline{A_{d3}} \frac{dT_{d3}}{dt} = A_{d3ext} I_{ext} - A_{d1ext} q_{d3,rad}$
T_{d4}	$d_a cp_a s_i \overline{A_{d4}} \frac{dT_{d3}}{dt} = A_{d4ext} I_{ext} - A_{d4ext} I_{amb} - A_{d2ext} q_{d4,rad} - A_{d4d6} q_{d4,rad}$
T_{d5}	$d_s cp_{sL} s_s \overline{A_{d5}} \frac{dT_{d5}}{dt} = A_{d5ext} q_{d6,rad} + A_{d2d5} q_{d2,cond} - A_{d5int} q_{d5,L} + A_{d1d5} q_{d1,cond}$
T_{d6}	$d_a cp_a s_i \overline{A_{d6}} \frac{dT_{d6}}{dt} = A_{d4d6} q_{d4,rad} - A_{d5ext} q_{d6,rad} - A_{d6ext} I_{amb}$

Table A.6 – Summary of equations set of the novel RADMOD validation sub-model for defective coatings, for the boiling liquid condition, $P \leq P_{sat}(T_L)$.

T_L	$\frac{dT_L}{dt} = 0$
T_V	$m_V cv_V \frac{dT_V}{dt} = q_V - q_{LV} - zz\phi \frac{RT_V}{M_W} + \frac{dm_L}{dt}\left(cv_V(T_V - T_L) - \frac{R}{M_W}T_L\right) + q_{d2,V}$
P	$\frac{dP}{dt} = zz\frac{\rho_V}{m_V}\left(\frac{P}{\rho_L}\frac{dm_L}{dt} + \frac{RT_V}{M_W}\frac{dm_V}{dt} + \frac{Rm_V}{M_W}\frac{dT_V}{dt}\right)$
L	$\frac{dL}{dt} = \frac{1}{2\rho_L W\sqrt{R^2 - (R-L)^2}}\frac{dm_L}{dt}$
m_L	$\frac{dm_L}{dt} = -\frac{(q_L + q_{LV})}{\Lambda}$
m_V	$\frac{dm_V}{dt} = \frac{(q_L + q_{LV})}{\Lambda} - \phi$
T_{15}	$d_s cp_s \frac{s_s}{2}\left(\frac{A_{15ext} + A_{15int}}{2}\right)\frac{dT_{15}}{dt} = A_{15ext}\frac{k_s}{s_s}(T_{iL} - T_{15}) - q_{L,boil}$
T_{26}	$d_s cp_s \frac{s_s}{2}\left(\frac{A_{26ext} + A_{26int}}{2}\right)\frac{dT_{26}}{dt} = A_{26ext}\frac{k_s}{s_s}(T_{iV} - T_{26}) - A_{26int}h_V(T_{26} - T_V) - q_{L,rad}$
T_{iL}	$\left(d_i cp_i \frac{s_i}{2}\left(\frac{\overline{A_{iL}} + A_{37int}}{2}\right) + d_s cp_s \frac{s_s}{2}\left(\frac{\overline{A_{iL}} + A_{15ext}}{2}\right)\right)\frac{dT_{iL}}{dt} = A_{37int}\frac{k_i}{s_i}(T_{37} - T_{iL}) - A_{15ext}\frac{k_s}{s_s}(T_{iL} - T_{15})$
T_{iV}	$\left(d_i cp_i \frac{s_i}{2}\left(\frac{\overline{A_{iV}} + A_{48int}}{2}\right) + d_s cp_s \frac{s_s}{2}\left(\frac{\overline{A_{iV}} + A_{26ext}}{2}\right)\right)\frac{dT_{iV}}{dt} = A_{48int}\frac{k_i}{s_i}(T_{48} - T_{iV}) - A_{26ext}\frac{k_s}{s_s}(T_{iV} - T_{26})$
T_{37}	$d_i cp_i \frac{s_i}{2}\left(\frac{A_{37int} + A_{37ext}}{2}\right)\frac{dT_{37}}{dt} = A_{37F}I_{extL} - A_{37A}I_{extL} - A_{37int}\frac{k_i}{s_i}(T_{37} - T_{iL})$
T_{48}	$d_i cp_i \frac{s_i}{2}\left(\frac{A_{48int} + A_{48ext}}{2}\right)\frac{dT_{48}}{dt} = A_{48F}I_{extV} - A_{48A}I_{extV} - A_{48int}\frac{k_i}{s_i}(T_{48} - T_{iV})$
T_{d1}	$d_s cp_{sL} s_s \overline{A_{d1}}\frac{dT_{d1}}{dt} = A_{d1ext}q_{d3,rad} - q_{d1,L} - A_{d1d5}q_{d1,cond}$
T_{d2}	$d_s cp_{sV} s_s \overline{A_{d2}}\frac{dT_{d2}}{dt} = A_{d2ext}q_{d4,rad} - q_{d2,V} - A_{d2d5}q_{d2,cond}$
T_{d3}	$d_a cp_a s_i \overline{A_{d3}}\frac{dT_{d3}}{dt} = A_{d3ext}I_{ext} - A_{d1ext}q_{d3,rad}$
T_{d4}	$d_a cp_a s_i \overline{A_{d4}}\frac{dT_{d3}}{dt} = A_{d4ext}I_{ext} - A_{d4ext}I_{amb} - A_{d2ext}q_{d4,rad} - A_{d4d6}q_{d4,rad}$
T_{d5}	$d_s cp_{sL} s_s \overline{A_{d5}}\frac{dT_{d5}}{dt} = A_{d5ext}q_{d6,rad} + A_{d2d5}q_{d2,cond} - A_{d5int}q_{d5,L} + A_{d1d5}q_{d1,cond}$
T_{d6}	$d_a cp_a s_i \overline{A_{d6}}\frac{dT_{d6}}{dt} = A_{d4d6}q_{d4,rad} - A_{d5ext}q_{d6,rad} - A_{d6ext}I_{amb}$

Ringraziamenti

Vorrei ringraziare anzitutto l'Ing. Landucci, relatore di questa tesi, per la guida, l'attenzione ed il supporto dato a questo lavoro.

Ringrazio il Prof. Bertini, controrelatore, per la disponibilità ed i consigli datami.

Un particolare ringraziamento va a Giordano, per la grande disponibilità al confronto e l'amicizia dimostratami.

Desidero ringraziare con il cuore in mano i miei genitori, Lorella e Pietro, e mio fratello Chicco per il loro incrollabile sostegno, che è stato la mia forza durante questi anni. Grazie per questa opportunità.

Ringrazio Anna, Sara e Angelo, che negli anni sono stati prima compagni di classe, poi amici e coinquilini, fino a ritrovarci in una famiglia a tutti gli effetti. Ringrazio inoltre Dario, che da solo è la mia squadra più forte, per esserci ed esserci sempre stato; il caro Frà che mi ha presa per mano ed accompagnata lungo questo percorso universitario e di vita; e Carmelo nel quale ho ritrovato un vero amico oltre ad un compagno di studi. Un grazie particolare ai miei compagni di corso: Bruno, Flavio, Gianluca, Giuseppe, Laura, Luigi e Luigi, Marina, Saverio e Vincenzo; con i quali ho condiviso davvero molto fuori e dento le mura di ingegneria. Vi voglio bene.

Vorrei ringraziare Giacomo, il mio fidanzato e colonna portante, per il supporto non quantificabile, soprattutto in questi ultimi mesi molto duri.

Un ultimo ringraziamento a tutte le persone a me vicine, in particolare a Martina, Silvia, Federico, Carletta e alla Federazione Cugini LON, tutta; ognuno di voi è stato parte di questo percorso.